The membrane trafficking protein myoferlin is a novel interactor of p97

Das Membrantransportprotein Myoferlin ist ein neuer Interaktor von p97

Doctoral thesis for a doctoral degree
at the Graduate School of Life Sciences,
Julius-Maximilians-Universität Würzburg,
Section: Biomedicine

submitted by
Mona Kawan

from
Stuttgart, Germany

Würzburg, 2022

Submitted on: ……..……..

Members of the Thesis Committee

Chairperson: Prof. Dr. Christoph Sotriffer

Primary Supervisor: Prof. Dr. Alexander Buchberger

Supervisor (Second): Prof. Dr. Hermann Schindelin

Supervisor (Third): Dr. Mathias Rosenfeldt

Date of Public Defence: ……..……

Date of Receipt of Certificates: ……..

Affidavit

I hereby confirm that my thesis entitled "**The membrane trafficking protein myoferlin is a novel interactor of p97**" is the result of my own work. I did not receive any help or support from commercial consultants. All sources and/or materials applied are listed and specified in the thesis.

Furthermore, I confirm that this thesis has not yet been submitted as part of another examination process neither in identical nor in similar form.

Place, Date Signature:

Eidesstattliche Erklärung

Hiermit erkläre ich an Eides statt, die Dissertation „**Das Membrantransportprotein Myoferlin ist ein neuer Interaktor von p97**" eigenständig, d.h. insbesondere selbständig und ohne Hilfe eines kommerziellen Promotionsberaters, angefertigt und keine anderen als die von mir angegebenen Quellen und Hilfsmittel verwendet zu haben.

Ich erkläre außerdem, dass die Dissertation weder in gleicher noch in ähnlicher Form bereits in einem anderen Prüfungsverfahren vorgelegen hat.

Ort, Datum Unterschrift

Table of contents

Abbreviations

AAA - ATPases - ATPases associated with diverse cellular activities

AD - Alzheimer's disease

ADP - adenosine diphosphate

ALS - amyotrophic lateral sclerosis

Amp - ampicillin

AMP - Adenosine monophosphate

APS - ammonium-peroxo-disulfate

ATG - autophagy-related gene

ATP - adenosine 5'-triphosphate

CAV1 - Caveolin-1

CD71 - Transferrin receptor protein 1

Cdc48 - cell division cycle 48

Co-IP - co-immunoprecipitation

CP - core particle

CRISPR - clustered regularly interspaced short palindromic repeats

DAPI - 4',6-diamidino-2-phenylindole

ddH_2O - double distilled water

DMSO - dimethyl sulfoxide

DNA - deoxyribonucleic acid

DSP - dithiobis[succinimidyl propionate]

DTT - 1,4-dithiothreitol

DUB - deubiquitinating enzyme

E1 - ubiquitin activating enzyme

E2 - ubiquitin conjugating enzyme

E3 - ubiquitin protein ligase

E. coli - *Escherichia coli*

ECL - enhanced chemiluminescence

EDTA - ethylene diamine tetra-acetic acid

EE - early endosome

EEA1 - early endosome antigen 1

EHD - Eps15 homology domain

ESCRT - endosomal sorting complexes required for transport

ER - endoplasmatic reticulum

ERAD - endoplasmatic reticulum associated degradation

ERC - endocytig recycling compartment

FTD - frontotemporal dementia

g - gravitational constant 9.81m/s2

G418 - geneticine disulfate

GAP - GTPase-activating protein

GEF - guanine nucleotide exchange factors

GFP - green fluorescent protein

Gly - glycine

GTP - Guanosine-5'-triphosphate

HA - hemagglutinin

HD - Huntington's disease

HECT - Homologous to the E6-AP Carboxyl Terminus

HEPES - 2-[4-(2-hydroxyethyl)piperazin-1-yl]ethanesulfonic acid

HRP - horseradish peroxidise

HRS - Hepatocyte growth factor-regulated tyrosine kinase substrate

IBM - inclusion body myopathy

IBMPFD - inclusion body myopathy associated with Paget's disease of bone and frontotemporal dementia

IgG - immunoglobulin G

ILV - intraluminal vesicle

IP - immunoprecipitation

KD - knockdown

kDa - kilo dalton

KO - knockout

LAMP1 - lysosome-associated membrane glycoprotein 1

LC3 - microtubule-associated protein 1A/1B-light chain 3

LE - late endosome

Leu - leucine

Lys – lycine

MAD - mitochondria-associated degradation

Met - methionine

M_r(K) - molecular weight (kilo dalton)

MSP - multisystem proteinopathy

MYOF - myoferlin

NP-40 - nonidet P-40

PBS - phosphate buffered saline

PCR - polymerase chain reaction

PDB - Paget disease of bone

PEG - polyethylene glycol

PLAA - phospholipase A-2-activating protein

PM - plasma membrane

PMSF - phenylmethylsulfonyl fluoride

PP1 - protein phosphatase-1

PQC - protein quality control

PtdIns(3)P - phosphatidylinositol 3-phosphate

PUB - PNGase/UBA or UBX containing proteins

PUL - PLAP, Ufd3, Lub1

PVDF - polyvinylidene fluoride

RBR - RING-between-RING

RE - recycling endosome

RFP - red fluorescent protein

RING - really interesting new gene

RNA - ribonucleic acid

RP - regulatory particle

rpm - rounds per minute

RQC - ribosomal quality control

RT - room temperature

S. cerevisiae - *Saccharomyces cerevisiae*

SDS - sodium dodecyl sulfate

SDS-PAGE - sodium dodecyl sulfate polyacrylamide gel electrophoresis

siRNA - small-interfering RNA

STAM - signal transducing adapter molecule 1

TBS - Tris-buffered saline

TBST - Tris-buffered saline with Tween

Ter94 - transitional endoplasmic reticulum 94

Tf - Transferrin

Tfr1 - Transferrin receptor protein 1 or CD71

TGN - trans Golgi network

Tris - tris (hydroxymethyl)aminomethane

UB - ubiquitin

UBA - ubiquitin-associated

UBL - ubiquitin-like

UBX - ubiquitin regulatory X

UFD1 - ubiquitin-fusion degradation protein 1

UIM - ubiquitin-interacting motif

UPS - ubiquitin-proteasome system

VBM - VCP-binding motif

VCP - valosin-containing protein

VIM - VCP-interacting motif

w/v - weight per volume

WT – wild-type

ZFAND1 - zinc finger AN1 type domain containing protein 1

1 Summary

p97 (also known as VCP, Cdc48 and Ter94) uses the energy of ATP hydrolysis to unfold and thereby segregate proteins. It is involved in various cellular processes such as proteasomal degradation, DNA damage repair, autophagy, and endo-lysosomal trafficking. The specificity for these processes is controlled by more than 30 regulatory cofactors.

Interactions of p97 with cofactors and target proteins are known to be highly dynamic and transient. To identify new interaction partners and to uncover novel cellular functions of p97, the interactome of endogenous p97 was determined by using *in cellulo* crosslinking followed by immunoprecipitation and mass spectrometry. Myoferlin was identified as a novel interactor of p97 and the interaction was validated in reciprocal immunoprecipitation experiments for different cell lines.

The ferlin family member myoferlin is a tail-anchored membrane protein containing multiple C2 domains. Myoferlin is involved in various membrane repair and trafficking processes such as the endocytic recycling of cell surface receptors. The myoferlin interactome was determined by mass spectrometry. Among others, the p97 cofactor PLAA, the transferrin receptor CD71 and Rab14 were identified as common interactors of p97 and myoferlin. Immunoprecipitation experiments with PLAA knockout cells revealed that the interaction between myoferlin and p97 depends on PLAA. Immunofluorescence microscopy showed a co-localization of myoferlin with Rab14 and Rab11, which are both involved in endocytic recycling pathways. Furthermore, immunofluoroscence experiments revealed that myoferlin and the p97 cofactor PLAA are localized to Rab14- and Rab5-positive endosomal compartments.

Using p97 inhibitors and p97 trapping mutants, the presence of p97 at myoferlin-positive and Rab14-positive structures could be demonstrated. Consistent with this finding, the endocytic recycling of transferrin was delayed upon inhibition of p97. Taken together, this work identified myoferlin as a novel interactor of p97 and suggests a role for p97 in the recycling of endocytic cargo.

Zusammenfassung

p97 (auch bekannt als VCP, Cdc48 und Ter94) nutzt die aus der ATP-Hydrolyse gewonnene Energie, um Proteine zu entfalten und dadurch zu trennen. Es ist an verschiedenen zellulären Prozessen wie dem proteasomalen Abbau, der Reparatur von DNA-Schäden, der Autophagie und dem endo-lysosomalen Transport beteiligt. Die Spezifität für diese Prozesse wird durch mehr als 30 regulatorische Cofaktoren gesteuert.

Wechselwirkungen von p97 mit Cofaktoren und Zielproteinen sind bekanntermaßen hochdynamisch und treten oft nur vorübergehend auf. Um neue Interaktionspartner zu identifizieren und neue zelluläre Funktionen von p97 aufzudecken, wurde das Interaktom von endogenem p97 unter Verwendung von *in cellulo* crosslinking, gefolgt von Immunpräzipitation und Massenspektrometrie bestimmt. Dabei wurde Myoferlin als neuartiger Interaktor von p97 entdeckt und diese Interaktion wurde in reziproken Immunpräzipitationsexperimenten und für verschiedene Zelllinien bestätigt.

Myoferlin gehört der Ferlin Familie an und besitzt mehrere C2-Domänen sowie eine Trans-membrandomäne. Myoferlin ist bekanntermaßen an verschiedenen Membranreparatur- und Transportvorgängen wie beispielsweise dem endozytischen Recycling von Zelloberflächenrezeptoren beteiligt. Das Interaktom von Myoferlin wurde durch Massenspektrometrie bestimmt. Dabei wurden unter anderem der p97 Cofaktor PLAA, der Transferrinrezeptor CD71 und Rab14 als gemeinsame Interaktoren von p97 und Myoferlin identifiziert. Durch Immunpräzipitationsexperimente mit PLAA Knockout Zellen wurde eine Abhängigkeit der Interaktion zwischen Myoferlin und p97 von PLAA nachgewiesen. Mit Immunfluoreszenzmikroskopie konnte eine Kolokalisation von Myoferlin mit Rab14 und Rab11, die beide an endosomalen Recycling-Wegen beteiligt sind, beobachtet werden. Des Weiteren zeigten Immunfluoreszenzexperimente, dass Myoferlin und der p97-Cofaktor PLAA an Rab14- und Rab5-positiven endosomalen Kompartimenten lokalisiert sind.

Durch die Verwendung von p97-Inhibitoren oder p97 Mutanten, die ATP nicht hydrolysieren können und so verstärkt Substrate anreichern, konnte gezeigt werden, dass p97 an Myoferlin-positiven und Rab14-positiven Strukturen nachgewiesen werden kann. In Übereinstimmung mit diesem Befund wurde das endozytische Recycling von Transferrin durch die Inhibierung von p97 verzögert. Zusammengefasst zeigt diese Arbeit, dass Myoferlin ein neuer Interaktor von p97 ist, und deutet auf eine Rolle von p97 beim Recycling von endozytischer Fracht hin.

2 Introduction

2.1 Protein homeostasis

To ensure normal cell function, synthesis, folding, disaggregation and degradation of proteins must be tightly controlled. For this purpose, a large number of cellular machines exist, such as ribosomes, chaperones, the ubiquitin-proteasome system, or lysosomes which control protein homeostasis (Labbadia & Morimoto, 2015; Jayaraj et al., 2020). Disturbed protein homeostasis is linked to aging and diseases such as Huntington's disease (HD), Alzheimer's disease (AD), or Multisystem proteinopathy (MSP).

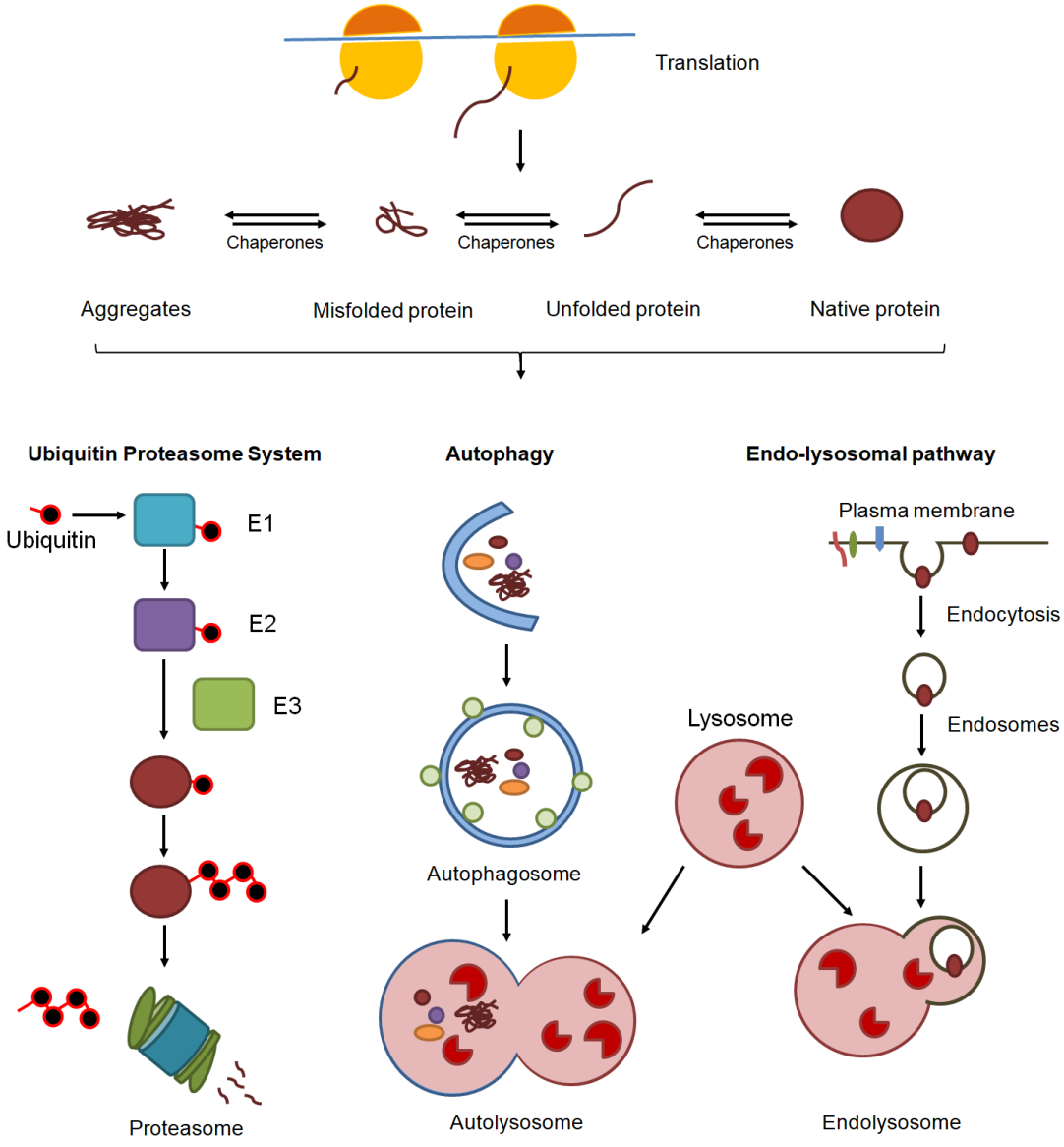

Figure 1: Cellular machines to maintain protein homeostasis. Cellular machinery and pathways involved in protein synthesis (ribosomes), folding (chaperones), and degradation (ubiquitin-proteasome system and lysosomal proteolysis via autophagy or the endo-lysosomal pathway) ensure proper protein homeostasis.

Proteins are synthesized at ribosomes which translate mRNA sequences and assemble the polypeptide chain based on the codon sequence (Figure 1). The polypeptide chain has to fold into the correct protein conformation to ensure the specific activity and functionality of the protein. In addition, misfolded proteins are prone to form aggregates linked to a multitude of human diseases. While some proteins are able to fold correctly individually during synthesis, most proteins require the aid of molecular chaperones to avoid misfolding. (Dobson et al., 1998 ; Kim *et al.*, 2013).

The cell must eliminate misfolded, damaged, or abnormal proteins. In addition, many processes such as the immune response, development, cell-cycle progression, signal transduction, transcriptional regulation, or endocytosis require a selective and regulated degradation of proteins (Hershko and Ciechanover, 1998).

There are two major systems for protein degradation in eukaryotes, the ubiquitin-proteasome system (UPS) and lysosomal proteolysis (Jayaraj et al., 2019). The UPS mostly targets single proteins marked by an ubiquitin chain for proteasomal degradation (Hershko & Ciechanover, 1998; Pohl & Dikic, 2019). Lysosomal proteolysis involves the lysosome, a membrane-enclosed organelle that contains hydrolyzing enzymes such as proteases, nucleases and lipases. Cytoplasmatic proteins, aggregates, or organelles are engulfed in vesicles during autophagy, which fuse with the lysosomes for digestion. Extracellular molecules and plasma membrane proteins are targeted via the endo-lysosomal pathway to the lysosomes. This process involves the endocytosis of molecules at the plasma membrane by the formation of vesicles, which mature and fuse with lysosomes for digestion (Jayaraj et al., 2020; Jackson & Hewitt, 2016).

2.2 Regulation of protein homeostasis via ubiquitin-proteasome system, autophagy and the endocytic pathway

2.2.1 The ubiquitin-proteasome system

2.2.1.1 Ubiquitin

Ubiquitin (Figure 2) is a small, 76 amino acid protein, which is highly conserved in eukaryotes (Goldstein et al., 1975). Ubiquitin is covalently attached to protein substrates either as a single molecule or in the form of polymeric chains with distinct topologies (Komander & Rape, 2012). The conjugation of ubiquitin to target proteins is called ubiquitination. Ubiquitination acts as signal in the

cell and has different cellular functions depending on the chain topologies (Komander & Rape, 2012). It is used as a signal for degradation by the proteasome or lysosome, acts as a sorting signal and alters protein localization. It can affect protein activity and influences protein interactions (Schnell and Hicke, 2003; Glickman and Ciechanover, 2002).

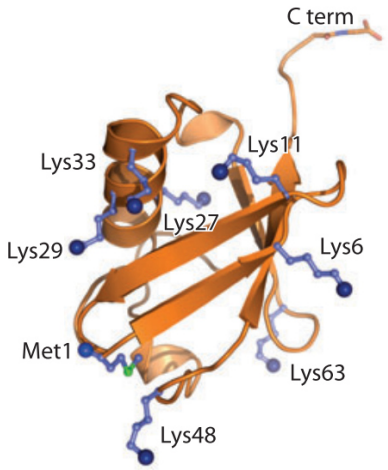

Figure 2: Structure of Ubiquitin. The seven lysine residues (Lys6, Lys11, Lys27, Lys29, Lys33, Lys48 and Lys63), the N-terminal Met1 and the C-terminus are labeled (Komander & Rape, 2012).

Ubiquitination is the attachment of ubiquitin to its substrate (Figure 3). This process is catalyzed by a cascade of three enzymes: E1 (ubiquitin activating enzyme), E2 (ubiquitin conjugating enzyme), and E3 (ubiquitin protein ligase) (Hershko et al., 1983; A. Hershko & Ciechanover, 1998). The process starts with the activation of ubiquitin by the enzyme E1 in an ATP-dependent reaction (Ciechanover et al., 1981). The ATP hydrolysis leads to the formation of an ubiquitin adenylate intermediate, followed by the formation of a thio-ester bond between the active site cysteine of enzyme E1 and the C-terminal glycine (Gly76) of ubiquitin. Finally, AMP is released (Ciechanover *et al.*, 1982; Hershko & Ciechanover, 1998; Pickart, 2001). Next, the activated ubiquitin is transferred via a trans-esterification reaction to the active site cysteine of an E2 enzyme (Hershkos et al., 1983). Classically, the E3 enzyme interacts with the ubiquitin-charged E2 enzyme and the substrate to form an isopeptide linkage between Gly76 of ubiquitin and the ε-amino group of a lysine residue of the substrate (Hershko and Ciechanover, 1998; Pickart, 2001; Fang and Weissman, 2004). There are different mechanisms how E3 enzymes ubiquitinate the target substrate. They can either bind directly or indirectly to promote the transfer of ubiquitin. There are three major classes of E3 enzymes: HECT ligases (Homologous to the E6-AP Carboxyl Terminus), RING ligases (Really Interesting New Gene) and RBR (RING-between-RING) ligases (Hershko and Ciechanover, 1998; Fang and

Weissman, 2004; Metzger et al., 2012; Walden & Rittinger, 2018). Ubiquitination is a reversible process: Deubiquitinating enzymes (DUBs) cleave ubiquitin from substrates (Komander & Rape, 2012).

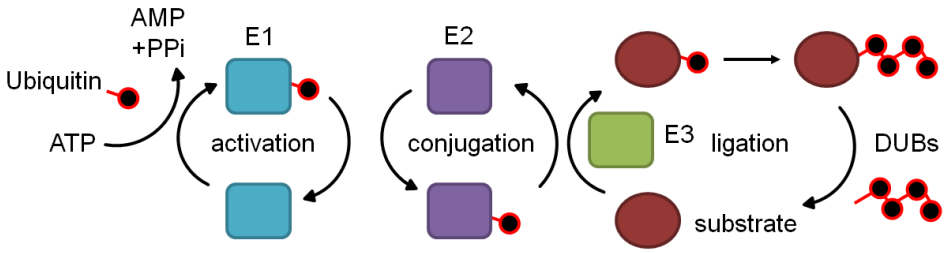

Figure 3: Enzymatic pathway of ubiquitin conjugation. Ubiquitin is covalently linked to the substrate by an ATP-dependent enzymatic cascade of three enzymes: the ubiquitin-activating enzyme (E1 - cyan), ubiquitin conjugating enzyme (E2 - violet) and ubiquitin ligase enzyme (E3 - green). Ubiquitinated substrates can be deubiquitinated by DUBs. Adapted from Pickart, 2001.

There are different types of ubiquitin modifications found on target proteins. Proteins can be tagged with a single ubiquitin moiety leading to monoubiquitinated proteins or by multiple ubiquitin molecules leading to multi-monoubiquitination (Figure 4). Furthermore, proteins can be polyubiquitinated with an ubiquitin chain.

This chain is formed by ubiquitin monomers connected to each other via isopeptide bonds. Since ubiquitin itself contains seven lysine residues (Lys6, Lys11, Lys27, Lys29, Lys33, Lys48, and Lys63) and an N-terminal methionine, multiple types of linkages, structures and lengths are possible (French et al., 2021).There are homotypic, branched, and mixed ubiquitin chains. Ultimately, the linkage type of the ubiquitin chain decides the fate of the substrate protein (Komander & Rape, 2012). For example, K48-linked ubiquitin chains typically target substrate proteins to the proteasome for degradation (Thrower et al., 2000), while K63-linked chains play a role in endocytic trafficking, DNA damage response, or intracellular signaling and K11-linked chains are involved in cell cycle control and immune signaling. Linear ubiquitin chains formed by M1-linked ubiquitin chains play a role in immune signaling (Akutsu et al., 2016).

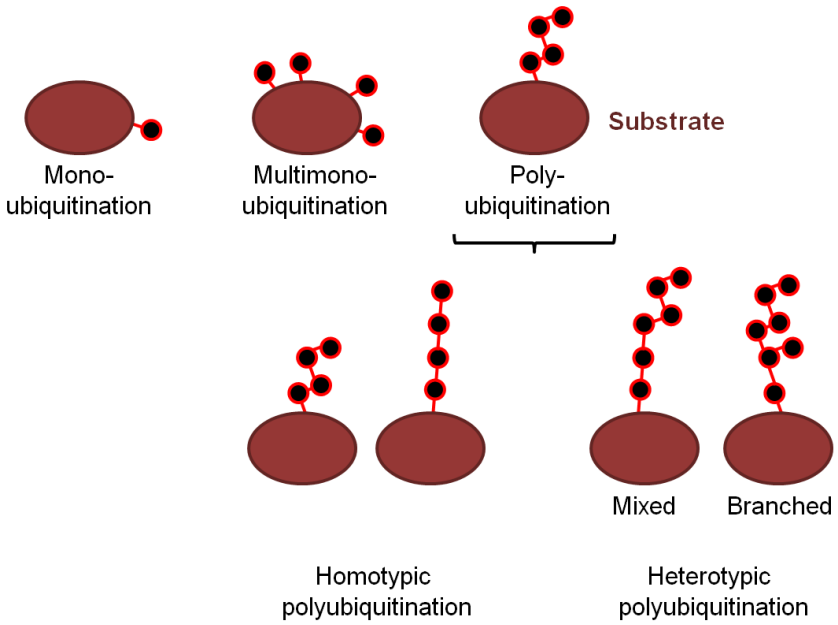

Figure 4: Ubiquitin chain topologies. Substrates can be modified with a single ubiquitin moiety leading to monoubiquitinated proteins, or by multiple ubiquitin molecules leading to multi-monoubiquitinated substrates. In addition, proteins can be polyubiquitinated with an ubiquitin chain. There are different types of ubiquitin chains: Homotypic chains are linked via the same residue of ubiquitin (for example K48-, or K63-linked chains), while heterotypic chains contain different linkage types. In addition, heterotypic chains can be branched whereby a single ubiquitin is modified with multiple ubiquitin molecules. Adapted from Komander & Rape, 2012.

2.2.1.2 The 26S proteasome

The 26S proteasome holoenzyme recognizes ubiquitinated target proteins by associated ubiquitin receptors, unfolds, deubiquitinates, and degrades them. It localizes to the cytosol and nucleus of eukaryotic cells (Coux et al., 1996). The proteasome consists of a 20S core particle (CP) with a barrel-like structure and one or two 19S regulatory particles (RP), which can bind to both sides of the CP facing in opposite directions. The RPs can be divided into a base and a lid subcomplex (Finley, 2009; Collins & Goldberg, 2017). The cylindrical CP consists of four heteroheptameric rings and each ring consists of seven different subunits. The two outer rings contain seven α-subunits and the inner rings consist of seven β-subunits (α7 β7 β7 α7) (Groll et al., 1997; Finley, 2009). The active sites are localized on three β-subunits (β1, β2 and β5) at the inner side of the barrel (Arendt and Hochstrasser, 1997; Finley, 2009). The N-termini of the outer α-ring subunits gate the access to the catalytic subunit and block the entrance in the channel. This gate can be opened by the ATPase ring complex of the base of the RPs (Collins & Goldberg, 2017). The RP is responsible for the recognition of ubiquitin-tagged proteins and their unfolding by the six ATPases of the base. The unfolded polypeptide chain is then gated through the pore of the CP in an ATP-dependent process and gets cleaved by the active sides of the CP into small peptides (Finley, 2009; Collins & Goldberg, 2017).

2.2.2 Autophagy

Autophagy is a conserved cellular degradation pathway in eukaryotes that targets cytoplasmatic material to the lysosomes. There are different types of autophagy: macroautophagy, microautophagy, and chaperone-mediated autophagy. During macroautophagy (hereafter called autophagy) cellular material such as long-lived proteins, protein complexes, aggregates, and damaged organelles are trafficked to the lysosome for proteolytic degradation (Figure 5) (Kaur & Debnath, 2015; Fleming et al., 2022).

During initiation and nucleation the formation of a lipid bilayer called phagophore starts. Substrates destined for degradation are engulfed by the phagophore via an unselective or a selective process. During unselective autophagy, cytoplasmatic substrates are randomly engulfed. In contrast, selective autophagy often requires the ubiquitination of substrates and their sequestration by adaptor proteins like p62 to the phagophore via interacting with receptor proteins like LC3-II, which is anchored into the membrane of the phagophore (Kaur & Debnath, 2015; Pohl & Dikic, 2019). LC3-II is also required for the expansion of the phagophore to form the autophagosome. Later, autophagosomes fuse with lysosomes to autolysosomes and their content is digested by hydrolytic enzymes (Kaur & Debnath, 2015).

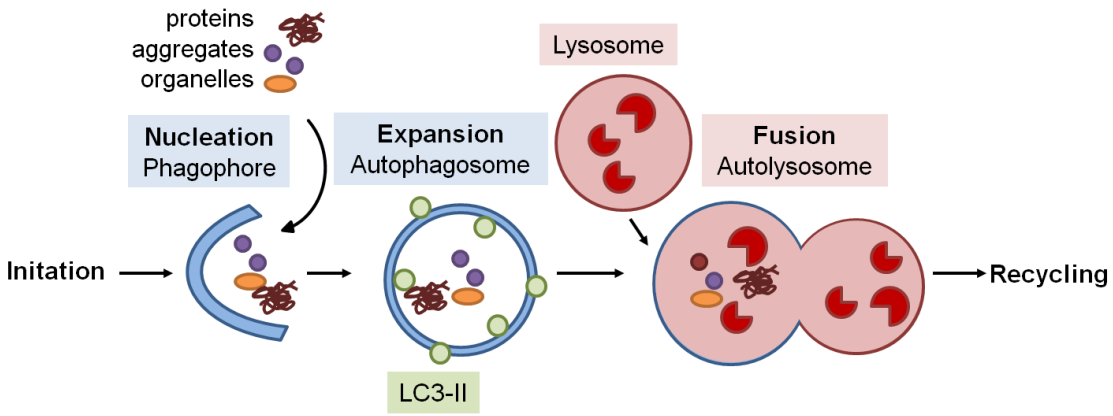

Figure 5: Overview of macroautophagy. Cytoplasmatic substrates such as proteins, protein complexes, aggregates, and damaged organelles are engulfed by a double membrane (phagophore – blue) leading to the formation of autophagosomes (blue). Autophagosomes fuse with lysosomes (red) to autolysosomes (red). Adapted from Kaur & Debnath, 2015.

2.2.3 The endocytic pathway

The plasma membrane contains membrane proteins which are important for essential functions such as signaling from the cell surface, nutrient uptake and transport, cell adhesion, migration, and maintaining cell polarity. The composition of the plasma membrane is controlled by the balance between anterograde protein transport along the secretory pathway and the endocytic pathway (Figure 6) (Cullen & Steinberg, 2018).

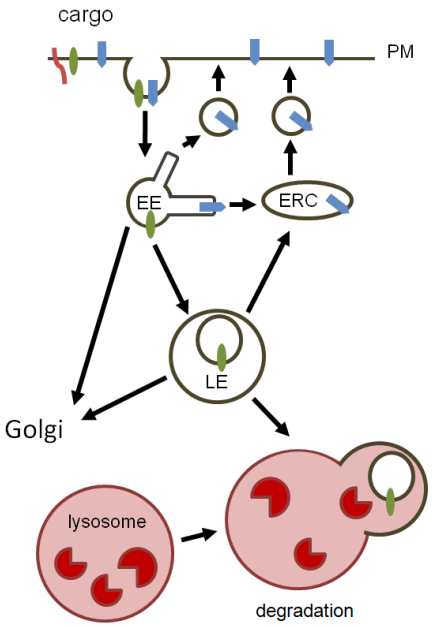

Figure 6: The endocytic pathway. Cargo is internalized by clathrin-dependent or clathrin-independent endocytosis and trafficked to early endosomes (EE). EEs can mature to late endosomes (LE). These endosomes are the sorting station for cargo. Cargo can be recycled by the fast and the slow recycling pathway via the endocytic recycling compartment (ERC) or degraded by internalization and the fusion of LEs with lysosomes.

Rab proteins of the Ras superfamily of small GTPases are important regulators of intracellular membrane trafficking, with many of them being involved in the endocytic trafficking (Sullivan & Lindsay, 2020; Wandinger-Ness & Zerial, 2014). Different Rabs can be found on specific membrane compartments of the endocytic pathway, such as early endosomes, late endosomes, and recycling endosomes, where they control the structural and functional identity of the different endosomes by interacting with specific effector proteins. Effector proteins have a wide range of functions such as selection of cargo into vesicles, coordination of vesicle budding, regulation of vesicle transport along actin filaments or microtubules, tethering of vesicles for fusion, and modulation of the lipid composition (Wandinger-Ness & Zerial, 2014).

Rabs switch between an active GTP-bound form induced by guanine nucleotide exchange factors (GEFs) and an inactive GDP-bound form induced by GTPase-activating proteins (GAPs) (Figure 7). The inactive form binds GDP dissociation inhibitor (GDI) and localizes to the cytosol. Active Rabs bind to membranes via their prenylated C-terminus and recruit specific effector proteins (Zhen & Stenmark, 2015; Homma et al., 2021).

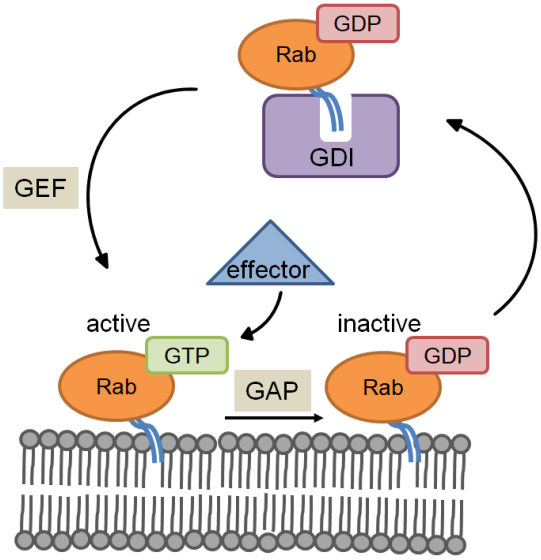

Figure 7: The Rab GTPase cycle. The canonical view of the Rab GTPase cycle is described here. Rab proteins switch between two conformations. The active Rab-GTP binds to the membrane and to their effectors. The inactive Rab-GDP form binds to GDP dissociation inhibitor (GDI) in the cytosol. The nucleotide exchange factor (GEF) activates the Rab and the GTPase-activating protein (GAP) inactivates the Rab. Adapted from Homma et al., 2021.

The endocytic pathway starts with endocytosis at the plasma membrane (Figure 6). Endocytosis is a process in which molecules, like lipids, proteins, fluids, other macromolecules, or pathogens are internalized by the cell. The process involves the selection of cargo and the internalization of the plasma membrane by the formation of vesicles. The destination of the internalized material of these primary endocytic vesicles is the early endosome (EE) (Kumari et al., 2010; Huotari & Helenius, 2011).

There are different types of endocytosis which differ in the selected cargo and the associated molecular machineries. In general, these pathways are defined as clathrin-dependent or clathrin-independent endocytosis, which includes phagocytosis, pinocytosis, and caveolin-dependent endocytosis (Mayor & Pagano, 2007). During clathrin-mediated endocytosis, clathrin-coated pits form domains at the plasma membrane which are stabilized by the presence of sorting motives and ubiquitin (Kumari et al., 2010). Ubiquitin, in form of multi-monoubiqitination or polyubiquitination (mostly K63-linked chains) can serve as a signal for internalization (Piper et al., 2014).

The early endosome (EE) or sorting endosome (Figure 6) receives the cargo from the plasma membrane and is the first endocytic structure of the pathway. EEs are the main sorting platform for the cargo and mature to late endosomes (LEs) (Huotari & Helenius, 2011; Naslavsky & Caplan, 2018). EEs consist of vesicular structures associated with tubular membrane extensions (Huotari & Helenius, 2011). On these structures, membrane domains with distinct composition are formed (Sönnichsen et al., 2000). These domains fulfill different functions, like trafficking of the cargo back to the plasma membrane (PM) or recycling endosomes (RE) or the trans Golgi network (TGN) (Sullivan & Lindsay, 2020). In addition to sorting of cargo for recycling, inwardly budding starts at EEs and intraluminal vesicles (ILVs) are formed. Cargo destined for degradation is sorted in these ILVs, a process which is mediated by the ESCRT machinery (Henne et al., 2011; Cullen & Steinberg, 2018).

EEs can be distinguished from other endosomes by their associated proteins. Several Rabs primarily localize to EEs and are enriched in distinct domains such as Rab14 or Rab4, which are involved in recycling of cargo, or Rab5 (Naslavsky & Caplan, 2018). Rab5 together with its effectors is a key component essential for shaping the identity of the organelle. Rab5 is activated by its GEF Rabex5 and recruits the Rab5 effector Rabaptin-5, which leads to the formation of a positive feedback by interacting with Rabex5, leading to the stabilization of active Rab5 on EEs (Jovic et al., 2010). Active Rab5 binds the VPS34 complex, composed of VPS34-VPS15-Beclin 1-UVRAG in mammals, and activates VPS34, which generates PtdIns(3)P (Ohashi, 2021). PtdIns(3)P is typically enriched on EEs and important for several functions, including the binding of the Rab5 effector EEA1 (early endosomal antigen 1), which acts as a tethering factor and supports vesicle fusion (Jovic et al., 2010). Other interactors of PtdIns(3)P include SNX3, which recruits the retromer complex involved in recycling of cargo to the TGN or the PM, and HRS, a subunit of ESCRT-0 complex and part of the ESCRT machinery (Gershlick & Lucas, 2017; Henne et al., 2011).

The endosomal sorting complexes required for transport (ESCRT) consist of four complexes: ESCRT-0, ESCRT-I, ESCRT-II, and ESCRT-III. The ESCRT mediates membrane remodeling and is involved in processes like viral budding, cytokinesis, nuclear membrane reformation, or the formation of intraluminal vesicles (Vietri et al., 2020). The sorting of cargo into ILVs and their formation, mediated by the ESCRT machinery, begins at EEs and continues during endosome maturation (Henne et al., 2011; Vietri et al., 2020). Usually, the sorting signal for proteins destined for degradation and targeted to ILVs is ubiquitin, either as monoubiquitin or K63-linked polyubiqutin chain. First, the ESCRT-0, consisting of STAM and HRS in mammalian cells, binds to PtdIns(3)P and to ubiquitinated cargo proteins (Figure 8) (Clague et al., 2012). Clathrin is recruited via HRS, which leads to clustering of ESCRT-0 complexes and the formation of subdomains with proteins destined for degradation.

Then ESCRT-I (TSG101, VPS28, VPS37, and MVB12 or UBAP1) and ESCRT-II (EAP45, EAP30, and EAP20) are recruited. Both are able to bind to ubiquitinated proteins and support the formation of these subdomains. The assembly of ESCRT-III starts, which consists of oligomers or polymers of CHMP proteins, and mediates the formation of ILVs. The cargo is deubiquitinated by USP8 and AMSH, and ESCRT-0, ESCRT-I, and ESCRT-II dissociate. The scission is mediated by the ATPase VPS4 (Henne et al., 2011; Vietri et al., 2020).

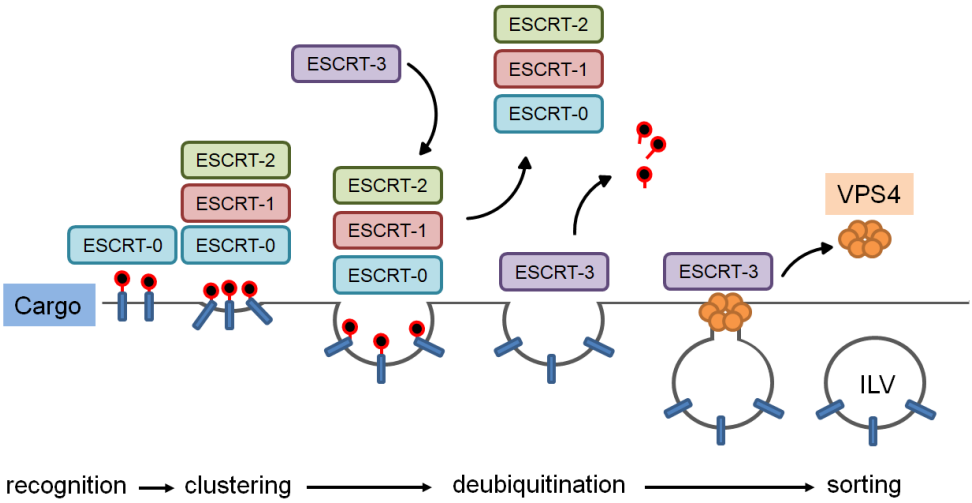

Figure 8: ESCRT-mediated cargo sorting into ILV. ESCRT-0 (cyan) binds to ubiquitinated cargo (blue). ESCRT-I (red) and ESCRT-II (green) bind and the cargo proteins are clustered. ESCRT-III (violet) mediates vesicle budding and the recruitment of DUBs. VPS4 (orange) leads to the disassembly of ESCRT-III and the scission of the ILV. Adapted from Henne et al., 2011.

The formation of ILVs at EEs continues during their maturation to LEs in the peripheral cytoplasm. Therefore, LEs contain more ILVs than EEs. LEs are part of the endo-lysosomal degradation pathway and move on microtubules to the perinuclear area and fuse with other LEs and lysosomes. During the maturation of EE to LE, strong changes in morphology and composition take place. LEs are roundish and contain the cargo destined for degradation in ILVs (Huotari & Helenius, 2011; Huotari & Helenius, 2011). In addition, lysosomal hydrolases and lysosomal membrane proteins like LAMP1 are enriched and are trafficked to the lysosomes for their maintenance (Saftig & Klumperman, 2009). Therefore, LEs are closer related to lysosomes than other endosomes and are more difficult to distinguish from lysosomes (Huotari & Helenius, 2011). During their maturation, EEs undergo a Rab5 to Rab7 transition (Poteryaev et al., 2010).

LEs contain Rab7, while Rab4 or Rab5 are usually excluded (Bottger et al., 1996). Rab7 has an analogous role for LEs as Rab5 for EEs. Therefore, Rab7 is a key regulator in late endosomal trafficking. It regulates movement of LEs on microtubules, interacts with tethering factors and fusion

machineries which enable fusion of LEs with LEs or lysosomes, supports biogenesis of lysosomes, and recruits the retromer core complex involved in the recycling of cargo (Guerra & Bucci, 2016).

In general, eukaryotic recycling starts with the formation of tubulovesicular membrane domains at EEs. Cargo destined for recycling such as receptors or lipids are separated from cargo destined for degradation and sorted into these tubular structures. Recycling can either be direct to the plasma membrane by a process called “fast recycling pathway” or indirect by the “slow recycling pathway” via recycling endosomes (RE) or via the TGN (Figure 6) (Cullen & Steinberg, 2018; Sullivan & Lindsay, 2020). Originally, the recycling of cargo was simply viewed as a default pathway which happens if the cargo fails to be sorted for degradation. However, some cargoes have been identified that carry specific sorting motifs for recycling. In addition, adaptors binding these sorting motifs and sorting machineries like the retriever complex or the retromer complex have been found (Cullen & Steinberg, 2018). The retromer complex, consisting of VPS26, VPS29, and VPS35, is involved in the recycling of cargo to the TGN or the PM. It is recruited to the endosomal membranes by sorting nexin 3 (SNX3) and Rab7 and binds cargo in a sequence-dependent manner by interacting with cargo adaptors such as SNX3 or SNX27 (Tu et al., 2020; Gershlick & Lucas, 2017).

Transferrin (Tf) and the transferrin receptor are frequently used to study the recycling pathway. Tf is a serum glycoprotein, which is important for iron (Fe^{3+}) uptake in cells for which it contains two binding sites (Kawabata, 2019). Binding of iron to Tf is pH dependent: It is bound at 7.4 pH and released at acidic pH (Princiotto & Zapolski, 1976). Diferric Tf enters the cell by binding to the transferrin receptor on the plasma membrane (Figure 9). There are two types of transferrin receptors: Tfr1 (CD71), which is ubiquitously expressed, and Tfr2, which is mostly found in tissues regulating iron metablolism. CD71 is a homodimer type 2 membrane protein with a high binding affinity to diferric Tf. Each CD71 monomer binds one Tf. It is internalized by clathrin-mediated endocytosis and trafficked to EEs (Mayle et al., 2012). In EEs, the acidification of the organelle starts, so the pH is lower. Therefore, iron is released but Tf remains bound to CD71. This complex is sorted to the tubular structures and then recycled back to the PM via the “fast recycling pathway” or the “slow recycling pathway”. At the plasma membrane, Tf is released due to the higher pH and a new cycle of iron uptake can start (Mayle et al., 2012; Kawabata, 2019).

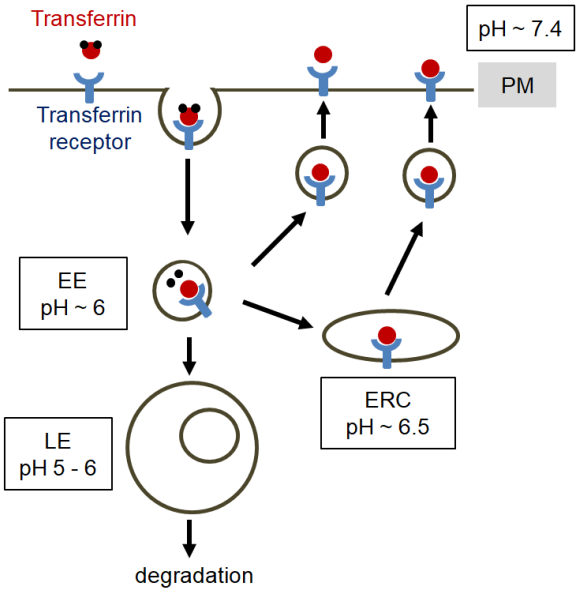

Figure 9: Overview of transferrin trafficking. Tf (red) binds to transferrin receptor (blue) and is internalized via clathrin-mediated endocytosis and trafficked to early endosomes (EE). Bound iron is released, and Tf-CD71 complex is recycled back to the plasma membrane (PM). Adapted from Maxfield & Mcgraw, 2004.

Recycling via the "fast recycling pathway" from EEs directly back to the PM has a half-time of about 2 minutes as shown for Tf (Mayor et al., 1993; Maxfield & Mcgraw, 2004). Proteins involved in the fast recycling pathway are Rab4, playing a role in Tf recycling (Daro et al., 1996), Rab35, AP-1, Snx17, and Snx27 (Naslavsky & Caplan, 2018).

Recycling via "the slow recycling pathway" includes an additional endosomal compartment, the REs. In some cell types, REs cluster in the perinuclear region and are therefore called endocytic recycling compartment (ERC) (Naslavsky & Caplan, 2018). Recycling from EEs to ERC has a half-life of about 2 min and about 10 min from ERC to the PM as shown for Tf (Maxfield & Mcgraw, 2004). Typical proteins found to be enriched at REs are Rab11 (Ullrich et al., 1996) and its effectors (Hales et al., 2001), EH domain-containing protein 1 (EHD1) (Naslavsky & Caplan, 2011), or Tf and CD71 (Naslavsky & Caplan, 2018). These marker proteins are primarily found on REs but can also be found on donor and acceptor compartments of REs (Sönnichsen et al., 2000; Li & DiFiglia, 2012). The Rab11 protein family consists of Rab11A, Rab11B, and Rab25. Rab11A is ubiquitous expressed and is involved in recycling pathways from EEs to REs and from RE to TGN or PM. Effector proteins such as the Rab11 family-interacting protein family consisting of Rab11-FIP1, FIP2, FIP3, FIP34, and Rip11 were shown to be involved in recycling of cargo, tethering and transport of vesicles via interaction with motor proteins (Hales et al., 2001; Kelly et al., 2012). Rab11B expression is enriched in the brain. While it was shown to have a similar localization in cells as Rab11A, different functions in recycling were suggested (Ferro et al., 2021).

EHD1 was shown to recycle a great number of receptors, including the transferrin receptor from REs to the PM. It was also shown to recycle cargo from EEs to ERC and to interact with the retromer core complex (Naslavsky & Caplan, 2011).

2.3 The ATPase p97

p97 (also known as VCP, Cdc48, and Ter94) plays a central and essential role in maintaining protein and organelle homeostasis and genome stability (van den Boom & Meyer, 2018). It is a AAA+ (ATPases associated with diverse cellular activities) ATPase, highly abundant in all tissues, and cell types and conserved in eukaryotes (Peters et al., 1990). The majority of p97 localizes to the cytosol and the nucleus (Peters et al., 1990; Madeo et al., 1998), but it also associates to membranes of organelles such as ER (Ye et al., 2001), Golgi (Rabouille et al., 1995), or lysosomes (Wang et al., 2011). p97 uses the energy of ATP hydrolysis to impose mechanical force on substrates to unfold them. It pulls proteins out of aggregates, complexes, membranes, or chromatin and segregates them (Meyer & Weihl, 2014; Buchberger et al., 2015; van den Boom & Meyer, 2018).

p97 is involved in various proteolysis pathways (Figure 10) including the UPS (van den Boom & Meyer, 2018; Meyer et al., 2012), autophagy (Ju et al., 2009; Papadopoulos et al., 2017), and the endo-lysosomal pathway (Ritz et al., 2011; Ramanathan & Ye, 2012), but it was also shown to be involved in non-degradative pathways such as reassembly of Golgi stacks (Kondo et al., 1997) or protein phosphatase-1 (PP1) maturation (Weith et al., 2018).

To carry out its role in these pathways, p97 is assisted by more than 30 cofactors. These cofactors have specific interaction domains and motifs to bind p97. Cofactors have diverse functions and they can act as DUBs, substrate or ubiquitin adaptors, or ubiquitin ligases (Buchberger et al., 2015). Cofactor binding to p97 has to be tightly regulated and is controlled by additional mechanisms such as competition to the same binding site, bipartite binding, and different binding stoichiometries (Buchberger et al., 2015). Most cofactors bind to the N domain of p97 (Figure 10), while only a few bind to the C-terminal tail (Buchberger et al., 2015). Cofactors can be divided functionally in substrate recruiting cofactors which mediate the binding of p97 to the substrate, substrate processing cofactors which are for example involved in ubiquitination or deubiquitination, and regulatory cofactors which sequester or recycle p97 hexamers. N domain interacting motifs and domains are UBX (ubiquitin regulatory X) and UBXL (UBX-like) domains, VIM (VCP-interacting motif), VBM (VCP-binding motif), and SHP box. In contrast, PUB (PNGase/UBA or UBX containing proteins)

and PUL (PLAP, Ufd3p, and Lub1p) domains were shown to interact with the C-terminal tail (Buchberger et al., 2015; Hänzelmann & Schindelin, 2017).

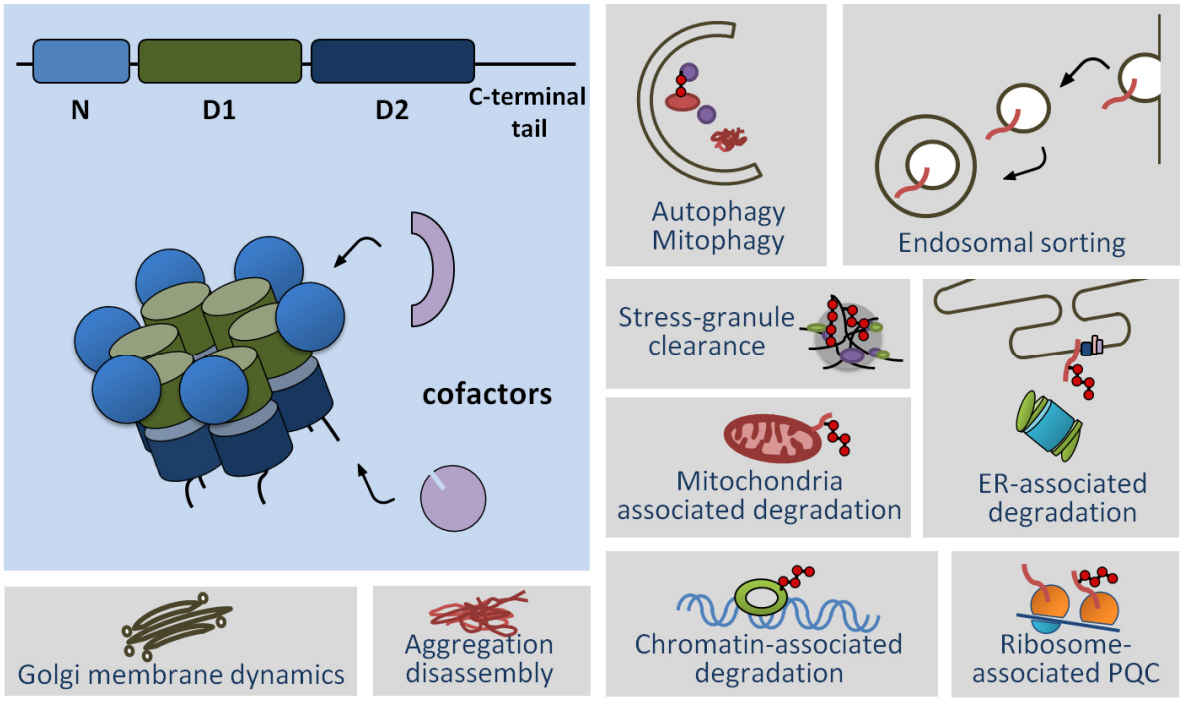

Figure 10: Overview of cellular functions of p97. p97 consists of an N domain, two ATPase domains, D1 and D2, and an C-terminal tail and forms homohexameric protein complexes. Cofactors can bind to the N domain or the C-terminal tail and mediate the functional role of p97 in diverse pathways. See text for details.

2.3.1 Structure and function of p97

Each monomer of the mammalian p97 consists of an N-terminal, globular N domain (residues 1–187), two ATPase domains, D1 (residues 209–460) and D2 (residues 481–763), and a C-terminal tail (residues 764–806).The N and D1 domain and the D1 and D2 domain are connected by two linker regions (residues 188–208 and 461–480) (Buchberger et al., 2015). The domains D1 and D2 form two stacked hexameric rings with a central pore (DeLaBarre & Brunger, 2003; Banerjee et al., 2020).

Both ATPase domains are able to hydrolyze ATP. The binding of ATP and its hydrolysis to ADP controls the conformation of the complex. The ATP cycle of the D1 domain influences the position of the N domain. It changes between a so-called “down conformation” to an “up conformation” (Figure 11). In the “down conformation”, ADP is bound and the N domains are coplanar with the D1 ring. The binding to ATP shifts the N domains upwards (“up conformation”). This change in conformation influences the binding to cofactors and substrates. Binding to substrates reduces ATP

hydrolysis of D1, so the ATP-bound form is favored (Bodnar & Rapoport, 2017a ; van den Boom & Meyer, 2018). In addition, the ATP hydrolysis cycle of the D2 domain is increased. The D2 domain provides the main driving force to unfold proteins. It was shown that ATP hydrolysis of the D2 domain leads to conformational changes in the pore-facing loops, rotation between D2 and D1 domain, and changes in the size of the pore (Milligan & Wilson-Kubalek, 2003; van den Boom & Meyer, 2018). These conformational changes cause the polypeptide chain to be pulled in the channel to facilitate the unfolding of the substrate protein (Bodnar & Rapoport, 2017a).

Recent publications have shown that the conformational changes of p97 caused by ATP hydrolysis lead to an unfolding of the substrate by a threading mechanism, in which substrates are pulled through the central pore of p97. In case of ubiquitinated substrates destined for proteasomal degradation, the p97-Ufd1-Npl4 complex recognizes and binds the ubiquitin chain (Figure 11). It was shown that unfolding starts from ubiquitin and moves on to the substrate. Ubiquitin refolds after being released from the pore (Ji et al., 2022).

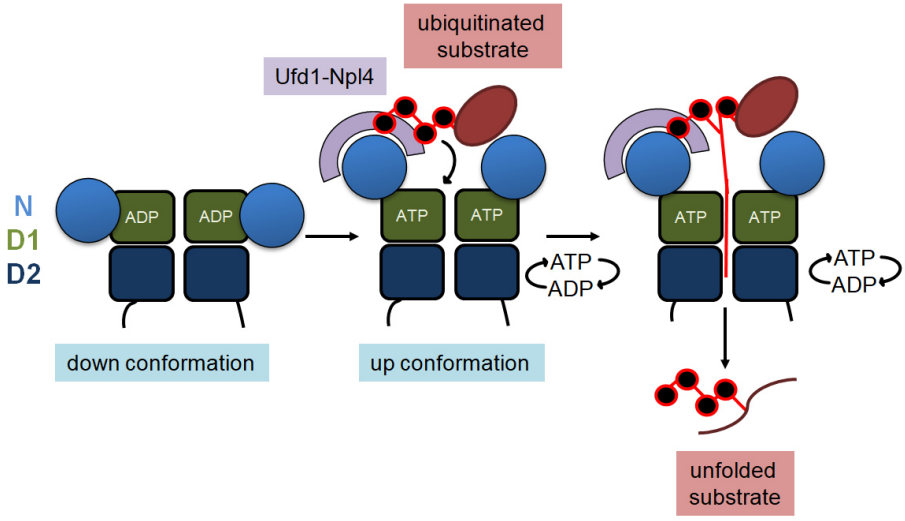

Figure 11: Function of p97. p97 switches from the "down conformation" to the "up conformation" by binding of ATP at the D1 domain. Ubiquitinated substrates (red) are bound at the N domain via cofactors (violet). The D2 domain hydrolyzes ATP and pulls ubiquitin into the pore and thereby unfolds it. Then the substrate is unfolded and ubiquitin refolds.

In case of PP1 maturation, the subunit I3 of the inactive SDS22-PP1-I3 complex is targeted by the p97-p37 complex leading to the threading of I3 into the pore of p97 and resulting in the disassembly of the complex. This process is independent of ubiquitin and mediated by the internal recognition sequences (IRS) of I3 recognized by the p97-p37 complex (Boom et al., 2021).

2.3.2 Role of p97 in the UPS, autophagy and the endocytic pathway

Proteins tagged with a K48-linked ubiquitin chain are destined for degradation via the UPS. p97 interacts with the Ufd1-Npl4 heterodimer to recognize and process these ubiquitin-tagged substrates. p97 was shown to assist the proteasome for the degradation of soluble proteins in the cytosol (Beskow et al., 2009; Olszewski et al., 2019). But more often, it is involved in several protein quality pathways which require the extraction of ubiquitinated target proteins from membranes or complexes and delivers them to the proteasome for degradation. In this context, p97 is involved in the ribosome-associated protein quality control (RQC), a pathway to recycle stalled ribosomes and to degrade the nascent polypeptide chains which are released from the peptidyl-tRNA through the p97 cofactor ANKZF1 (Yip et al., 2019). The p97-Ufd1-Npl4 complex directly extracts the ubiquitinated nascent polypeptide chains from 60S ribosomes for proteasomal degradation (Figure 10) (Brandman & Hegde, 2016). ER-associated degradation (ERAD) is another pathway relying on the function of p97. Misfolded or damaged proteins in the ER are recognized and retrotranslocated to the cytosol for proteasomal degradation. The p97-Ufd1-Npl4 complex is recruited to the membrane to pull out the proteins. The p97-Ufd1-Npl4 complex is also involved in the extraction of proteins from mitochondria via mitochondria-associated degradation (MAD) (Taylor & Rutter, 2011) or the chromatin associated degradation important for regulation of transcription, DNA damage response and the cell cycle, or nucleotide excision repair (Franz et al., 2016).

p97 was shown to be involved in autophagy. First, enlarged vesicles positive for p62 and LC3-II were found in patient cells carrying p97 disease-causing mutations (J. Ju et al., 2009). In addition, abnormal autophagosome formation and lysosome morphology defects were observed in context with p97 (van den Boom & Meyer, 2018). p97 was shown to play a role in the targeted degradation of damaged lysosomes via autophagy. The cofactors involved are PLAA, UBXD1, and YOD1, forming a complex with p97 (ELDR complex - endo-lysosomal damage response). The ELDR complex is recruited to damaged lysosomes and removes K48-linked ubiquitin conjugates, which supports the degradation of the damaged organelle via autophagy (Papadopoulos et al., 2017).

In the endo-lysosomal pathway, p97 was shown to be involved in the degradation of CAV1. CAV1 is a membrane protein involved in organizing cholesterol-rich microdomains and important for the formation of caveolae at the PM, which are important for signaling, endocytosis, and maintenance of the plasma membrane. CAV1 is monoubiquitinated and sorted into ILVs for degradation (Hayer et al., 2010; Kirchner et al., 2013), a process which involves p97 and its cofactor UBXD1. It was shown that both interact with CAV1 and this interaction is important for the internalization of CAV1 into ILVs

(Ritz et al., 2011a). Moreover, it was demonstrated that inhibition of p97 affected sorting and degradation of EGFR in the endo-lysosomal pathway (Ritz et al., 2011a). p97 was also shown to localize to EEs and bind to the tethering factor EEA1. It was suggested that p97 influences the oligomeric state of EEA1 and therefore affects the size of EEs. (Ramanathan & Ye, 2012). In addition, the p97 cofactor PLAA was shown to be involved in receptor trafficking at the endo-lysosomal pathway (Hall et al., 2017).

2.3.3 Multisystem proteinopathy 1

Mutations in the gene encoding human p97 cause a fatal genetic multisystem degenerative disorder called multisystem proteinopathy 1 (MSP1), previously classified as inclusion body myopathy with frontotemporal dementia, Paget's disease of bone, and amyotrophic lateral sclerosis (IBMPFD/ALS) (Korb et al., 2020). More than 50 autosomal dominant mutations were found and patients with disease-causing mutations show a combination of four main disease manifestations: Inclusion body myopathy (IBM), Paget disease of bone (PDB), frontotemporal dementia (FTD) and amyotrophic lateral sclerosis (ALS) (Korb et al., 2020). Mutations are usually found at the interface of the N domain and the D1 domain of p97 (Tang & Xia, 2016), suggesting that the communication between these domains is disturbed (Meyer & Weihl, 2014) leading to perturbed cofactor binding (Fernández-Sáiz & Buchberger, 2010; Hayer et al., 2010; Schuetz & Kay, 2016).

Around 90% of MSP1 patients have myopathy and suffer from progressive weakness and atrophy of skeletal muscles. This weakness progresses to the respiratory muscles and heart, leading to respiratory failure, cardiomyopathy, or cardiac failure. In cells, cytoplasmic rimmed vacuoles and inclusions positive for proteins such as ubiquitin and TDP-43 were found (Korb et al., 2020). About 42% of the patients suffer from PDB. In PDB, osteoclasts are deregulated and overactive, causing increased bone turnover and weakness (Nalbandian et al., 2011). Osteoclasts contain ubiquitinated nuclear and cytoplasmic inclusions positive for proteins like ubiquitin and p62. FTD occurred in about 30% of the patients, which suffer from neurodegeneration of the brain, affecting the frontal and anterior temporal lobes. This leads to a change in personality, behavior, and executive function. Ubiquitin-positive inclusions and aggregates have been found in neurons. ALS can be found in 9% of the patients. It affects upper and lower motor neurons and patients display muscle atrophy and weakness which progress to other muscles leading to death from respiratory failure (Nalbandian et al., 2011; Korb et al., 2021).

On a cellular level, the disease-causing mutations affect a subset of p97 functions. Inclusions and aggregates positive for ubiquitin suggest that the pathogenic mutations of p97 influence protein degradation and trafficking (Korb et al., 2020). Early studies showed an accumulation of ERAD substrates and suggested impaired proteasomal degradation (Weihl et al., 2006). However, this finding could not be confirmed in more recent studies, which could not detect impairment of the UPS (Tresse et al., 2010). Meanwhile, several other functions of p97 were shown to be implicated in MSP1. p97 disease mutations were shown to cause impaired sorting of CAV1 leading to an accumulation of CAV1 at endosomes (Ritz et al., 2011). In addition, autophagosomes positive for LC3-II and p62 accumulated (Ju et al., 2009), and impaired autophagosome maturation was observed (Tresse et al., 2010). Thus, autophagy and endosomal sorting were linked to p97 disease-causing mutations. In addition, impaired stress granule clearance was also implicated in neurodegenerative diseases and also shown to be involved in MSP1. Stress granules are membrane-less, cytoplasmic assemblies of mRNPs stalled in translation initiation and usually induced by different stress conditions. p97 is involved in the clearance of stress granules via autophagy (granulophagy) or the proteasome via ZFAND1 mediated recruitment (Buchan et al., 2013; Turakhiya et al., 2018).

2.4 Aims

p97 is involved in diverse cellular pathways and processes mediated by a large number of regulatory cofactors. However, many of its functions are still poorly understood. The aim of this thesis was to identify novel p97 interaction partners to gain a better understanding of its cellular functions.

3 Results

3.1 Myoferlin is a novel interactor of p97

3.1.1 Crosslinking stabilizes the p97 interactome

To identify novel interactors of p97, immunoprecipitation (IP) combined with mass spectrometry was applied. Several publications showed different approaches to identify or stabilize p97 interactors, reaching from expression of tagged p97 wild-type (WT) or ATPase-deficient substrate-trapping mutants to treatment with p97 inhibitors or crosslinking (Raman et al., 2015; Ritz et al., 2011; Her et al., 2016; Xue et al., 2016). Since p97 interactions are known to be transient and highly dynamic (Xue et al., 2016), an *in cellulo* crosslinking approach with the crosslinker dithiobis(succinimidyl propionate) (DSP) was tested to stabilize interactions in the native environment. In the first step, the efficiency of the crosslinking was determined by comparing cells treated with DSP to untreated cells.

DSP is a homo-bifunctional crosslinker with two terminal N-hydroxysuccimide esters as reactive groups, which react with primary amines (Figure 12 A). It is cleavable by reducing the disulfide bond in the spacer and membrane-permeable. Therefore, DSP was directly added to intact HeLa cells to stabilize p97 interactions before lysis.

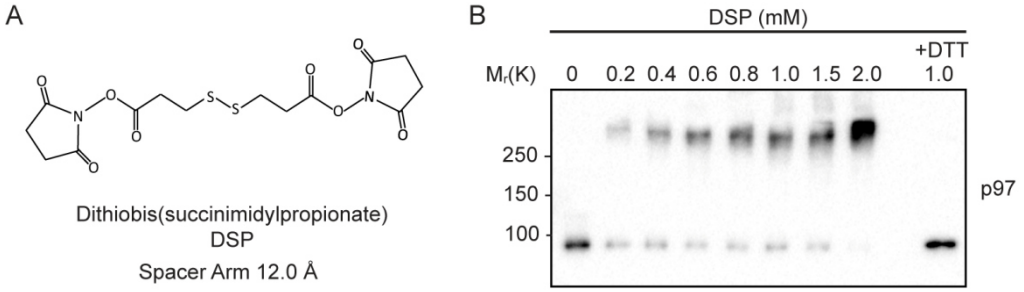

Figure 12: Crosslinking with DSP produces SDS-resistant p97 oligomers. (A) Chemical structure of DSP. DSP contains two reactive groups and a disulfide bridge which is cleaved upon addition of DTT. (B) HeLa cells were treated with the indicated concentrations of DSP before lysis. Western blot performed by Maria Körner née Schultz (Körner/Schultz, 2018).

To identify a low DSP concentration which still ensures efficient crosslinking, different DSP concentrations were tested and monomers as well as oligomers of p97 were detected by western blot (Figure 12 B). Without crosslinking, the p97 complex was disassembled into its monomers due to

the denaturing conditions of SDS-PAGE. The addition of the crosslinker leads to the formation of SDS-resistant p97 oligomers visible in the high molecular weight area. The proportion of p97 in high molecular weight complexes increased with increasing concentration of DSP. The addition of dithiothreitol (DTT) to the sample buffer reduced the disulfide bond of DSP, and p97 monomers were regained. A concentration of 0.8 mM DSP was selected for all following crosslinking experiments to prevent over crosslinking. At this concentration, p97 is mostly crosslinked, but there are still monomers left, while at higher concentrations (2.0 mM) most of the remaining p97 monomers were gone.

In order to determine if crosslinking stabilizes p97 interactions, co-immunoprecipitations of p97 were performed using untreated HeLa cells and HeLa cells crosslinked with DSP (Figure 13). Crosslinking did not interfere with the binding of the antibody to its epitope, since similar levels of p97 were immunoprecipitated for both conditions. To test the effect of the crosslinker on p97 interactions, the known p97 cofactors FAF1 and UBXD1 were analyzed for co-precipitation. Whereas UBXD1 interacted with p97 in both conditions, FAF1 interaction was only detectable with crosslinking, showing that crosslinking indeed stabilized the interaction of p97 with FAF1.

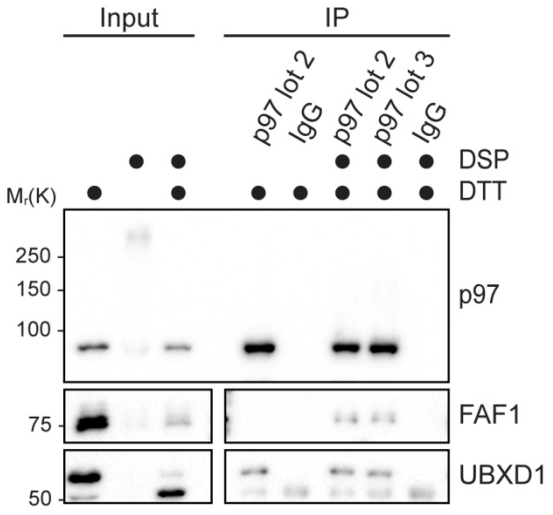

Figure 13: Crosslinking stabilizes the interaction of p97 with its cofactor FAF1. Comparison of cells treated with and without DSP. Lysates were subjected to immunoprecipitation with two different lots of p97 antibody and control IgGs, respectively. Input and immunoprecipitation samples were analyzed by western blot using the indicated antibodies.

To determine if crosslinking stabilizes p97 interactions in general, immunoprecipitation of p97 complexes from crosslinked and non-crosslinked control samples were performed and analyzed by mass spectrometry. The dataset was first evaluated for known p97 cofactors (Figure 14 A), and both

conditions were directly compared. Without crosslinking, seven known cofactors, including UBXD1 were identified. All seven cofactors were also identified with crosslinking together with 12 additional cofactors, including FAF1 and UBXD1 (Figure 14 B). This experiment confirmed the previous result (Figure 13) and verified that crosslinking stabilizes the interaction of p97 with known cofactors. The total amount of hits with a significance of one or two was strongly increased by the crosslinking approach from 29 to 399.

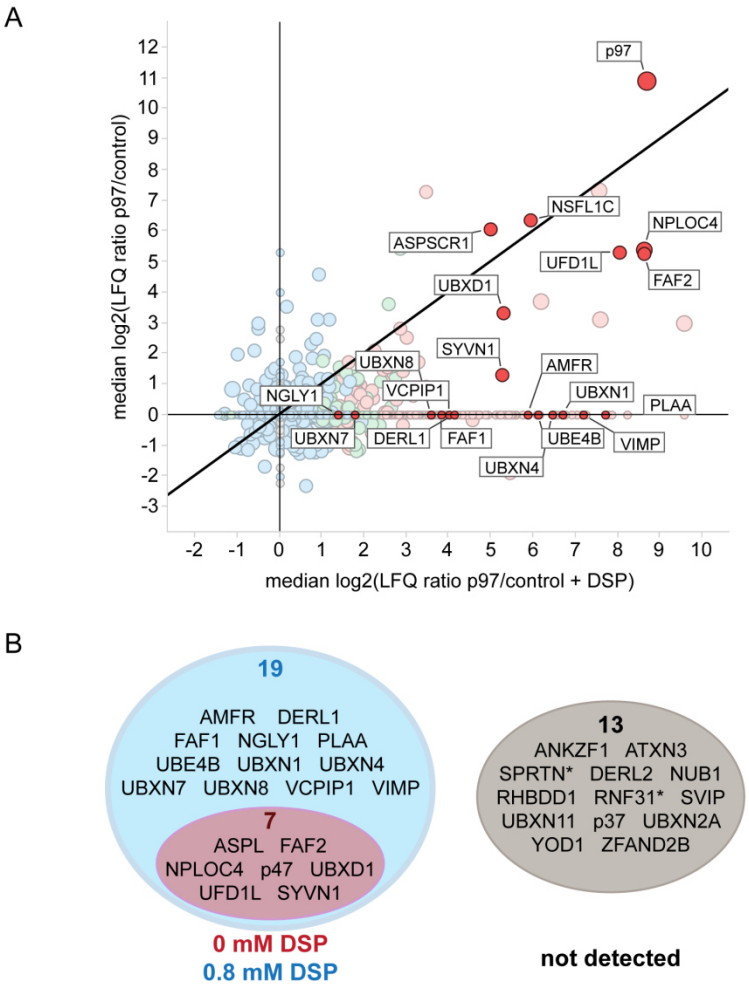

Figure 14: Crosslinking stabilizes cofactor interactions with p97. (A) Comparison of cells treated with (p97/control (DSP)) and without DSP (p97/control). Identification of cofactors interacting with p97 by co-immunoprecipitation and mass spectrometry. p97/control: n=3 (see 7.1); p97/control(DSP): n=4 (see 7.2); one replicate performed by Maria Körner (Körner/Schultz, 2018). (B) Venn diagram of p97 cofactors: Cofactors detected with crosslinking (blue), cofactors detected without crosslinking (red) and known cofactors which were not detected (grey).*- Interaction with p97 not confirmed for SPRTN and RNF31.

3.1.2 Identification of myoferlin as a novel interactor of p97

The p97 interactome obtained by crosslinking was further analyzed for known p97 interactors to confirm the reliability of the data (Figure 15). p97 unfolds ubiquitinated substrates and many of its

cofactors possess ubiquitin-binding domains (Buchberger et al., 2015). As expected, ubiquitin, which is derived from several ubiquitin-fusion proteins (RPS27A; UBB; UBC; UBA52), was identified. In addition, p97 is known to be involved in unfolding and extraction of target proteins in various proteasomal degradation pathways. The exact mechanism how the unfolded target proteins are delivered to the proteasome and how the proteasome and p97 coordinate their degradation is not fully understood (Hänzelmann et al., 2019). Most proteasomal subunits from the 20S core particle as well as the 19S regulatory particle with the lid and base subunits were found to be significantly enriched.

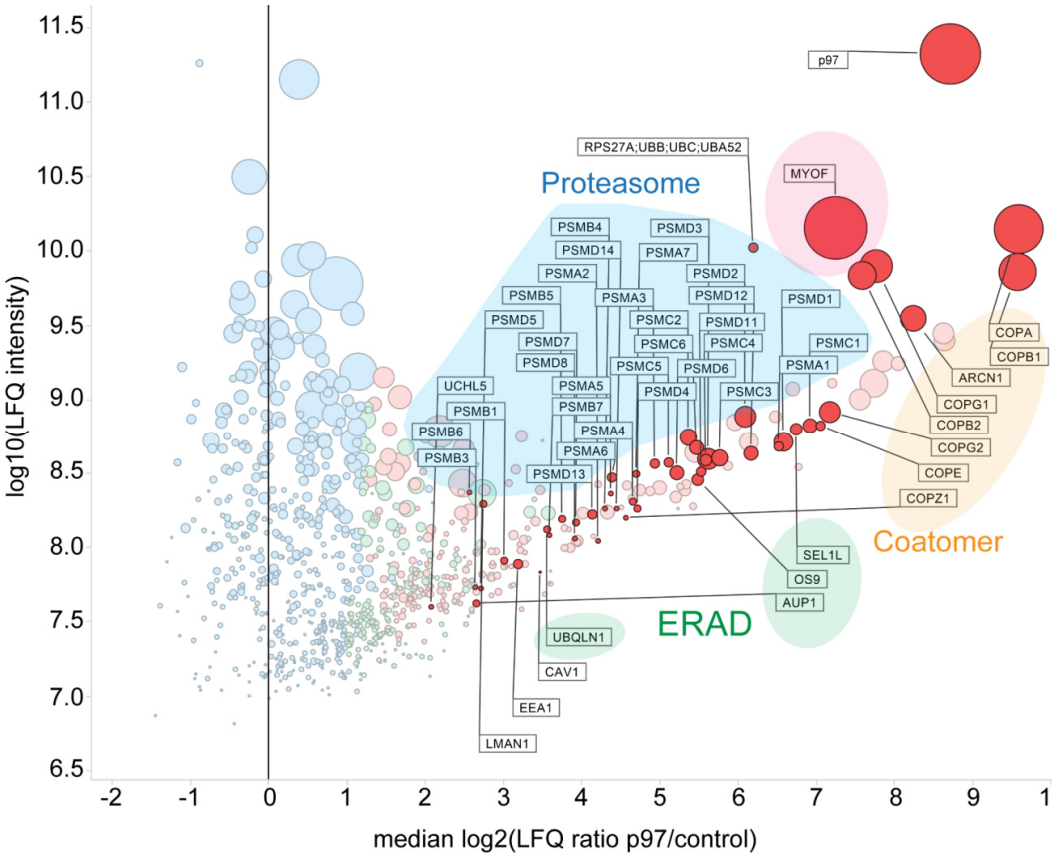

Figure 15: Mass spectrometry analysis for p97 binding proteins. Interactors of p97 were identified by co-immunoprecipitation and mass spectrometry (see 7.2). Proteasomal subunits are highlighted in blue, proteins involved in ERAD are marked in green, the coatomer subunits of COPI are marked in yellow and MYOF in red. For details on the replicates see legend of Figure 14.

It should be noted that crosslinking with DSP does not only stabilize direct interactions of p97 but also indirect interactors linked via cofactors or other interactors to p97. Therefore, whole complexes such as the proteasome are stabilized.

In addition, several proteins involved in ERAD were identified: OS9 and SEL1L, involved in substrate recognition, p97 cofactors involved in retrotranslocation such as DERL1, UFD1L, NPLOC4, FAF2 and the E3 ligase SYVN1 (Figure 14), as well as AUP1 and UBQLN1 (Lopata et al., 2020). Besides these complexes, known p97 interactors involved in trafficking such as CAV1 (Ritz et al., 2011), EEA1 (Ramanathan & Ye, 2012), and LMAN1 (also known as ERGIC-53) (Haines et al., 2012) were found. Crosslinking also revealed an interaction of p97 with the coat protein complex I (COPI) (Arakel & Schwappach, 2018). All subunits of this complex were identified with crosslinking, even though COPA and COPB2 were also identified without crosslinking (see 7.1), again showing that crosslinking stabilizes complexes. In addition, myoferlin (MYOF) was among the most strongly enriched proteins and therefore considered as a strong candidate to be a novel interactor of p97.

3.1.2.1 Confirmed interaction of myoferlin and p97

In order to validate the interaction between MYOF and p97, immunoprecipitations of HeLa cells treated with DSP were performed using two different antibodies raised against the C-terminal part of p97 (Figure 16). p97 #1, which was used in the previous experiments (Figure 13, 14 and 15), is a rabbit polyclonal antibody raised against residues 750-806, whereas p97 #2 is a mouse monoclonal antibody raised against residues 792-806. For both antibodies, co-immunoprecipitation of MYOF with p97 was confirmed.

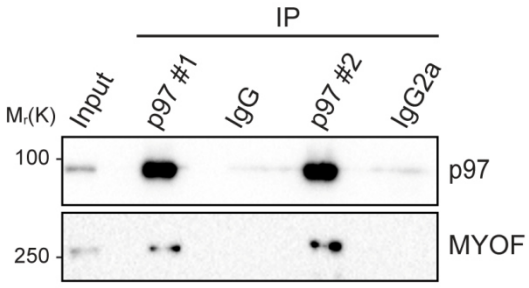

Figure 16: p97 interacts with MYOF. HeLa cells were crosslinked with DSP (30 min, RT). Lysate was subjected to immunoprecipitation (IP) with two different p97 antibodies (p97 #1: A300-589A; p97 #2: sc-57492) and matched unspecific IgGs, respectively. Input and IP samples were analyzed by western blot for MYOF and p97.

Importantly, the interaction was also confirmed by reciprocal co-immunoprecipitations of HeLa cells treated with DSP, using two different MYOF antibodies: MYOF #1, a rabbit polyclonal antibody raised against residues 700-800, and MYOF #2, a mouse monoclonal antibody raised against residues 88-198 (Figure 17).

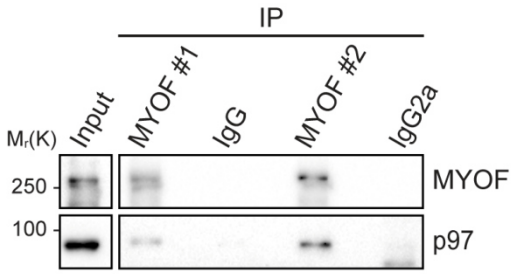

Figure 17: MYOF interacts with p97. HeLa cells were treated with DSP (30 min, RT). Lysate was subjected to anti-MYOF immunoprecipitation (IP). Two antibodies targeting different epitopes of MYOF were tested (MYOF #1: ab190264; MYOF #2: sc-376879) and analyzed for MYOF and p97 using immunoblot.

So far, the interaction of MYOF and p97 could only be observed with crosslinking, but not without (Table 14 7.1), suggesting a weak or transient interaction. In order to exclude the possibility that the observed interaction is a crosslinking artefact, stable HeLa cell pools with a doxycycline-inducible, ectopic expression of FLAG-tagged p97 variants were generated using the pINDUCER20 lentiviral system (Meerbrey et al., 2011). Five cell pools were generated: a negative control carrying the empty lentiviral plasmid (empty) and four different variants of FLAG-tagged p97, including wild-type (WT) and the mutants E305Q, E578Q and E305QE578Q (EQEQ) (Figure 18 A). Residues E305 and E578 are located on the D1 and D2 domain, respectively. Mutations of the conserved glutamate residue of the Walker B motifs to glutamine generated ATP hydrolysis deficiency in their respective domain (Ye et al., 2003). E578Q mutations are commonly used to enrich and stabilize p97 interactions (Ritz et al., 2011; Papadopoulos et al., 2017; Turakhiya et al., 2018). Upon treatment with doxycyline, HeLa cells expressed the different variants and p97 levels were slightly increased compared to uninduced cells or the control cell line (Figure 18 B).

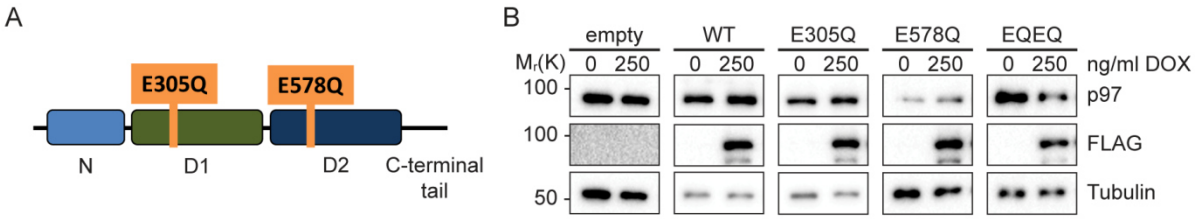

Figure 18: Stable HeLa cell pools expressing p97 mutants. (A) Schematic representation of ATP-hydrolysis deficient mutations, E305Q at the D1 domain of p97 and E578Q at the D2 domain of p97. (B) p97 variants were expressed upon induction by doxycyline treatment for 22 h and detected by western blot.

The expression of the FLAG-tagged p97 variants was further confirmed by confocal immunofluoroscence microscopy (Figure 19). The cells were induced with doxycycline and their expression was observed with an anti-FLAG antibody and compared to an anti-p97 antibody.

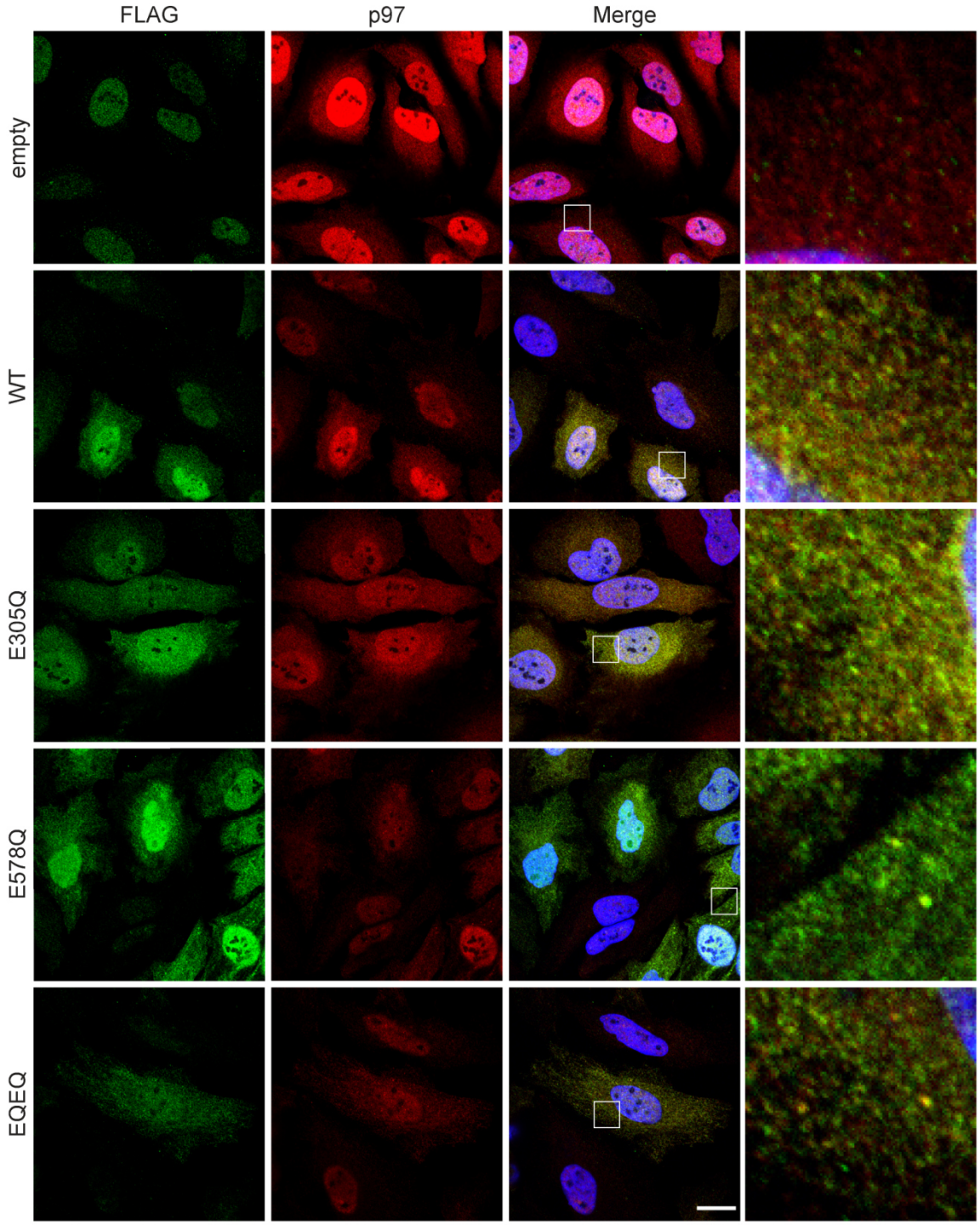

Figure 19: Stable HeLa cell pools expressing Flag-tagged p97 mutants upon doxycycline induction. Confocal microscopy was used to visualize the localization of p97 and FLAG-p97. Scale bar, 20 µm.

Cells expressing the p97 variants showed an increased cytoplasmic and nuclear FLAG staining compared to the control cell line. In general, the signals for FLAG and p97 overlapped. Usually, p97 appeared as a diffuse cytoplasmic and nuclear staining, in line with Peters et al.. The cytoplasmic distribution is visible for all p97 variants. However, cells with high expression of E578Q or EQEQ showed a less diffuse distribution of p97, and puncta, positive for both FLAG and p97 were identified, suggesting that the p97 variants get integrated into p97 complexes.

The specificity of the p97 antibody was evaluated by immunofluoroscence microscopy and p97 KO cell pools were compared to control cell pools (Figure 20 A and B). The cell pools were generated by CRISPR/Cas9-mediated gene editing and cells were selected for 4 days only. p97 is essential for HeLa and p97 KO cells do not survive long, whereas the surviving cells maintain low expression levels of p97. Nevertheless, most of the signal in the cytoplasm and nucleus was lost in p97 KO cell pools, demonstrating the specificity of the p97 antibody.

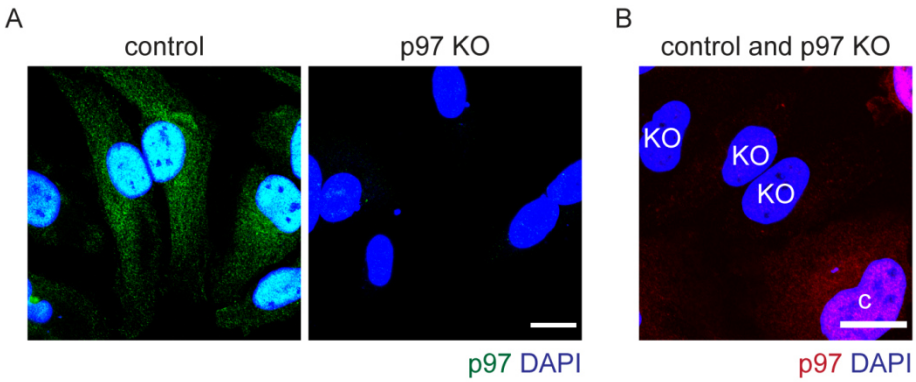

Figure 20: The p97 antibody is specific for p97. p97 KO cell pools and control cell pools were used to detect endogenous p97 with confocal immunofluoroscence microscopy (Antibody VCP #2). (A) p97 (green) in control cells and p97 KO cells. (B) Control cell pools and p97 KO cell pools were seeded together and expression of p97 (red) was determined. Scale bar, 20 µm.

The generated cell pools were induced with doxycycline to express the p97 variants, and a FLAG-IP was performed in the absence of crosslinker (Figure 21). Importantly, a co-immunoprecipitation of MYOF was observed for the p97 substrate-trapping mutants E578Q and EQEQ. In addition, the interaction of p97 with its cofactor PLAA, which was lost during conventional p97 immunoprecipitation but was identified upon addition of crosslinker (Figure 14), was also stabilized by the expression of E578Q and EQEQ (Figure 21), consistent with previous data (Ritz et al., 2011). UBXD1 was shown to bind stably to p97 without crosslinking (Figure 13 and Figure 14), but the interaction is enhanced in the presence of E578Q and EQEQ (Figure 21). This experiment confirmed the interaction of p97 and MYOF in the absence of crosslinker, excluding that it is a crosslinking artefact.

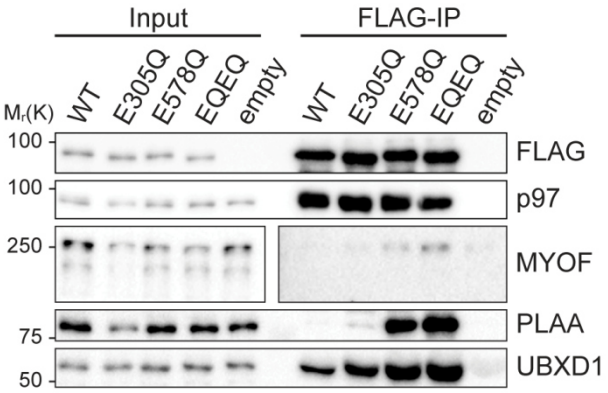

Figure 21: p97 trapping mutants stabilize the interaction with MYOF in the absence of crosslinker. The indicated p97 variants were induced for 20 h with doxycycline and lysates were subjected to anti-FLAG immunoprecipitation. Indicated proteins were detected by western blot.

In order to determine if the interaction between p97 and MYOF can also be observed in other cell lines, the lung cancer cell line A549, which has higher MYOF expression levels (ProteomicsDB: median protein expression: Intensity 6.12; The Human Protein Atlas: RNA expression: nTPM: 206.3), was compared to HeLa cells (ProteomicsDB: median protein expression: Intensity 5.71; The Human Protein Atlas: RNA expression: nTPM: 80.8). The cells were treated with the crosslinker and MYOF was immunoprecipitated (Figure 22). The interaction was confirmed for HeLa and A549, even though the ratio of MYOF interacting with p97 is lower in A549 compared to HeLa cells.

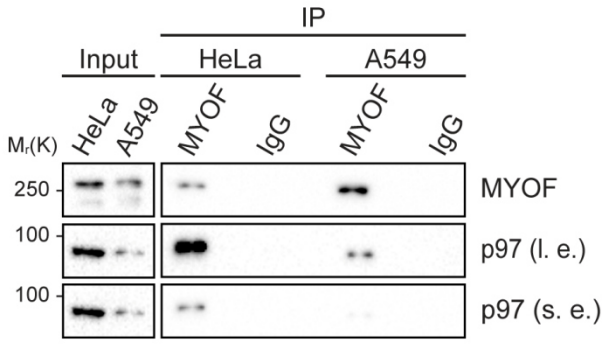

Figure 22: Interaction between endogenous MYOF and p97 in HeLa and A549. HeLa and A549 cells were subjected to crosslinking using DSP (30 min, RT). Immunoprecipitation of endogenous MYOF was performed. Indicated proteins were detected by western blot.

Moreover, HEK293T cells (HEK293 ProteomicsDB: median protein expression: -; The Human Protein Atlas: RNA expression: nTPM: 0.9) were transfected with a plasmid encoding MYOF-HA, crosslinked, and anti-HA, anti-MYOF, or anti-p97 immunoprecipitations were performed (Figure 23), confirming

the interaction of p97 and MYOF for all conditions. Taken together, these experiments confirmed MYOF as a novel interactor of p97.

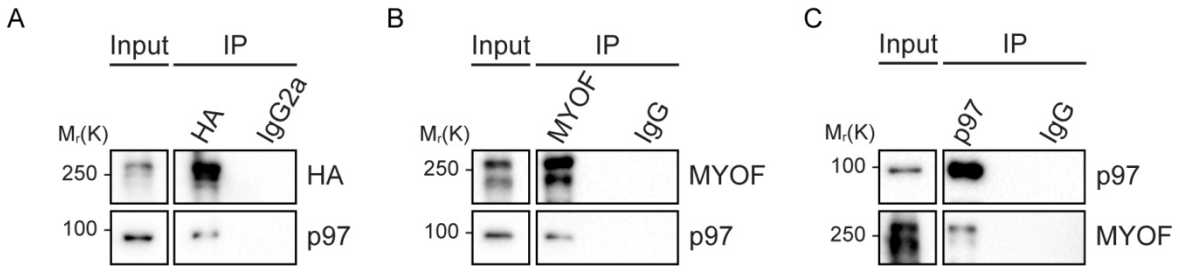

Figure 23: Ectopically expressed MYOF-HA interacts with p97 in HEK293T cells. HEK293T cells were transfected with a plasmid encoding MYOF-HA. Cells were crosslinked with DSP (30 min RT). Lysates were subjected to (A) anti-HA, (B) anti-MYOF and (C) anti-p97 immunoprecipitation (IP). Indicated proteins were detected by western blot.

The ferlin family member MYOF has a molecular weight of 230 kDa and is expressed in different splicing variants (Peulen et al., 2019). It contains seven C2 domains, implicated in interacting with phospholipids and proteins, as well as a DysF domain, and FerI, FerA and FerB domains which are all located in the cytoplasm (Figure 24), and a carboxy-terminal single-pass transmembrane domain (Shumer, 2017; Bulankina & Thoms, 2020). MYOF localizes to the plasma membrane, to vesicles in the perinuclear region and in the cytoplasm, and to the nucleus (Davis et al., 2002; Redpath et al., 2016). Originally, MYOF was shown to be important for myoblast fusion during embryonic development, muscle regeneration and repair (Davis et al., 2002; Doherty et al., 2005; Demonbreun, et al., 2010). In addition, MYOF plays a role in various trafficking pathways such as endocytosis (Bernatchez et al., 2009), the endocytic recycling pathway (Doherty et al., 2008; Demonbreun et al., 2010) and in degradation via the endo-lysosomal pathway (Turtoi et al., 2013; Redpath et al., 2016). Moreover, MYOF was also reported to function in lysosome-mediated exocytosis (Miyatake et al., 2018) and involved in reducing membrane stress at lysosomal membranes (Gupta et al., 2021).

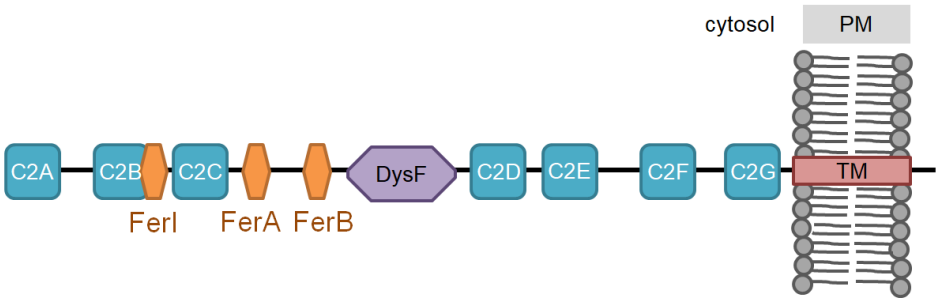

Figure 24: Schematic structure of MYOF. MYOF has seven C2 domains (cyan), FerI, FerA and FerB domains (orange), DysF (violet) domain, and a single C-terminal transmembrane domain (red). Database: SMART

3.2 Myoferlin localizes to the endocytic pathway

3.2.1 Identification of the myoferlin interactome

In order to get a better understanding of the function of MYOF, the MYOF interactome was determined by mass spectrometry. HeLa cells were crosslinked and IP of endogenous MYOF was performed (Figure 25). As expected, p97 was significantly enriched compared to the control IP, confirming the interaction of MYOF and p97. In addition, the p97 cofactor PLAA was identified as a significant interactor of MYOF.

The MYOF interactome was analyzed for proteins involved in the endocytic pathway. As expected, Rab7a, a marker for late endosomes, was identified (Redpath et al., 2016; Zhang et al., 2018). However, several proteins involved in endocytic recycling pathways were also significantly increased, including the Rab proteins Rab14 (Linford et al., 2012; Reed et al., 2013) and Rab11A/B (Ullrich et al., 1996; Ferro et al., 2021) and the effector proteins RUFY1 (Yamamoto et al., 2010) and Rab11-FIP1 (Peden et al., 2004), as well as EHD1 and EHD4 (Naslavsky & Caplan, 2011). In previous publications MYOF was shown to interact with EHD proteins like EHD2 and EHD1 (Doherty et al., 2008; Posey et al., 2011), confirming this finding. In addition, SNX3 and VSP26A, involved in retromer-mediated recycling, and the transferrin receptor CD71 were identified, consistent with the role of MYOF in endocytic trafficking and in particular in endocytic recycling.

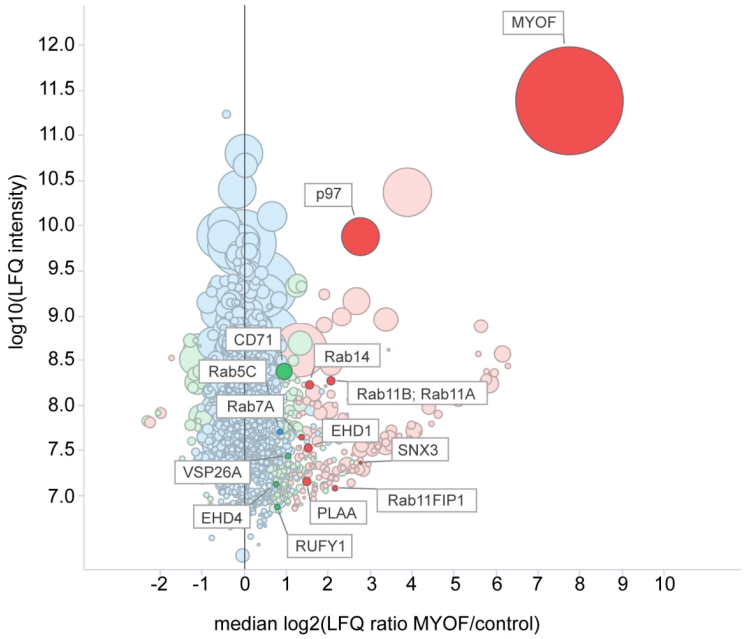

Figure 25: Mass spectrometry analysis for MYOF binding proteins. Identification of proteins interacting with MYOF by co-immunoprecipitation and mass spectrometry (see 7.3). Median values calculated from triplicate experiments were plotted. MYOF, p97, PLAA and proteins involved in the endocytic pathway are labeled.

3.2.2 Co-localization of myoferlin with various markers of the endocytic pathway

Several proteins involved in the endocytic pathway were identified (Figure 25). To confirm the localization of MYOF to this pathway, co-localization of MYOF with various marker proteins of the endocytic pathway were tested by immunofluoroscence microscopy experiments (Figure 26-30).

The experiments were performed with HeLa and A549 cells and antibodies targeting different epitopes of MYOF were used (Figure 26 A). First, the specificity of the MYOF antibodies was confirmed. Both antibodies show a strong co-localization with each other (Figure 26 C), suggesting that they target the same structures. In addition, MYOF knockdown was performed and most MYOF signal was lost compared to the non-targeting control siRNA for HeLa and A549 cells, proving the specificity of the antibody (Figure 26 B). The distribution of MYOF was observed by immunofluoroscence microscopy from the top of the cells to the bottom. In line with previous reports (Davis et al., 2002; Redpath et al., 2016), MYOF localizes to the plasma membrane and to vesicles in the cytosol and perinuclear region in HeLa and A549 cells (Figure 26 C).

To test for localization of MYOF with EEs, plasmids encoding EGFP-Rab5WT or Rab5WT-pmRFP and the dominant active GFP-Rab5QL, which leads to enlarged EEs, were transfected. Strong co-localization of MYOF to Rab5-positive vesicles was observed for both cell lines (Figure 27 A and B). This result was confirmed by using an antibody targeting the early endosomal marker EEA1 (Figure 27 C), again confirming a previous report (Redpath et al., 2016).

Localization of MYOF to late endosomes was tested by transfection of a plasmid encoding pEGFP-Rab7-WT and co-localization with MYOF was observed (Figure 28 A), verifying the interaction identified by the mass spectrometry approach (Figure 25). Moreover, co-localization of MYOF with the late endosomal and lysosomal markers LAMP1 and CD63 was observed for both cell lines (Figure 28 B and C), proving that MYOF localizes to late endosomes and lysosomes as suggested (Redpath et al., 2016).

Even though co-localization of MYOF with markers of the endo-lysosomal pathway was confirmed, prominent co-localizations were also observed with the recycling endosome marker Rab11 (Figure 29 A). In addition, MYOF also showed a strong localization to endosomes positive for Rab14 (Figure 29 B). Rab14 localizes to EEs and TGN and is involved in recycling of cargo proteins such as CD71 (Yamamoto et al., 2010; Linford et al., 2012) and GLUT4 (Reed et al., 2013). In addition, strong co-localization with CD71 (Figure 30), a cargo of the recycling pathway, was observed.

Together, these experiments clearly reveal a localization of MYOF to the endocytic pathway for both tested cell lines. Available data of MYOF suggested a role in trafficking of receptors, for the endo-lysosomal pathway, but also for the recycling pathway (Doherty et al., 2008; Demonbreun et al., 2010; Turtoi et al., 2013; Redpath et al., 2016). The MYOF interactome gained by mass spectrometry (Figure 25) and the observed co-localization with markers for the endocytic pathway (Figure 26-30) supports trafficking of MYOF to the recycling and the degradation routes. It is still unclear how the sorting of MYOF for one of these pathways is regulated and which additional interactors of MYOF are involved in the sorting of MYOF and its cargo proteins for degradation or recycling.

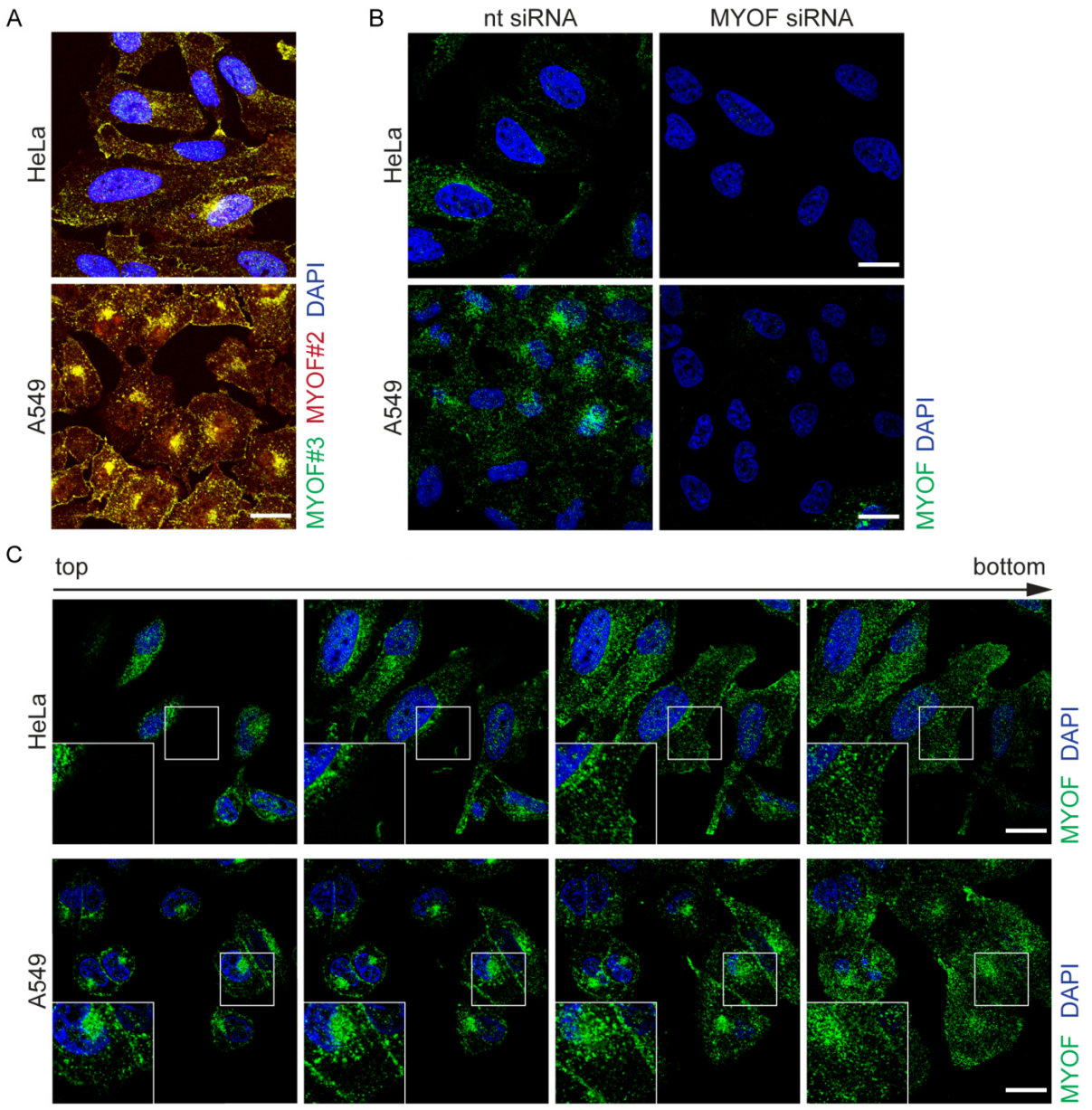

Figure 26: MYOF localizes to vesicles and the plasma membrane. Confocal immunofluoroscence microscopy was performed to visualize MYOF. (A) Two antibodies targeting different epitopes of MYOF were tested (MYOF #3, HPA014245 - green and MYOF #2, sc-376879 - red). (B) HeLa and A549 cells were transfected with siRNA (50 nM, 72 h) targeting MYOF and compared to cells transfected with the non-targeting (nt) control siRNA to confirm the specificity of MYOF #3, HPA014245 antibody. (C) Localization of MYOF in HeLa and A549 cells was observed from the top to the bottom of the cells and Z-stacks of 4 confocal planes were imaged. Scale bar, 20 µm.

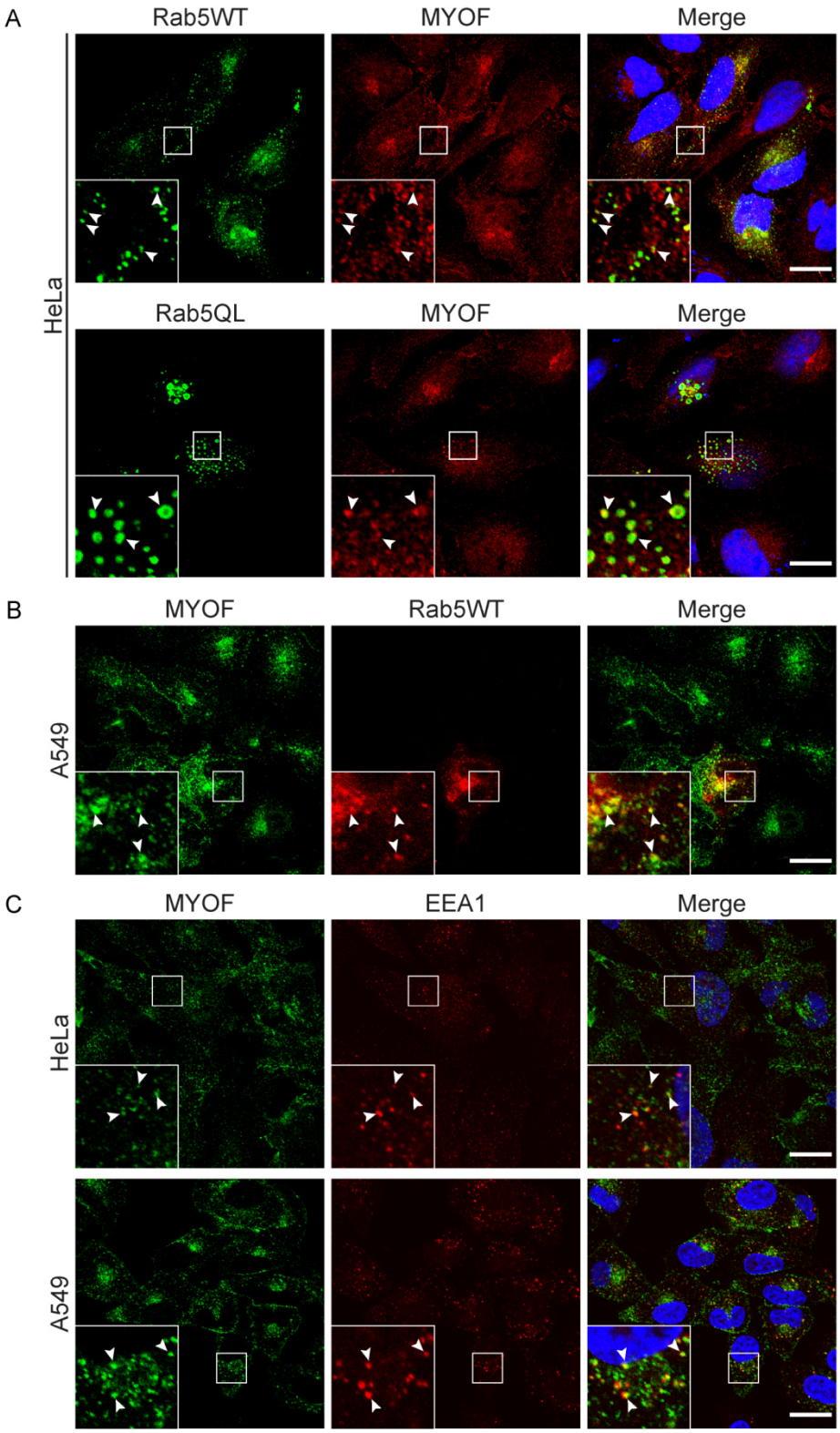

Figure 27: MYOF localizes to early endosomes. (A) HeLa cells were transfected with plasmids encoding EGFP-Rab5WT or GFP-Rab5CA (Q79L). Confocal microscopy was performed to visualize MYOF and GFP. (B) A549 cells were transfected with a plasmid encoding Rab5WT-pmRFP. Confocal microscopy was used to visualize RFP and MYOF. (C) Localization of endogenous EEA1 and MYOF in HeLa and A549 cells visualized by confocal microscopy. Scale bar, 20 µm.

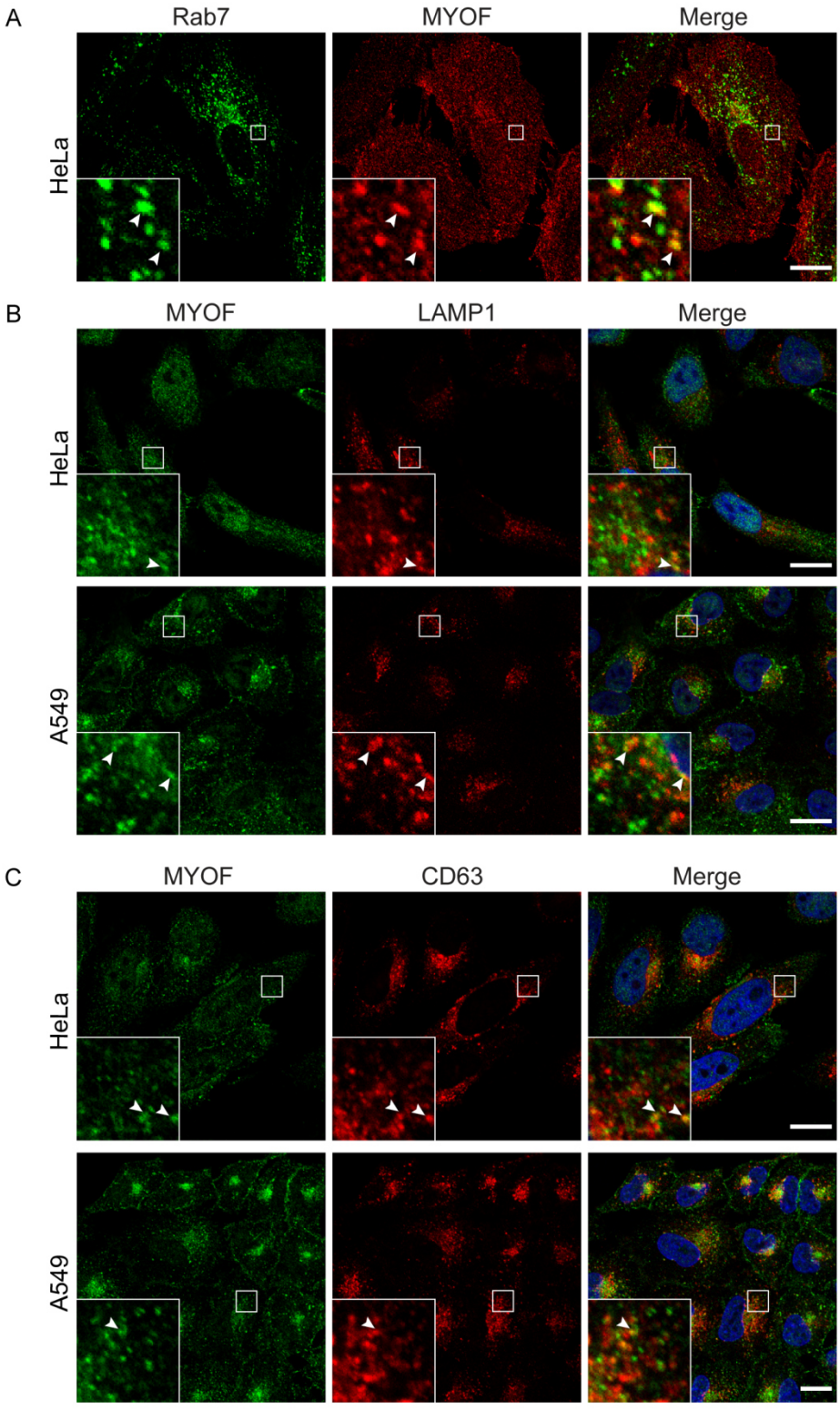

Figure 28: MYOF shows co-localization with late endosomal/lysosomal markers. (A) HeLa cells were transfected with a plasmid encoding pEGFP-Rab7-WT. Confocal microscopy was performed to visualize MYOF and GFP. (B) Confocal microscopy was performed to visualize the localization of endogenous MYOF and LAMP1 or (C) CD63. Scale bar, 20 µm.

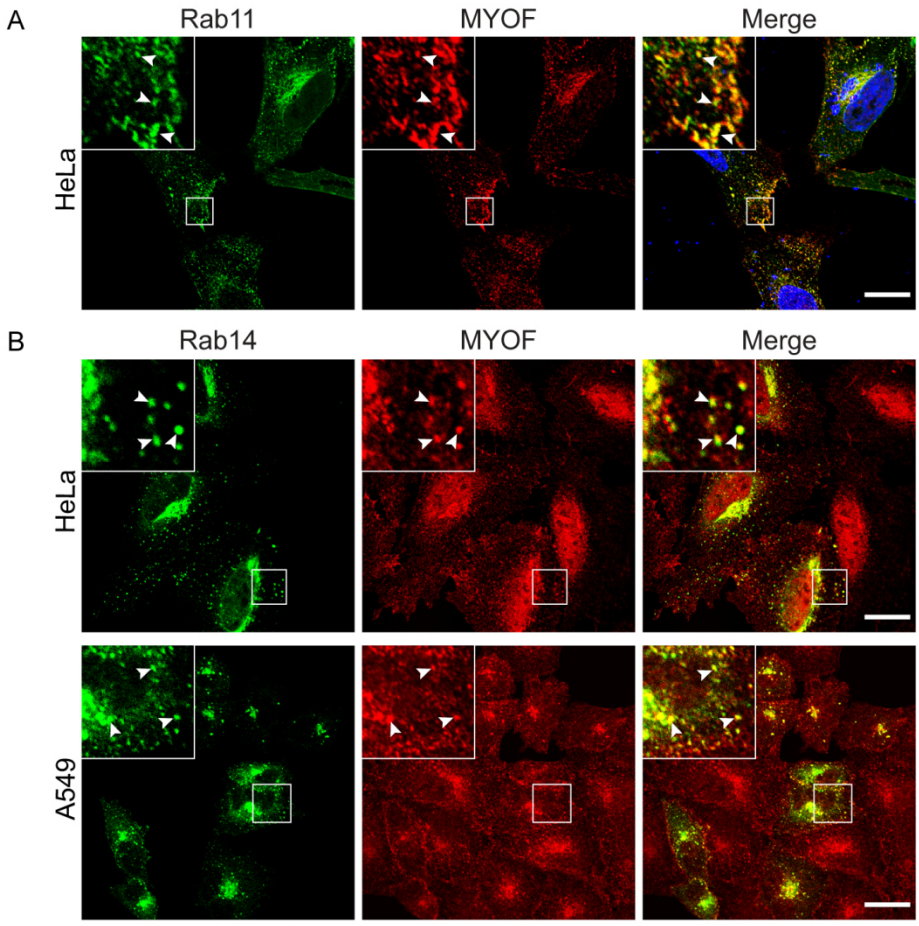

Figure 29: MYOF localizes to recycling endosomes. (A) HeLa cells were transfected with a plasmid encoding GFP-Rab11. Confocal microscopy was performed to visualize MYOF and GFP. (B) HeLa and A549 cells were transfected with a plasmid encoding pEGFP-Rab14. Confocal microscopy was used to visualize GFP and MYOF. Scale bar, 20 µm.

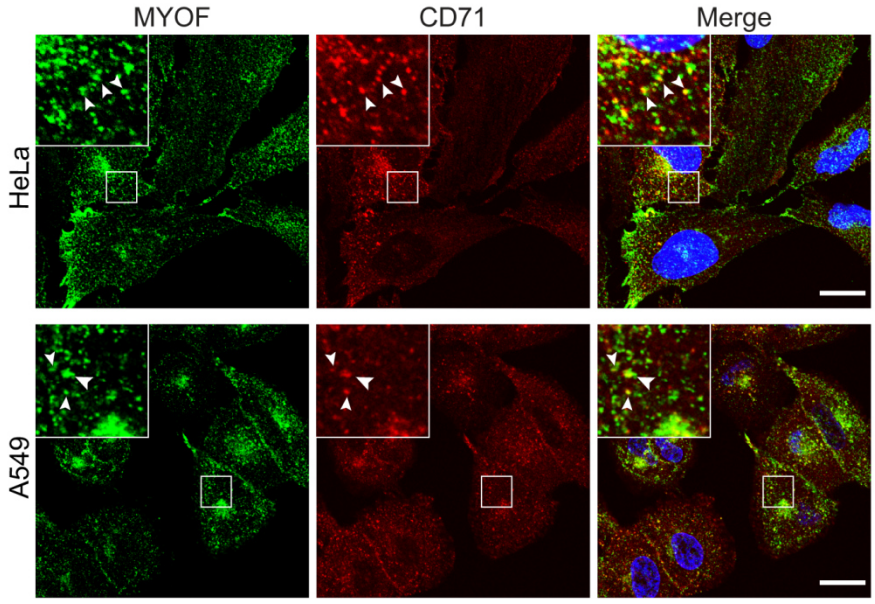

Figure 30: Co-localization of MYOF with transferrin receptor CD71. Localization of CD71 and MYOF in HeLa and A549 cells was visualized by confocal microscopy. Scale bar, 20 µm.

3.3 Role of p97 in the endocytic pathway

3.3.1 Partial co-localization of p97 and myoferlin

MYOF was identified as a novel interactor of p97 by reciprocal IP experiments. However, the function and the subcellular localization of this interaction were so far unknown. To investigate these open questions, the potential co-localization of MYOF with p97 was studied by immunofluoroscence microscopy. Since expression of the p97 trapping mutants (E578Q and EQEQ) stabilized its interaction with MYOF (Figure 21), co-localization of MYOF and p97 was investigated by using the pINDUCER20 cell lines expressing the different ATP hydrolysis-deficient FLAG-tagged variants of p97 (Figure 31).

As shown before (Figure 19), control cells (empty) and cells expressing p97 WT and E305Q displayed a mostly diffuse staining of p97, and no co-localization with MYOF could be observed. By contrast, cells with high expression of E578Q and EQEQ showed a number of distinct puncta positive for both, p97 and MYOF.

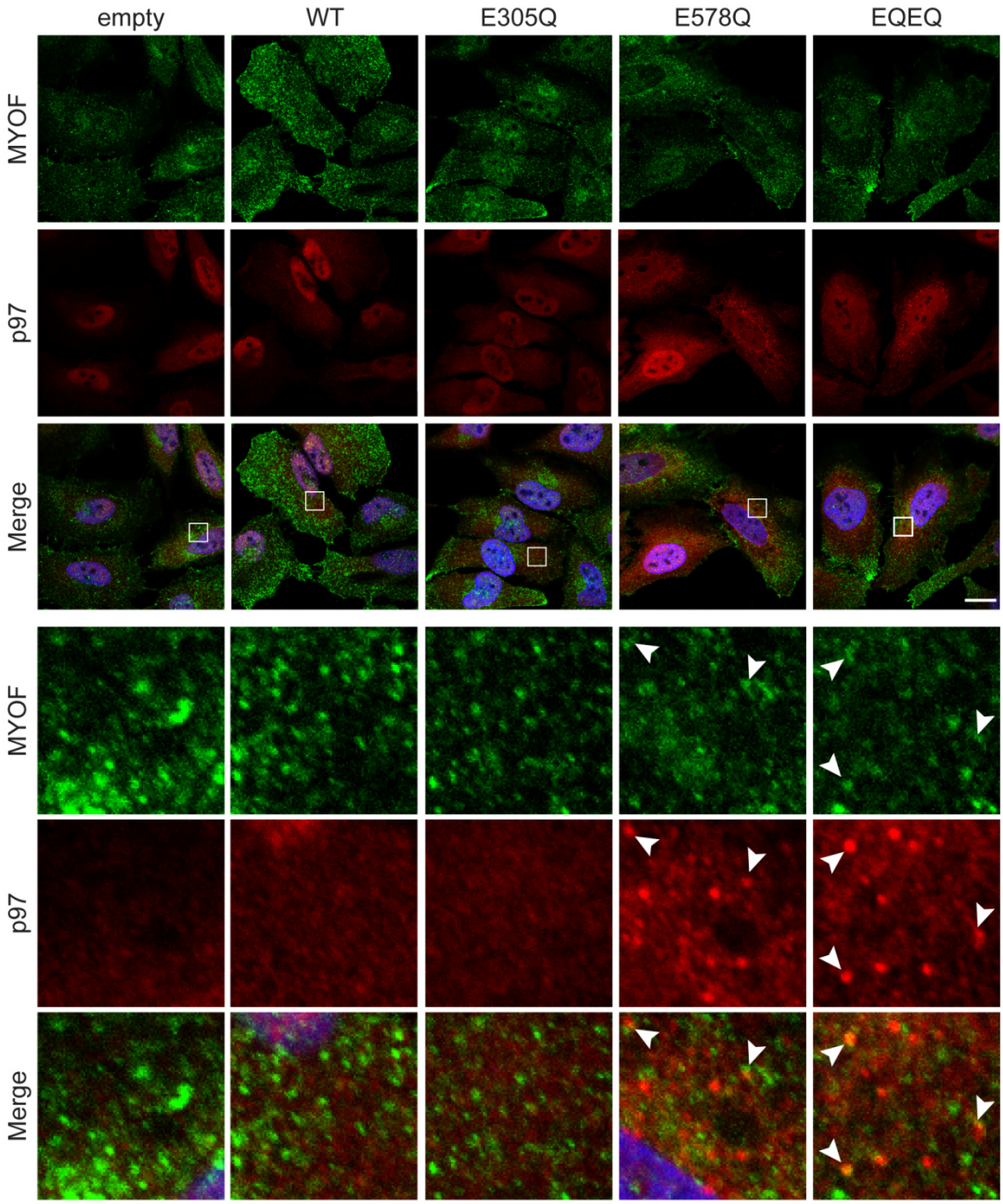

Figure 31: Increased co-localization of MYOF with p97 ATP hydrolysis-deficient mutants. Stable HeLa cell pools expressed Flag-tagged p97 mutants upon doxycycline (500 ng/ml; 22 h) induction. Endogenous MYOF and p97 were detected by confocal microscopy. Scale bar, 20 µm.

To confirm the observed co-localization of MYOF with p97, HeLa cells were treated with the p97 inhibitors NMS-873 and CB-5083 for 3 h, which resulted in the formation of puncta positive for p97 (Figure 32). In general, the distribution of p97 in inhibitor-treated cells was similar to cells expressing E578Q and EQEQ. Importantly, a partial co-localization of MYOF with some p97-positive puncta was observed in the presence of both inhibitors, confirming the result with the p97 trapping mutants (Figure 31). With these experiments, the interaction of MYOF and p97 was further validated, and co-localization at defined structures was shown.

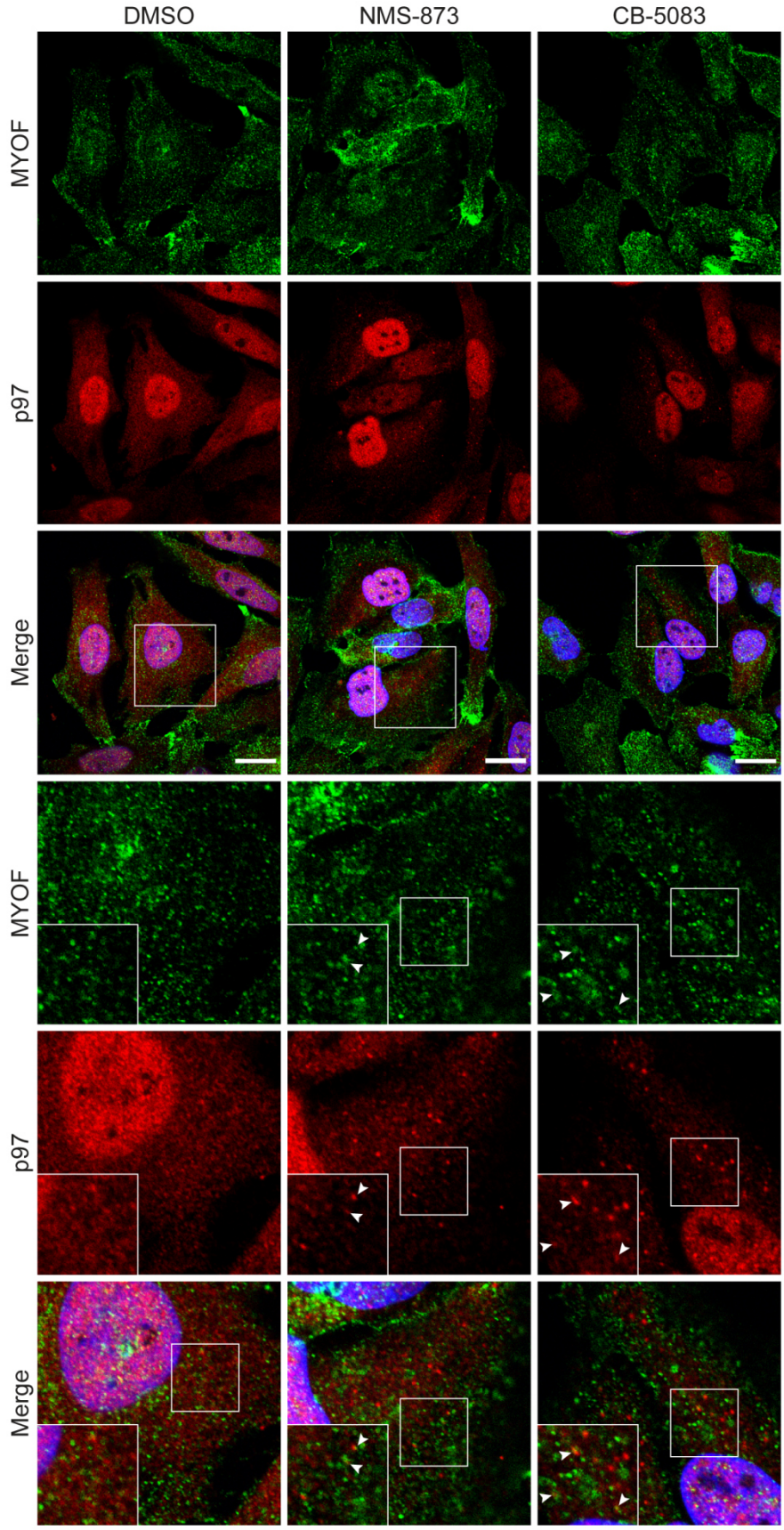

Figure 32: p97 inhibition reveals partial co-localization of MYOF and p97. HeLa cells were treated with DMSO, NMS-873, (10 µM), or CB-5083 (10 µM) for 3 h. Endogenous MYOF and p97 were detected by confocal microscopy. Scale bar, 20 µm.

3.3.2 p97 and myoferlin share interactors involved in the endocytic pathway

In order to determine at which subcellular structures MYOF and p97 may interact, the interactome of both proteins was compared and shared interactors were determined (Figure 33). Interestingly, several proteins involved in the endocytic pathway were found in both data sets, such as Rab7a, Rab14, and the transferrin receptor CD71 (Figure 33 A). The Rab proteins Rab5 and Rab11A/B were also identified, but were either not significantly enriched in both interactomes or only in one of them. In addition, the p97 cofactor PLAA, which has been shown to be involved in the endo-lysosomal pathway (Hall et al., 2017), was found to be significantly enriched in both interactomes. In total, 43 proteins were identified as shared interactors (Figure 33 B).

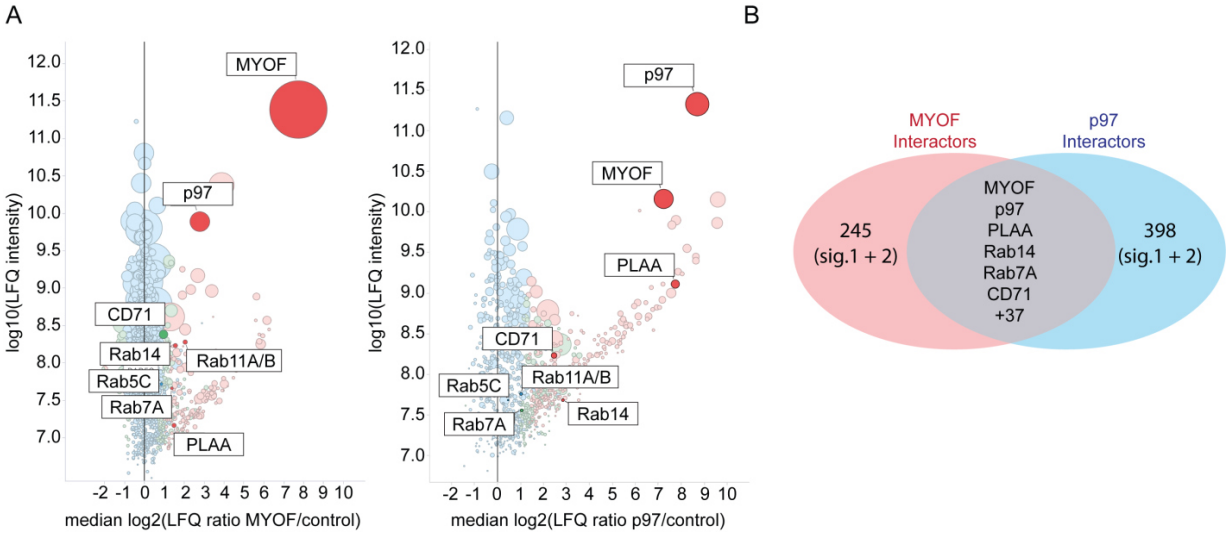

Figure 33: Comparison of p97 and MYOF interactome for proteins involved in the endocytic pathway. (A) Rab proteins (Rab5C, Rab7A, Rab14, and Rab11A/B), the transferrin receptor CD71 and the p97 cofactor PLAA were identified. (B) Venn diagram for identified MYOF (red) and p97 (blue) interactors with a significance of 1 and 2. In total, 43 proteins were identified as interactors for MYOF and p97 (violet) and selected proteins involved in the endocytic pathway are shown (see 7.4).

3.3.3 Localization of p97 to Rab14-positive endosomes

Rab14 was identified as a significant interactor of both p97 and MYOF (Figure 34). To test if p97 co-localizes with Rab14, HeLa cells were transfected with a plasmid encoding Rab14-GFP and treated with p97 inhibitors. Several p97-positive puncta visible upon inhibition of p97 indeed showed a partial co-localization with Rab14-positive vesicles. This confirmed the interaction of p97 with Rab14 and the localization of p97 to vesicles of the endocytic pathway.

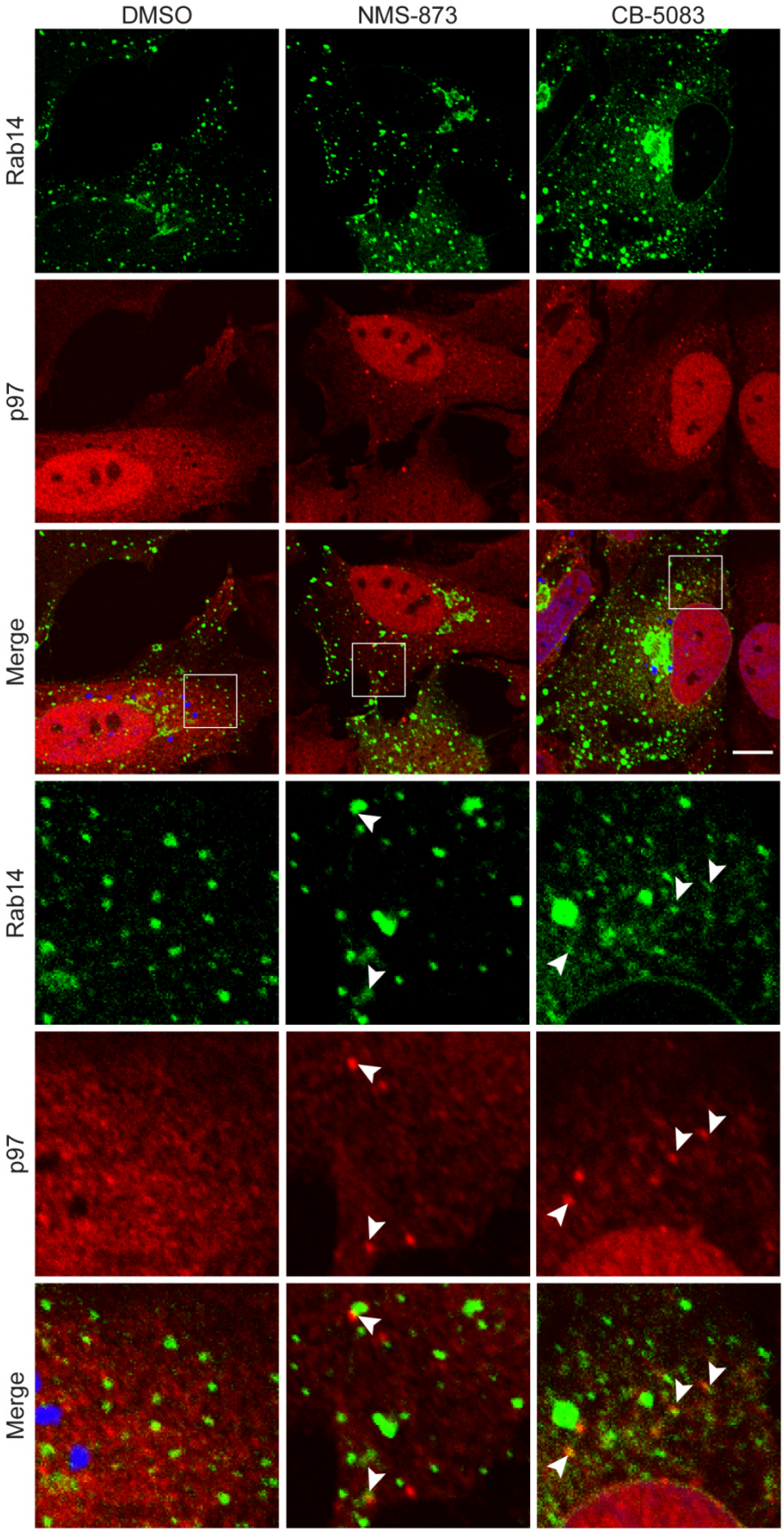

Figure 34: p97 inhibition reveals partial co-localization of p97 and pEGFP-Rab14. HeLa cells were transfected with a plasmid encoding pEGFP-Rab14. After 20 h the cells were treated with DMSO, NMS-873 (10 µM), or CB-5083 (10 µM) for 3 h. Confocal microscopy was used to detect GFP and p97. Scale bar, 10 µm.

3.3.4 The interaction of p97 and myoferlin depends on PLAA and UBXD1

The p97 cofactor PLAA was identified as a shared interactor of MYOF and p97 (Figure 33). In addition, expression of p97 E578Q and EQEQ stabilized the interaction of p97 with both, PLAA and MYOF (Figure 21). To test if the interaction between p97 and MYOF depends on PLAA, PLAA KO HeLa cell pools were generated by CRISPR/Cas9-mediated gene editing. In p97 immunoprecipitations, PLAA KO cells showed reduced co-immunoprecipitation levels of MYOF compared to control cells, hinting to an involvement of PLAA in the interaction (Figure 35 A). The experiment was performed two times and the intensity of the co-immunoprecipitation levels of MYOF was normalized to the band intensity of p97 and then normalized to the control immunoprecipitation (Figure 35 B). The first experiment showed a 28% reduction for MYOF in the absence of PLAA. The quantification of this western blot was difficult due to the running behavior of the bands (Figure 35 A) and the re-run of the same samples revealed a reduction of 58% for MYOF. The second experiment confirmed the finding and co-immunoprecipitation levels of MYOF in PLAA KO showed a reduction of 77% compared to the control.

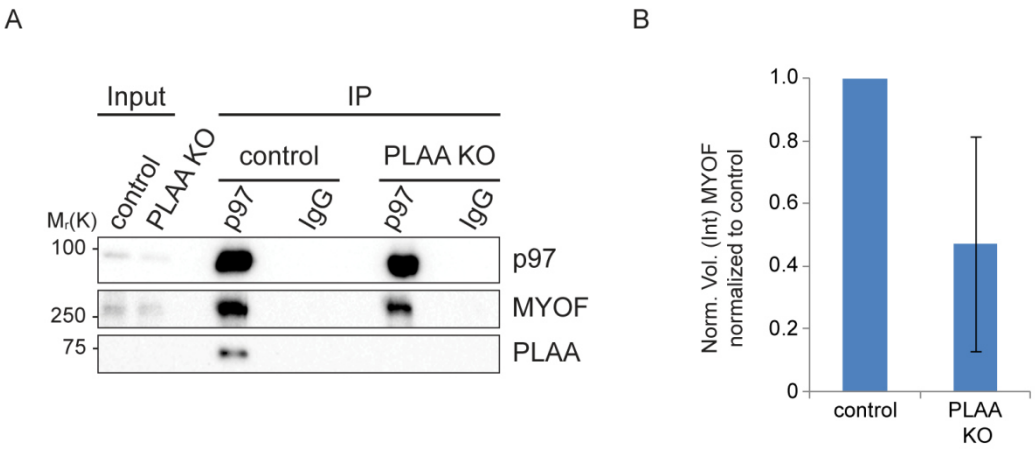

Figure 35: The interaction of p97 with MYOF depends on p97 cofactor PLAA. (A) PLAA KO HeLa cell pools and control cells were crosslinked with DSP (30 min, RT). Immunoprecipitation of endogenous p97 was performed and indicated proteins were detected by western blot. (B) Quantification of MYOF levels: MYOF volume intensity was normalized to the amount of immunoprecipitated p97 and then normalized to the control. Shown are mean ± SD, n=2.

PLAA was shown to play a role in the trafficking of cargo proteins to ILVs leading to their degradation via the endo-lysosomal pathway (Hall et al., 2017). Therefore, protein levels of MYOF and CD71, which is normally not targeted for degradation via the endo-lysosomal pathway, were analyzed in the PLAA KO and control cell pools (Figure 36). A loss of PLAA did not change the protein levels of CD71 and MYOF, suggesting that these proteins were not affected by a trafficking defect to the endo-

lysosomal pathway and that the interaction with PLAA is not related to its function in the endo-lysosomal pathway.

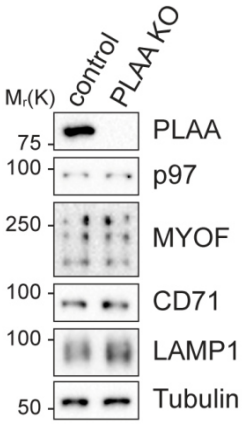

Figure 36: Protein levels in PLAA KO and control HeLa. PLAA KO HeLa and control cells were lysed. Indicated proteins were detected by western blot.

PLAA has been shown to function together with UBXD1 and YOD1 in the p97-dependent removal of K48-linked ubiquitin conjugates from damaged lysosomes to support their removal via lysophagy (Papadopoulos et al., 2017). In addition, a role of UBXD1 in endo-lysosomal sorting was published (Ritz et al., 2011). To test if UBXD1 also plays a role in the interaction of p97 with MYOF, UBXD1 KO HeLa cells from single clones (Figure 37) and UBXD1 KO cell pools generated by CRISPR/Cas9 mediated gene editing (Figure 38) were used. p97 immunoprecipitation showed that a loss of UBXD1 reduced the level of interaction of p97 with MYOF. Together, these experiments reveal that the interaction between p97 and MYOF depends on the cofactors PLAA and UBXD1.

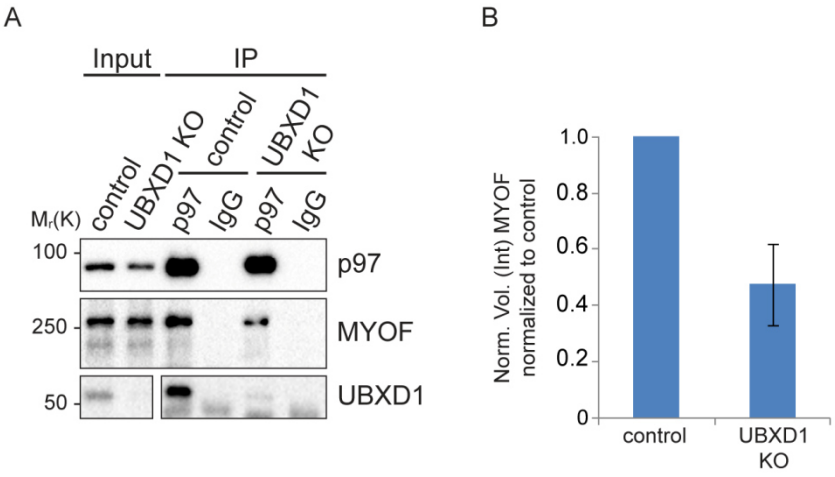

Figure 37: Interaction of p97 with MYOF depends on the p97 cofactor UBXD1. (A) Single clone UBXD1 KO HeLa cells and control cells were crosslinked with DSP (30 min, RT). Immunoprecipitation of endogenous p97 was performed and indicated proteins were detected by western blot. (B) Quantification of MYOF levels: MYOF volume intensity was normalized to immunoprecipitated p97 and then normalized to the control. Shown are mean ± SD, n=3.

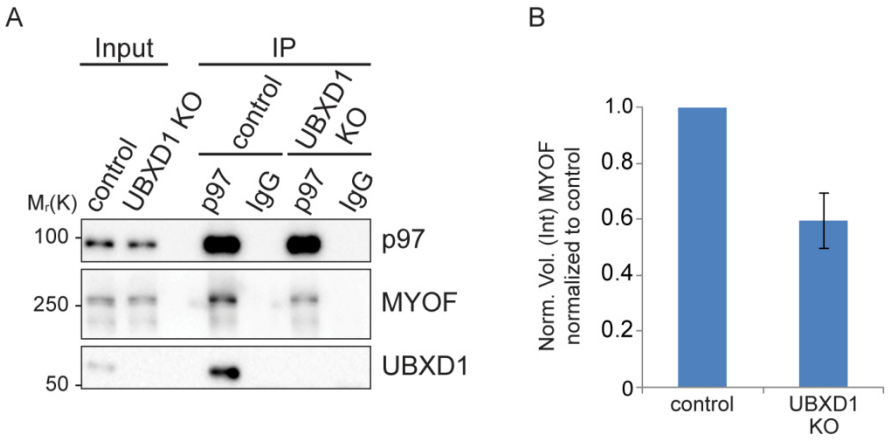

Figure 38: Interaction of p97 with MYOF depends on the p97 cofactor UBXD1. (A) UBXD1 KO HeLa cells and control cells were crosslinked with DSP (30 min, RT). Immunoprecipitation of endogenous p97 was performed and indicated proteins were detected by western blot. (B) Quantification of MYOF levels: MYOF volume intensity was normalized to immunoprecipitated p97 and then normalized to the control. Shown are mean ± SD, n=2.

3.3.5 PLAA co-localizes with Rab5- and Rab14-positive endosomes and with myoferlin

Interaction between MYOF and p97 was shown to depend on the cofactor PLAA (Figure 35). Therefore, it was investigated if PLAA and MYOF localized to the endocytic pathway and to compartments positive for Rab proteins identified in the shared MYOF and p97 interactome (Figure 33). As it was recently proposed that PLAA functions in internalization of cargo in ILVs (Hall et al., 2017), HeLa cells were transfected with a plasmid encoding Rab5QL-pmRFP and the localization of PLAA was determined using two different rabbit polyclonal antibodies: PLAA#1 raised against residues 397-493 and PLAA#2 raised against residues 495-584 (Figure 39 A).

With both antibodies, PLAA was visible as a diffuse signal in the cytoplasm and the nucleus. In addition, an accumulation of PLAA could be observed on the surface of Rab5QL-positive vesicles. This co-localization could be confirmed with both antibodies and was largely lost in PLAA KO cells, indicating that PLAA indeed localizes to the endocytic pathway at Rab5QL-positive vesicles. PLAA localization to Rab5QL-RFP positive vesicles was further visualized by structured illumination microscopy. PLAA accumulates mostly on the surface of Rab5QL-positive vesicles (Figure 39 B).

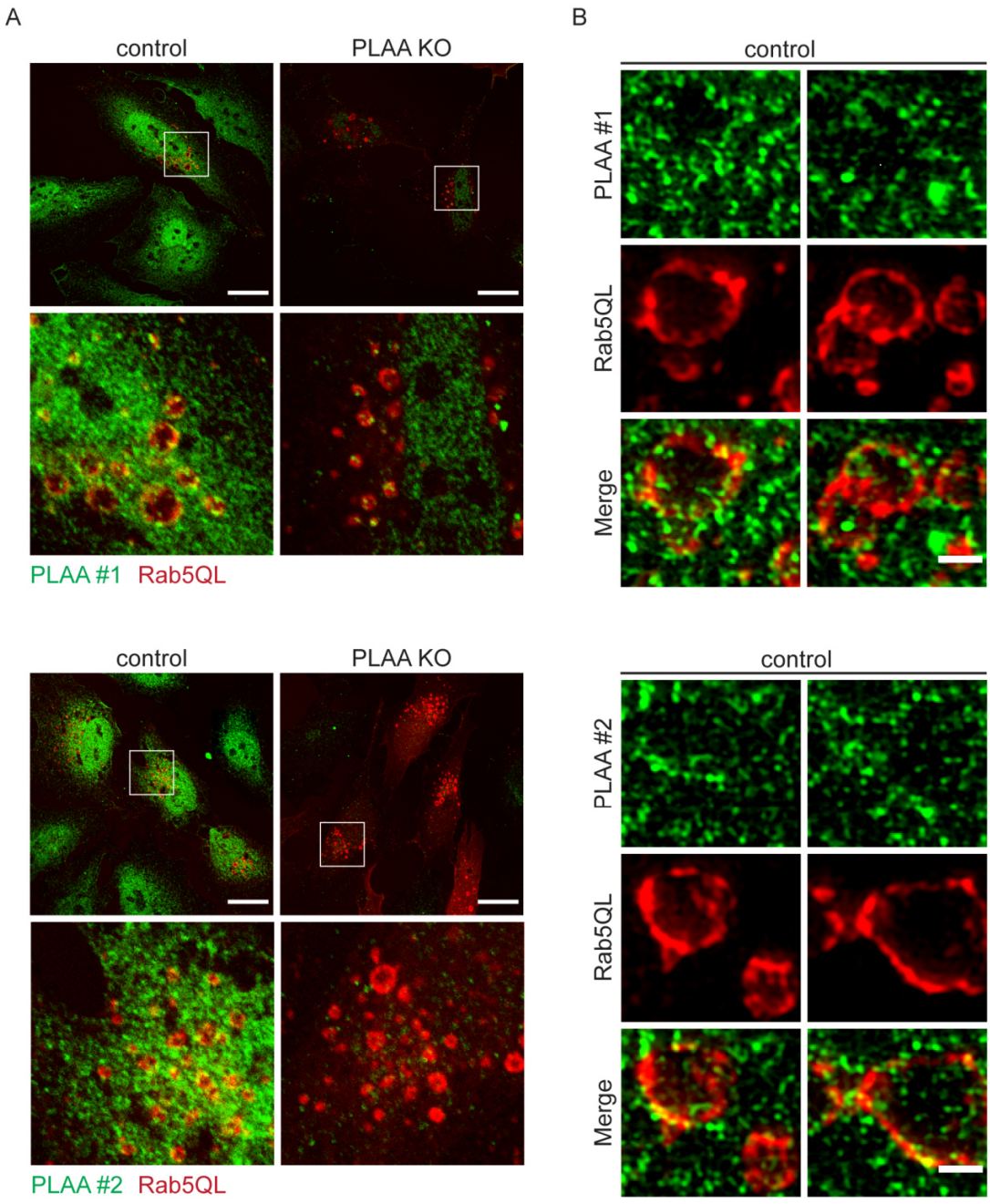

Figure 39: PLAA localizes to Rab5-positive endosomes. (A) PLAA KO HeLa and control cells were transfected with a plasmid encoding Rab5QL-pmRFP. Confocal microscopy was performed to visualize PLAA and RFP. Two different antibodies were tested (PLAA#1: HPA020996 and PLAA#2: HPA020994). Scale bar, 20 µm. (B) Control HeLa cells were transfected with a plasmid encoding Rab5QL-pmRFP. SIM microscopy was used to visualize RFP and PLAA. Scale bar, 1 µm.

Expression of Rab5QL leads to abnormal endosomal structures, because in the presence of the dominant active form of Rab5, Rab7 is recruited to endosomes, but Rab5 fails to dissociate from the endosomes. This results in enlarged vesicles, which accumulate early endosomal markers like EEA1 or transferrin as well as late endosomal markers like LAMP1, leading to perturbed lysosome biogenesis (Rosenfeld et al., 2001; Rink et al., 2005).

Therefore, HeLa cells were transfected with plasmids encoding Rab5WT-pmRFP, which does not lead to these abnormal endosomal structures, (Rosenfeld et al., 2001) and Rab5QL-pmRFP, to validate the previous finding (Figure 39), and to confirm co-localization of PLAA and MYOF with early endosomes (Figure 40 A). In addition, co-localization of PLAA and MYOF with GFP-RAB14 was tested by immunofluoroscence microscopy (Figure 40 B). Indeed, co-localization of PLAA and MYOF with endosomes positive for Rab5 and Rab14 could be observed.

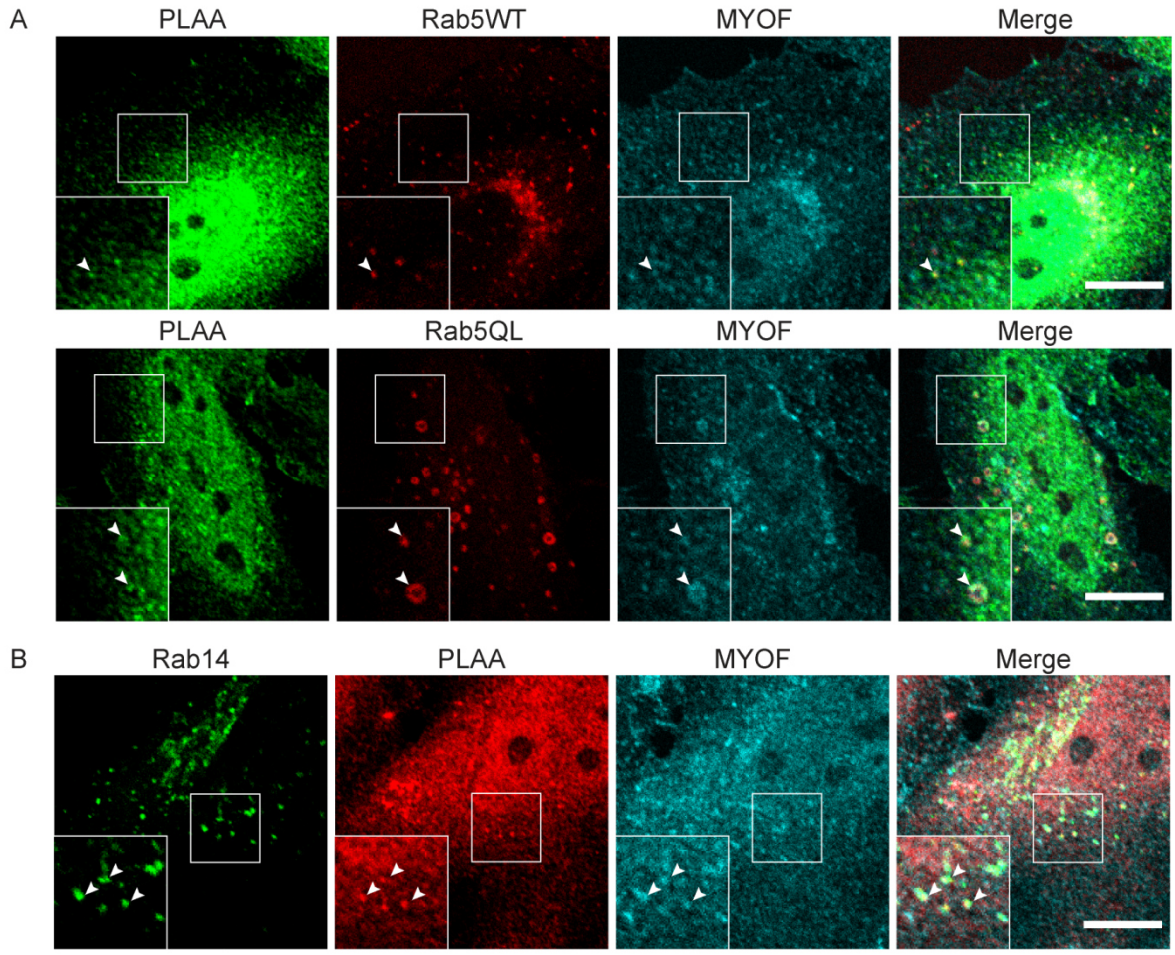

Figure 40: Co-localization of PLAA and MYOF with Rab14- and Rab5-positive endosomes. (A) HeLa cells were transfected with plasmids encoding Rab5WT-pmRFP and Rab5QL-pmRFP. Confocal microscopy was performed to visualize PLAA, RFP and MYOF. (B) HeLa cells were transfected with a plasmid encoding pEGFP-Rab14. PLAA, GFP and MYOF were visualized by confocal microscopy. Scale bar, 10 µm.

3.3.6 p97 promotes transferrin recycling

The localization of MYOF, PLAA and p97 to early and recycling endosomes raised the possibility that p97 is involved in the recycling pathway. In addition, Rab14, known to be involved in recycling of transferrin (Yamamoto et al., 2010; Linford et al., 2012), and transferrin receptor CD71 were identified as interactors for both MYOF and p97 (Figure 33).

To that end, transferrin recycling assays were performed with fluorescent labeled transferrin, which is commonly used as marker to observe the recycling of endocytic cargos. Therefore, HeLa cells were labeled with transferrin conjugated with Alexa Fluor™ 594 and analyzed by microscopy. During labeling, transferrin is taken up by the cell via endocytosis and is trafficked to early endosomes. Then, unbound transferrin was washed off and the cells were chased with full media for different time periods. At 0 min, endosomes positive for transferrin were visible and distributed throughout the cell (Figure 41 A). After 10 min, less transferrin-positive vesicles were visible and the vesicles localized closer to the perinuclear region. After 30 min, most signal for transferrin in the cells disappeared due its recycling and release to the media. To quantify these results, cells were harvested and prepared for FACS analysis of the fluorescent transferrin signal. This quantitative analysis showed that the transferrin signal is reduced after 10 min and drops quickly until 30 min. After 30 min only a slight decrease in the signal can be observed (Figure 41 B and C).

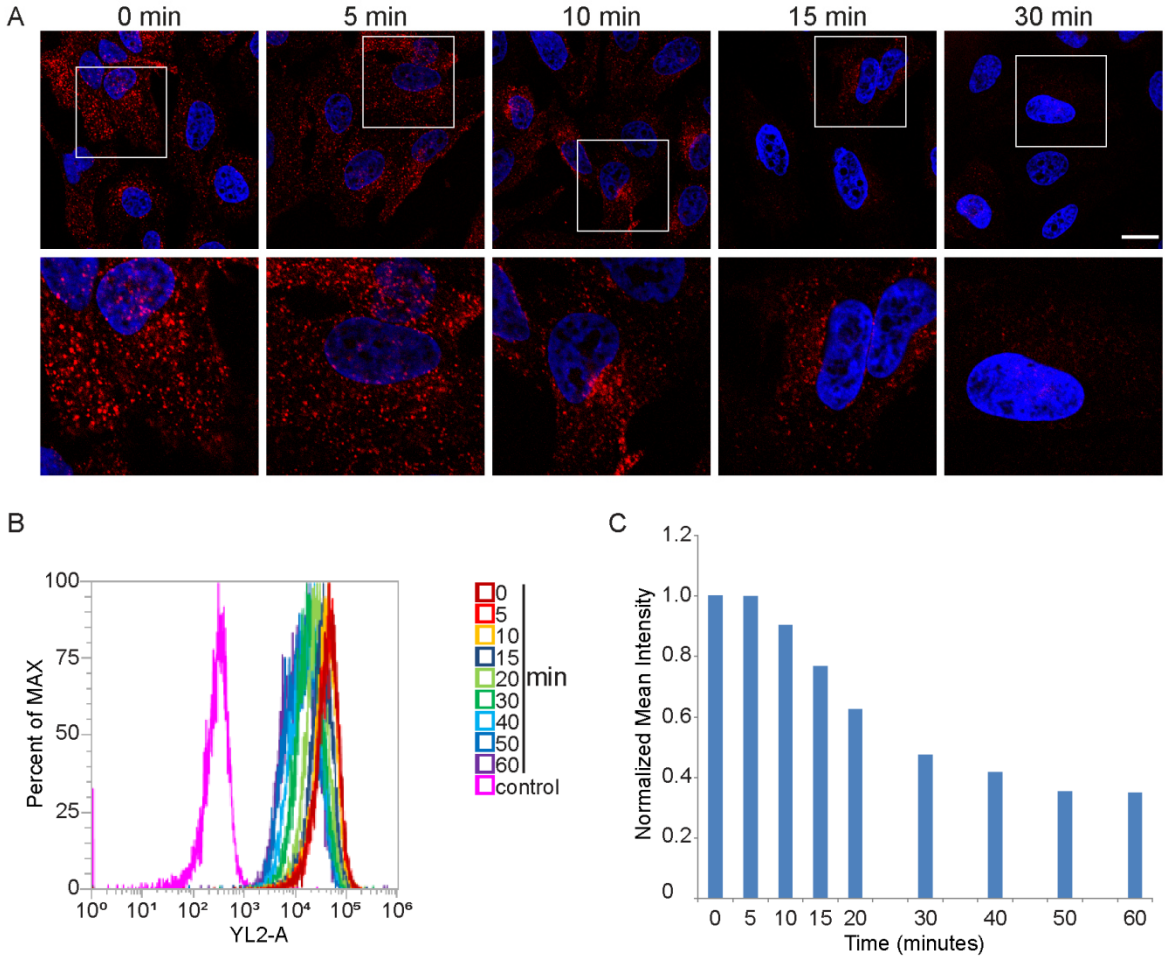

Figure 41: Recycling of transferrin in HeLa. HeLa cells were labeled with transferrin. (A) Transferrin was chased for 0, 5, 10, 15, and 30 min and confocal microscopy was used to visualize the distribution of transferrin (red) during the chase experiment. (B) HeLa cells were labeled with transferrin and chased for 0, 5, 10, 15, 20, 30, 40, 50, and 60 min and the fluorescence signal of labeled transferrin was measured using FACS. Overlay of the chase for the different time points. (C) Mean intensity of the transferrin signal normalized to time point 0 min. Scale bar, 20 µm.

In order to confirm the localization of transferrin to the recycling pathway, HeLa cells were labeled with transferrin as described and co-localization with several marker proteins was tested by immunofluoroscence microscopy. The internalized transferrin showed co-localization with CD71 and with Rab5 (Figure 42 A and B), but only little co-localization with the late endosomal and lysosomal marker LAMP1 (Figure 42 C), suggesting that most transferrin is recycled to the PM.

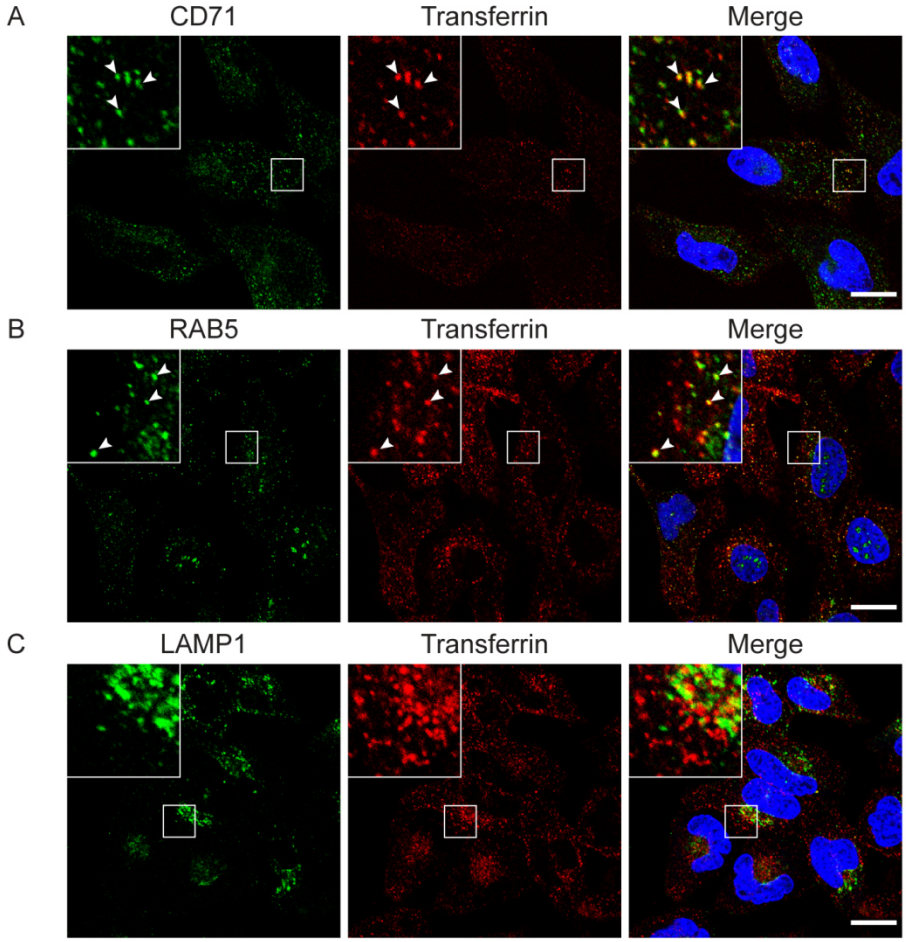

Figure 42: Co-localization of transferrin to CD71 and endocytic markers. (A) HeLa cells were labeled with transferrin on ice and chased for 5 min at 37°C. Confocal microscopy was performed to visualize transferrin and CD71. (B) HeLa cells were labeled for 5 min at 37°C. Localization of transferrin and Rab5 was determined by using confocal microscopy. (C) HeLa cells were labeled with transferrin for 30 min at 37°C and localization of LAMP1 and transferrin was determined. Scale bar, 20 µm.

Co-localization of transferrin and CD71 with Rab14 and Rab11, and trafficking via Rab14- and Rab11-positive endosomes was shown previously (Ullrich et al., 1996; Junutula et al., 2004). To confirm these findings, the transferrin chase experiments were performed with HeLa cells transfected with plasmids for GFP-Rab11 or pEGFP-Rab14 (Figure 43 A and B). Both Rabs showed a strong co-localization with transferrin after 10 min. The amount of co-localization decreased for Rab14 at 20 min, while Rab11 still showed strong co-localization with transferrin. These experiments

confirmed that transferrin was internalized and recycled via Rab11 and Rab14-positive vesicles, as expected.

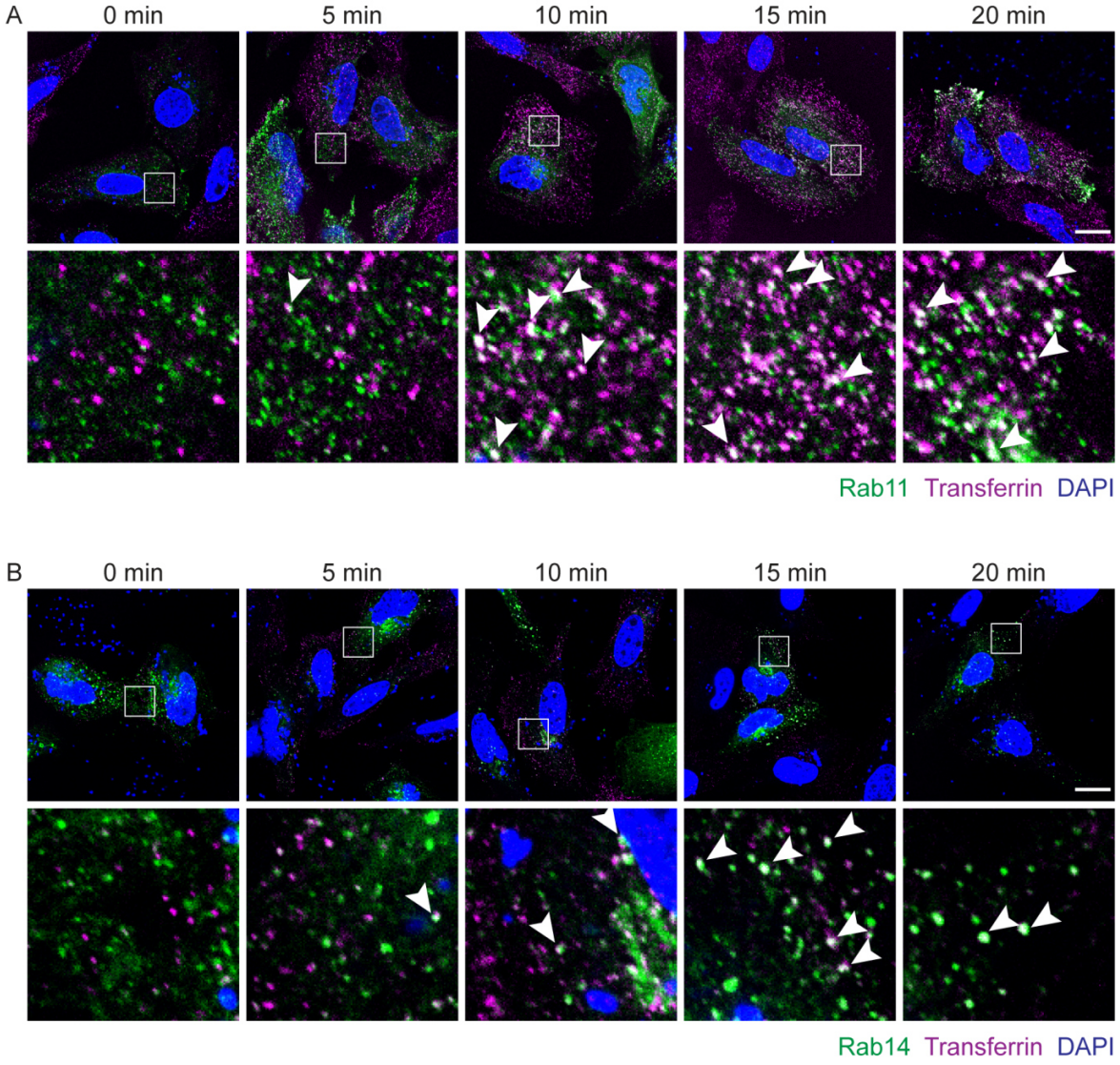

Figure 43: Co-localization of labeled transferrin with markers of recycling endosomes. (A) HeLa cells were transfected with plasmids encoding GFP-Rab11, labeled with transferrin and chased for 0, 5, 10, 15, and 20 min. Co-localization of GFP-Rab11 and transferrin was visualized by confocal microscopy. (B) HeLa cells transfected with plasmids encoding pEGFP-Rab14, labeled with transferrin and chased for 0, 5, 10, 15, and 20 min. Co-localization of pEGFP-Rab14 and transferrin was visualized by confocal microscopy. Scale bar, 20 µm.

Next, it was tested if p97 has a function in the recycling of transferrin. First, HeLa cells with FLAG-tagged p97 variants (WT, E305Q, E578Q, EQEQ and negative control empty), generated by using the pINDUCER20 lentiviral system, were induced with doxycyline and then labeled with transferrin to analyze the recycling via FACS (Figure 44 A and B). A slight increase in the intensity of the transferrin signal could be observed for E578Q and EQEQ after about 20 min, suggesting a weak delay in recycling at best. However, the interpretation of these results is complicated by the fact that the

majority of cells in the pool showed only a low expression of the p97 variants that might mask defects in the few strongly expressing cells.

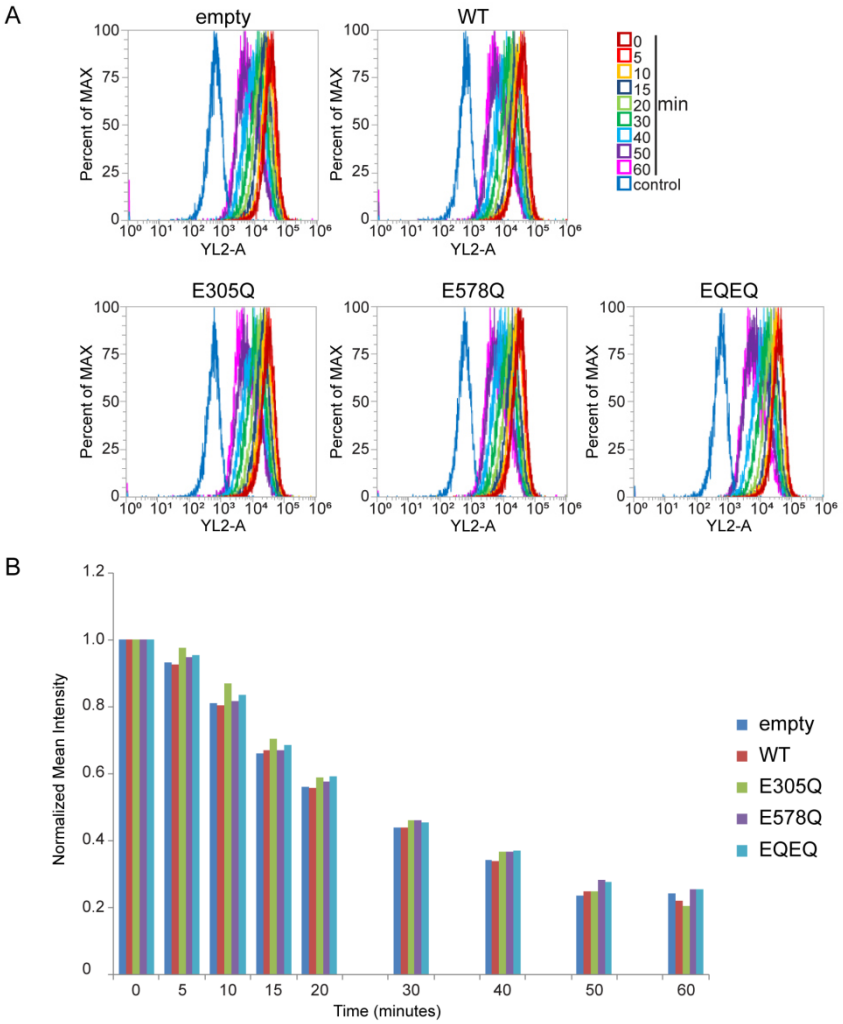

Figure 44: p97 ATP-hydrolysis deficient mutants show a weak delay in recycling of transferrin. Expression of p97 variants was induced for 20 h with doxycycline. Cells were labeled with transferrin and chased for 0, 5, 10, 15, 20, 30, 40, 50, and 60 min and the fluorescence signal of labeled transferrin was measured using FACS. (A) Overlay of the chase for the different p97 variants. (B) Mean intensity of the transferrin signal normalized to time point 0 min for all p97 variants.

To equally affect most analyzed cells, p97 inhibitors were used to test the role of p97 in transferrin recycling. HeLa cells were treated with the inhibitors, labeled with transferrin and then chased for the indicated time periods. The transferrin intensities determined by FACS revealed a significant delay in the recycling of transferrin upon NMS-873 treatment after 15 min chase. A slightly weaker delay in recycling could be observed for CB-5083 (Figure 45 A and B). CB-5083 showed significant differences at 10 min, 15 min and 60 min, but several time points slightly missed the threshold for significance of $p \leq 0.05$ (20 min: 0.054; 30 min: 0.061; 50 min: 0.055). These results could be confirmed by microscopy (Figure 45 C). Together, these results show that p97 promotes the endocytic recycling of receptor proteins like the transferrin receptor with transferrin.

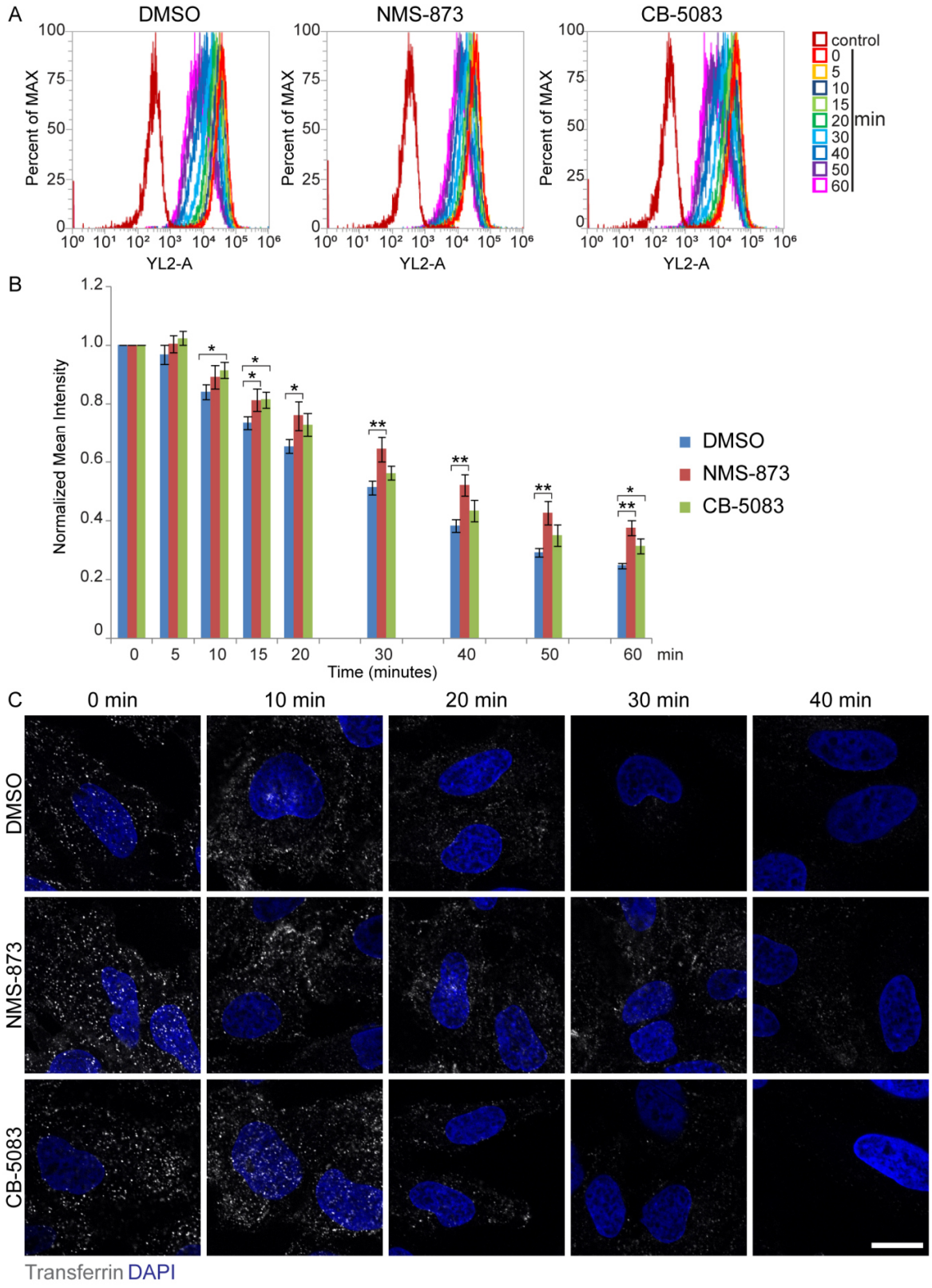

Figure 45: HeLa cells display delayed recycling of transferrin upon p97 inhibition. Cells were treated with DMSO, NMS-873 (10 µM), or CB-5083 (10 µM) for 4 h and then labeled with transferrin and chased for 0, 5, 10, 15, 20, 30, 40, 50, and 60 min. (A) The fluorescence signal of labeled transferrin was measured using FACS. Overlay of the chase. (B) Mean ± SD of the mean intensity of the transferrin signal from n=3 normalized to time point 0 min for all conditions. *t*-test; two tailed, unpaired, equal variance; *p≤0.05, **p≤0.01. (C) Confocal microscopy to visualize the distribution of transferrin (grey) during the chase experiment. Scale bar, 10 µm.

4 Discussion

In this work, MYOF, which plays a role in various membrane repair and trafficking events, was identified as a novel interactor of p97. MYOF localizes to the endocytic pathway, and co-localization of endogenous MYOF with Rab14 and Rab11, which are both involved in endosomal recycling pathways, was revealed. The interaction of p97 and MYOF was partially dependent on the p97 cofactors PLAA and UBXD1. Consistent with the presence of p97 and PLAA at early and recycling endosomes, the data suggest a role of p97 in endocytic recycling.

4.1 Identification of MYOF as novel p97 interactor by in-cell crosslinking

In this work, the interactome of p97 in HeLa cells was investigated. Therefore, an *in cellulo* crosslinking protocol was used to covalently link p97 interactors in their native environment and to prevent the loss of interactions during subsequent steps like lysis or immunoprecipitation. In contrast to other approaches to stabilize p97 interactions, such as expression of p97 trapping mutants or treatment with p97 inhibitors, which are likely to affect protein homeostasis due to prolonged interference with normal p97 function, the addition of crosslinker to cells stabilizes p97 interactions without directly affecting p97 functions. However, crosslinking has potential disadvantages, such as over-crosslinking, or the enrichment of indirect interactors. Therefore, this experimental setup requires different approaches to evaluate the identified interactors and to confirm them as novel interactors of p97.

First, it was tested if known p97 interactors can be stabilized in their interaction with p97 by the crosslinking approach. For this purpose, p97 cofactors were investigated and the number of cofactors detected with crosslinking was compared to cofactors identified in the absence of the crosslinker. Seven p97 cofactors were found without crosslinking (Figure 14). The addition of the crosslinker increased the amount of detected cofactors to 19, showing that p97 interactors are stabilized by this approach. Overall, 13 known or putative p97 cofactors could not be identified in the HeLa p97 interactome presented here (Figure 14 B). Potential reasons are low expression levels, such as for UBXN10, which is not expressed in HeLa cells, or a difficult identification by mass spectrometry due to technical reasons like the size of the protein or the availability of trypsin cleavage sites. Furthermore, several functions of p97 are known to be related to different stress responses. Therefore, some cofactor interactions with p97 might only occur under certain stress conditions to restore normal protein homeostasis. Examples include ZFAND1, which recruits p97 to arsenite-

induced stress granules (Turakhiya et al., 2018), YOD1, which is part of the ELDR complex and involved in removal of damaged lysosomes (Papadopoulos et al., 2017), and ANKZF1, which recruits p97 to mitochondria under oxidative stress conditions (Heo et al., 2010). Since the p97 interactome of HeLa was determined under steady state conditions, such cofactor interaction might not occur at all or at too low levels to detect them via mass spectrometry.

Next, the identified cofactors were compared to available, published data of endogenous p97 immunoprecipitation followed by mass spectrometry. Two studies that investigated the p97 interactome with tagged variants of p97 were excluded (Ritz et al., 2011; Raman et al., 2015). Her et al. investigated the p97 interactome in HCT116 cells. They immunoprecipitated endogenous p97 of cells treated with NMS-873 to investigate the binding of cofactors compared to control conditions. Xue et al. examined the p97 interactome of HEK293 and BJ fibroblasts by treating the cells with NMS-873 or the proteasome inhibitor MG132, then stabilized the p97 interactions directly in the cells by DSP crosslinking, and compared the generated interactomes to crosslinked control cells. The identified cofactors are largely similar between these approaches (Table 1). Some differences in identified p97 cofactors can be explained by the fact that different antibodies were used to immunoprecipitate endogenous p97 complexes by Her et al., Xue et al. and in this study.

Most of the cofactors identified in this study in the absence of DSP were also identified by Her et al., confirming the result. The interactome identified upon the addition of DSP revealed the same set of cofactors as identified by Xue et al. in HEK293, with the exception of UBXN2A and of p37/UBXN2B, which was only identified once in HeLa (Table 1). In contrast to the strong increase in the number of identified p97 cofactors by the crosslinking approach in this study, Xue et al. noticed an increase in the amount of the detected cofactors, since they identified most cofactors also without crosslinking. In addition, slight differences between the two tested cell lines were observed. This might explain the different results obtained by the crosslinking approach in HeLa compared to Xue et al. who investigated HEK293 and BJ fibroblasts. Surprisingly, and in contrast to Her et al. and Xue et al. the p97 cofactor UBXN2A was not identified in this study. Instead, VCPIP1, which is involved in the post-mitotic reassembly of the Golgi apparatus, was significantly enriched. In addition, SVIP was identified as in one of the crosslinked immunoprecipitation samples. SVIP is a small protein with about 8 kDa, explaining the difficulty in identification and reproducibility via mass spectrometry. This comparison shows that the p97 cofactors found in this study are comparable to published data and the crosslinking approach successfully stabilizes interaction of p97 with its cofactors. Therefore, this approach was used to identify novel p97 interactions.

Table 1: Comparison of p97 cofactor interactions identified in this work with published mass spectrometry data. The numbers correspond to the number of replicates in which the cofactor was detected in this work (-DSP: n=3; +DSP: n=4). Significantly enriched cofactors are marked in green and undetected ones in red. This color scheme was transferred to the other studies by Xue et al. and Her et al., where no statement can be made about significance levels. Cofactors marked in blue were identified but only in one immunoprecipitation experiment and therefore, not considered as significant.

	Figure 14		Xue et al., 2016		Her et al., 2016
	HeLa		HEK293		HCT116
Cofactor	- DSP	+DSP	-DSP	+DSP	-DSP
ASPL	3	4			
FAF2	3	4			
NPLOC4	3	4			
NSFL1C (p47)	3	4			
SYVN1	2	4			
UBXD1	3	4			
UFD1L	3	4			
AMFR		4			
DERL1		4			
FAF1		4			
NGLY1		4			
PLAA		4			
UBE4B		4			
UBXN1		4			
UBXN4		4			
UBXN7		4			
UBXN8		2			
VCPIP1		4			
VIMP		4			
UBXN2B (p37)		1			
SVIP		1			
DERL2					
UBXN2A					
RHBDD1					
ANKZF1					
ATXN3					
NUB1					
RNF31					
SPRTN					
UBXN10					
UBXN11					
YOD1					
ZFAND2B					
ZFAND1					

The total number of significantly enriched p97 interactors strongly increased from 29 to 399 interactors upon crosslinking. Many identified interactors are involved in pathways and processes with a known role of p97, such as ERAD, trafficking pathways, the UPS with the 26S proteasome and ubiquitin (Figure 15), which strongly suggests that crosslinking stabilizes physiologically relevant interactions.

MYOF was identified as a candidate interactor of p97, strongly enriched in the p97 interactome upon crosslinking. This enrichment might not only be caused by stabilization of the transient interaction with DSP, but also due to the fact that MYOF is a large 230 kDa protein, allowing an easier detection in mass spectrometry by the availability of many tryptic peptides. In addition, MYOF might even form dimers or oligomers, which would also increase the amount of immunoprecipitated MYOF due to stabilization of the dimers or oligomers by crosslinking. To confirm MYOF as a novel interactor, its interaction with p97 was further validated: Different antibodies were tested in immunoprecipitation experiments to exclude the possibility, that MYOF cross-reacts with the p97 antibody. Therefore, another p97 antibody was tested (Figure 16), reciprocal co-immunoprecipitations with two different MYOF antibodies were performed (Figure 17), and HA-tagged MYOF was ectopically expressed and immunoprecipitated (Figure 23). The interaction could be confirmed for all tested antibodies targeting p97, MYOF or the HA-tag. Furthermore, to demonstrate the relevance of the interaction, different cell lines were investigated and the interaction was confirmed for all tested cell lines such as HeLa, A549 and HEK293T (Figure 22 and 23). Interestingly, the amount of MYOF interacting with p97 was different between the cell lines: HeLa cells showed a stronger interaction in comparison to A549 cells which express MYOF at higher levels, and compared with the ectopic expression of MYOF in HEK293T cells (Figure 23). This finding might indicate a different regulation in various cell lines. To rule out the possibility that the interaction of MYOF with p97 is caused only by the addition of the crosslinker, different approaches were tested in the absence of the crosslinker: Cells were treated with inhibitors such as the p97 inhibitor CB-5083 or the proteasome inhibitor MG132 to stabilize or enrich the interaction (data not shown). However, these approaches failed to reproduce the result. Therefore, the interaction is probably highly transient but could be confirmed in the absence of DSP by the expression of p97 trapping mutants (Figure 21). Taken together, these results confirmed that MYOF is a novel interactor of p97.

4.2 Role of myoferlin in the endocytic pathway

MYOF was shown to play a role in several membrane trafficking pathways, but its exact function is still unknown. MYOF is localized to the plasma membrane and vesicles (Davis et al., 2002; Redpath et al., 2016). In particular, localization to EEs and LEs was shown, with a weaker co-localization with LAMP1 or with transferrin. Thus, a role in late-endosomal to lysosomal trafficking of cargo was proposed (Redpath et al., 2016). However, this study was conducted using ectopically expressing MYOF constructs, which might lead to problems caused by overexpression, such as an increased risk of misfolding and aggregation, and modulation of pathways influenced by MYOF. Therefore, the localization of endogenous MYOF in HeLa and A549 cells was determined by immunofluoroscence microscopy in this work. While the observed co-localization of MYOF with early (Figure 27) and late endosomal markers (Figure 28) confirmed the previous report (Redpath et al., 2016), a strong co-localization of MYOF with markers of recycling endosomes such as Rab11, Rab14 (Figure 29), or CD71 (Figure 30) was observed. Indeed, a role of MYOF in the trafficking of cargo via the endocytic recycling pathway or via the endo-lysosomal pathway for degradation has been shown for various cargo proteins (Doherty et al., 2008; Demonbreun et al., 2010, Turtoi et al., 2013). MYOF null myoblasts exhibit defects in endocytic recycling of transferrin and insulin-like growth factor 1 (IGF1). Transferrin accumulated in the cells and was delayed in recycling (Doherty et al., 2008; Demonbreun et al., 2010). In this context, MYOF interacted with EHD2, which functions in the recycling of vesicles in the endocytic pathway. MYOF null myoblasts had reduced levels of EHD2 (Doherty et al., 2008). It was also shown that the IGF1 receptor (IGF1R) was misdirected for degradation in the endo-lysosomal pathway in MYOF null muscle and myoblasts (Demonbreun et al., 2010). In addition, a role of MYOF in the endo-lyososomal pathway was observed. Depletion of MYOF impaired the degradation of epidermal growth factor receptor (EGFR) in breast cancer cells, resulting in its accumulation (Turtoi et al., 2013).

To get a better understanding of potential functions of MYOF in HeLa cells, the interactome of endogenous MYOF was determined by the *in cellulo* crosslinking mass spectrometry approach in this study (Figure 25). Several Rab proteins were identified to be significantly enriched and some of them are known to function in the endocytic pathway, such as Rab7a, Rab14, and Rab11A/B. Recent publications also supported this finding by immunoprecipitation experiments and bioinformatics analysis (He et al., 2021; Zhang et al., 2018). Interestingly, Rab11 and Rab14 play a role in endocytic recycling. Rab14 was first associated with trafficking between Golgi and endosomes (Junutula et al., 2004), but subsequently, co-localization with RAB4 and RAB5 as well as EEA1 (Proikas-Cezanne et al., 2006; Yamamoto et al., 2010; Reed et al., 2013) on early endosomes, and with transferrin

(Yamamoto et al., 2010) and RAB11 at recycling endosomes (E. Kelly et al., 2010), was observed. A function of Rab14 in the recycling pathway between endosomes and Golgi has been proposed for GLUT4 trafficking (Reed et al., 2013). In addition, it was suggested that Rab14 forms an intermediate compartment in the recycling pathway, which is localized between endosomes positive for Rab5 and Rab4 and recycling endosomes positive for Rab11, and which is involved in recycling of transferrin (Linford et al., 2012). In this study, in addition to Rab14, two Rab14 effector proteins, RUFY1 and Rab11FIP1 (also known as RCP), were identified in the MYOF interactome (Figure 25). Both were shown to be involved in endocytic recycling, including in the recycling of transferrin. RUFY1 is a common effector of Rab14 and Rab4 (Yamamoto et al., 2010), and Rab11FIP1 is a common effector of Rab14 and Rab11 (E. Kelly et al., 2010). Mass spectrometry data of the RCP interactome identified Rab11, Rab14, and MYOF as interactors (Gundry et al., 2017), consistent with the interactions of MYOF identified in this work (Figure 25). Other known interactors of MYOF involved in the endocytic pathway such as EHD1 (Doherty et al., 2008; Posey et al., 2011) and EHD4, were also identified (Figure 25). Interestingly, the transferrin receptor CD71, a protein commonly used as a model cargo to study endocytic recycling, was also found to be significantly enriched (Figure 25). In addition, SNARE proteins involved in membrane fusion and proteins like SNX3 and VSP26A, involved in retromer-mediated recycling, were found. Taken together, the identified interactors support the localization of MYOF to the endocytic pathway as observed by immunofluoroscence microscopy, in particular to recycling endosomes.

In summary, MYOF localized to the endocytic recycling pathway and the endo-lysosomal pathway. Treatment of A549 cells with chloroquine, which was suggested to influence the endo-lysosomal pathway by impairing the trafficking of cargo to the degenerative compartments (Mauthe et al., 2018), resulted in the accumulation of enlarged vacuoles positive for MYOF, which was not observed to this extent in HeLa cells (data not shown), suggesting that endocytic recycling of MYOF might be stronger in HeLa cells compared to A549 cells. Since immunoprecipitation experiments (Figure 22) showed that the amount of MYOF interacting with p97 was stronger in HeLa cells compared to A549 cells, the question arose if p97 plays a role in the sorting of MYOF, and influences its trafficking either to the endocytic recycling pathway or to the endo-lysosomal pathway.

4.3 Role of p97 in the endocytic pathway

Therefore, the localization of endogenous p97 was investigated by immunofluroscence microscopy and p97 showed a diffuse staining in the cytoplasm (Figure 19), although many of p97 functions involve its association with membranes of organelles such as ER in ERAD, mitochondria in MAD or the Golgi apparatus. A possible explanation for this observation is that p97 interactions with membranes and organelles are known to be transient and short-lived. To observe a potential co-localization of p97 with MYOF in this study, transient interactions were stabilized by treatment with p97 inhibitors (Figure 32) or by the ectopic expression of p97 trapping mutants (Figure 31). Both conditions lead to the formation of p97-positive puncta which showed a partial co-localization with MYOF. p97 was also significantly enriched in the MYOF interactome and, in addition, the p97 cofactor PLAA was significantly enriched (Figure 25). p97 was shown to function in the endo-lysosomal degradation of CAV1, a process involving p97 and its cofactor UBXD1 (Ritz et al., 2011; Kirchner et al., 2013). In addition, inhibition of p97 affected sorting and degradation of EGFR in the endo-lysosomal pathway (Ritz et al., 2011). The p97 cofactor PLAA was also shown to function at the endo-lysosomal pathway, supporting internalization of cargo in ILVs (Hall et al., 2017). Furthermore, it was proposed that p97 interacts with the tethering factor EEA1 at EEs to influence the oligomeric state of EEA1 and, therefore, regulate the size of EEs (Ramanathan & Ye, 2012). It was hypothesized that p97 and its cofactor PLAA play a role in endocytic trafficking and in endocytic sorting of MYOF. Therefore, the interactomes of MYOF and p97 were compared and analyzed for shared interactors (Figure 33). Several proteins involved in the endocytic pathway were identified in both interactomes, such as Rab proteins like Rab5, Rab7a, Rab14, and Rab11A/B but also the cargo CD71. Co-localization of p97 with EEs in cells expressing Rab5QL was published previously, and knockdown of p97 was shown to lead to enlarged EEs (Ramanathan & Ye, 2012).

This further suggests that p97 and MYOF play a role in the endocytic pathway and therefore, shared significantly enriched interactors were validated. Rab14 was identified as common interactor of MYOF and p97, co-localization of p97 with Rab14-positive endosomes was confirmed upon p97 inhibitor treatment (Figure 34). PLAA was also identified as a common interactor, and its depletion reduced the interaction of p97 with MYOF (Figure 35). Co-localization of PLAA with Rab5- and Rab14-positive endosomes, which were also positive for MYOF, was observed (Figure 40). This interaction was visible without the addition of p97 inhibitors or the expression of p97 trapping mutants. These results support the hypothesis that MYOF interacts with p97 and PLAA on Rab5- and Rab14-positive endosomes.

Protein sorting occurs at EEs, where cargo proteins are either sorted in ILVs for degradation or sorted for recycling to the PM (Naslavsky & Caplan, 2018). Localization with EEs but also with REs has been demonstrated for Rab14 and it was shown to function in the endocytic recycling pathway, including recycling of transferrin (Yamamoto et al., 2010; Linford et al., 2012). Since MYOF is also known to play a role in transferrin recycling (Doherty et al., 2008), it seemed plausible that p97 plays a role in the endocytic recycling pathway as well. It was previously shown that cells treated with Eeyarestatin I, which was believed to be a specific p97 inhibitor at that time, had a delayed trafficking of transferrin (Ramanathan & Ye, 2012). However, Eeyarestatin I was meanwhile shown to affect the Sec61 translocon, leading to perturbed Ca^{2+} homeostasis (Gamayun et al., 2019), and raising doubts about the validity of the conclusions made by Ramanathan and Ye. Therefore, transferrin recycling was reanalyzed in the present work, by treating the cells with p97 inhibitors (Figure 45) or by expression of p97 trapping mutants (Figure 44). Expression of p97 trapping mutants showed only a slight delay in the recycling in comparison to the control cells (Figure 44). This is probably due to the fact that only a small fraction of cells within the stable cell pools express the p97 constructs at high levels inducing trapping, whereas the majority of low-expressing cells might mask a potential effect. To obtain more uniform effects, the two p97 inhibitors CB-5083 and NMS-873 were tested and both caused a delay in recycling of transferrin (Figure 45 A and B), even though the effects varied between NMS-873 and CB-5083. A possible explanation for the observed differences in the delay of transferrin recycling could be the different mechanisms of action of the inhibitors. CB-5083 targets the D2 domain of p97 reversibly and competitively (Zhou et al., 2015), while NMS-873 is a reversible and allosteric inhibitor (Magnaghi et al., 2013). This might result in differences in the efficiency of stabilization of certain cofactor interactions with p97. The results observed by FACS analysis could also be confirmed by immunofluoroscence microscopy (Figure 45 C). These data suggest a role of p97 in the endocytic recycling pathway for receptor proteins such as CD71 and its interactor transferrin.

In summary, MYOF was identified as novel interactor of p97 and was shown to interact with p97 in part via the p97 cofactors PLAA and UBXD1 (Figure 46). PLAA was observed to localize to Rab5- and Rab14-positive endosomes. Therefore, it was hypothesized that p97 interacts with MYOF at endosomes positive for Rab5 and Rab14. p97 promotes endocytic trafficking and supports the sorting of MYOF and its cargo proteins such as transferrin and CD71 for endocytic recycling.

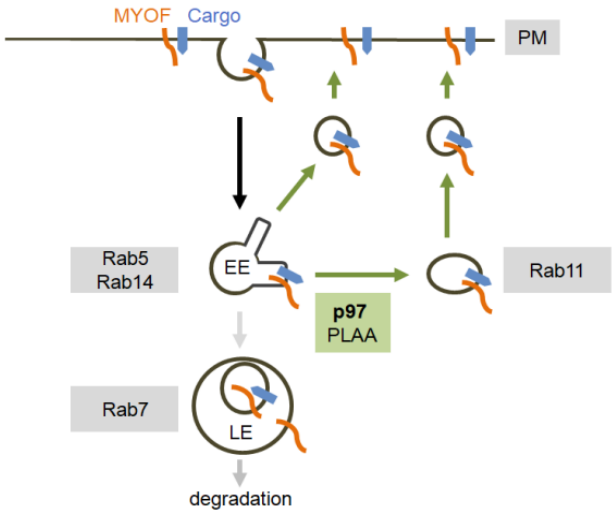

Figure 46: Model for the role of p97 in trafficking. MYOF localizes to the PM and is internalized. At EEs positive for Rab5 and Rab14, MYOF is involved in the sorting of proteins either for degradation or for recycling to the PM. MYOF transits to LEs or REs. p97 interacts with MYOF via PLAA and UBXD1 and promotes to the recycling of proteins to the PM at Rab5- and Rab14- positive endosomes.

4.4 Outlook

In this work the trafficking protein MYOF was identified as a novel interactor of p97. However, a number of questions regarding the interaction and the function are still open and require further investigation.

It remains unclear if MYOF interacts directly or indirectly with p97 and which domain of MYOF mediates the interaction with p97. The interaction of p97 with MYOF was decreased upon knockout of PLAA (Figure 35) or UBXD1 (Figure 37 and 38), suggesting that these cofactors are involved in the interaction. In order to map the interaction domain of MYOF with p97, MYOF variants, lacking various domains, were generated. However, the truncations resulted in altered subcellular localization, as observed by immunofluoroscence microscopy (data not shown), and therefore the variants were not useful to map the interaction domain. Other approaches such as crosslinking mass spectrometry like XL-MS, using mass spectrometry to identify crosslinked peptides and their linkage side, should be taken into account to determine if MYOF interacts directly with p97.

Another open question is if MYOF is ubiquitinated and a substrate of p97. Ubiquitin is an important regulator of the endocytic trafficking at the level of endocytosis (Piper et al., 2014) as well as during ESCRT-mediated sorting of proteins to the endo-lysosomal pathway (Clague et al., 2012). So far, the functional role of p97 in the endocytic pathway was linked to monoubiquitinated substrates like CAV1 or EEA1 (Ritz et al., 2011; Ramanathan & Ye, 2012). In addition, in this work the p97 cofactor

PLAA, which contains two ubiquitin binding domains and does not possess catalytic activity (Mullally et al., 2006; Hall et al., 2017), was identified as interactor of MYOF (Figure 25). Therefore, it was investigated if MYOF is ubiquitinated, which is shown by several studies, summarized in the database BioGRID. However, no shift in the band pattern of MYOF was observed by western blot of HeLa cells treated with the E1 inhibitor TAK-243 or the DUB inhibitor PR-619 (data not shown). This experiment might not exclude the possibility of ubiquitination of MYOF, as eventually longer treatment times might be needed to observe an effect. However, this finding would be consistent with the function of MYOF in endocytic recycling, because the sorting of proteins to the recycling pathway depends on sorting motifs or bulk membrane flow rather than on ubiquitin (Cullen & Steinberg, 2018). A localization of MOYF to late endosomal and lysosomal markers was also observed (Figure 28) and different studies suggested that MYOF is not sorted for degradation (Redpath et al., 2016), but MYOF was shown to localize to the lysosomal membrane of pancreatic cancer cells (Gupta et al., 2021). These findings also exclude an ubiquitin-dependent targeting of MYOF to ILVs. Addressing the question if MYOF is a substrate of p97, MYOF interaction with p97 was stabilized by expression of p97 trapping mutants, indicating that MYOF might be a substrate of p97. However, this observation can also be explained by an indirect interaction of MYOF with p97 and therefore, MYOF may not be a substrate. Supporting this hypothesis, p97 inhibition (data not shown), proteasome inhibition (data not shown) or PLAA KO did not change protein levels of MYOF, suggesting that MYOF is not targeted for degradation, and therefore might not be a classical substrate of p97.

In this work, a role of p97 in recycling of transferrin was observed (Figure 45). However, the precise function of p97 in mediating the recycling of cargo is unclear. MYOF has roles in membrane fusion and endocytic trafficking and is involved in sorting of cargo for degradation, but also recycling (Figure 15). Therefore, we hypothesize that the functional role of p97 in cargo recycling is linked to MYOF. Based on known functions of p97 in trafficking and sorting, there are several possibilities how p97 might influence and regulate functions of MYOF. So far, the role of p97 in endosomal sorting and trafficking was linked to the regulation of the oligomeric state of EEA1 (Ramanathan & Ye, 2012), and CAV1 (Ritz et al., 2011). Therefore, p97 might influence MYOF-mediated processes by regulating its oligomeric state. Based on its homology to dysferlin (Davis et al., 1999), which was shown to form dimers via interaction of C2 domains and TM domains (Xu et al., 2011), and oligomerization was observed upon crystallization for different domains of dysferlin (Sula et al., 2014), it can be speculated that MYOF forms dimers or oligomers, an aspect which needs to be further investigated. Other potential functions of the p97 interaction might be related to the proposed role of MYOF in membrane fusion via its C2 domains. Proteins containing C2 domains, like synaptotagmin, are known to be involved in membrane fusion (Hui et al., 2012). It was observed that the C2A domain of MYOF binds to a negatively charged phospholipid mixture containing phosphatidylserine (PS) (Davis et al.,

2002; Doherty et al., 2005), which is enriched at early and recycling endosomal membranes and at the plasma membrane (Leventis & Grinstein, 2010). In addition, the C2 domains C2ABC showed an additive effect in the binding to negatively charged lipids and calcium binding enhanced the activity, resulting in altered lipid membranes (Marty et al., 2014). p97 together with its cofactors p47 and VCPIP1 is known to support membrane fusion processes like the membrane fusion of the post-mitotic Golgi apparatus. However, the p97 cofactors shown to be involved in membrane fusion processes were not identified in mass spectrometry. Instead, SNARE proteins were identified in the MYOF interactome (see 7.3), supporting the proposed role of MYOF in membrane fusion. p97 interacting with MYOF might regulate or influence the interaction of MYOF with key regulators of endocytic trafficking and support cargo trafficking to the recycling pathway. A similar function in protein trafficking of p97 and its cofactor UBXD1 was reported for LMAN1 (also known as ERGIC-53). p97-UBXD1 complex regulates trafficking by influencing the binding of associated trafficking factors of LMAN1 (Haines et al., 2012). The MYOF interactome revealed several key regulators of endocytic trafficking such as Rab, EHD (Figure 25), and SNARE proteins (see 7.3) and p97 might regulate the interaction of MYOF with these interactors by binding and blocking interaction sites.

Finally, both p97 and MYOF are linked to human diseases. Mutations in the *VCP* gene encoding human p97 cause MSP1 and one of the four main disease manifestations is inclusion body myopathy (IBM) (Korb et al., 2020). 90% of MSP1 patients suffer from myopathy and show progressive weakness, leading to respiratory failure, cardiomyopathy, or cardiac failure. In patient cells, cytoplasmic rimmed vacuoles and inclusions positive for proteins such as ubiquitin and TDP-43 were found (Korb et al., 2020). In addition, myoblasts from patients had defective cell fusion (Vesa et al., 2009), and it was reported that CAV3 mislocalized from the sarcolemma to LAMP2-positive structures in muscle tissue from patients (Ritz et al., 2011), showing a role of p97 in sorting of cargo in myoblasts and muscle cells. MYOF was shown to be involved in cardiomyopathy, limb-girdle type muscular dystrophy and cancer, where it is involved in proliferation, invasion and migration (Zhu et al., 2019). MYOF was reported to function in myoblast fusion during embryonic development, but also in muscle regeneration and repair (Shumer, 2011). Other ferlin family members, including otoferlin and dysferlin, are linked to human diseases. Dysferlin causes a range of muscle diseases called dysferlinopathies, with limb-girdle muscular dystrophy type 2B (LGMD2B) and Miyoshi myopathy (Barefield et al., 2021). Recently, a patient with a combination of cardiomyopathy and limb-girdle type muscular dystrophy caused by a truncating variant of MYOF was identified (Kiselev et al., 2019). Mutations in the genes of MYOF and p97 are linked to different types of myopathies. However, trafficking and the endocytic pathway which is connected to lysosomes and autophagy are often linked to myopathies (Dowling et al., 2008; Korb et al., 2020; Yarwood et al., 2020). Therefore, it will be interesting to investigate MYOF in the context of p97 disease-causing mutations.

5 Materials and Methods

5.1 Materials

5.1.1 Chemicals and reagents

Commonly used chemicals were obtained from Roth, Sigma Aldrich, Merck, and Serva unless otherwise indicated (see Table 2; or Methods).

Table 2: List of chemicals and reagents

Chemical	Company	Identifier
Dimethylsulfoxid (DMSO)	Thermo Fisher	D12345
Dithiobis(succinimidyl propionate) (DSP)	Thermo Fisher	PG82081
Polyethylenimine (PEI)	Polysciences	23966-1
Polybrene	Santa Cruz	sc-134220

5.1.2 Plasmids

Table 3: List of plasmids used in this study

Plasmid	Source	Lab collection number: pAB
psPAX2	Addgene - 12260	2522
pMD2.G	Addgene - 12259	2523
Rab5WT-pmRFP	a kind gift from Dr. Seiichi Koike (The University of Tokyo)	3034
Rab5QL-pmRFP	a kind gift from Dr. Seiichi Koike (The University of Tokyo)	3035
EGFP-Rab5	Addgene - 49888	3023
GFP-Rab5CA (Q79L)	Addgene - 35140	3021
GFP-Rab11	Addgene - 12674	3013
pEGFP-Rab7-WT	Pavlos et al., 2010	3031
pEGFP-Rab14	Pavlos et al., 2010	2997
MYOF-HA	Addgene - 22443	2905
pINDUCER20 empty	Addgene - 44012, via AG Gaubatz	3021
pINDUCER20 FLAG-p97WT	Buchberger lab collection, S. Meyer	3041
pINDUCER20 FLAG -p97E305Q	Buchberger lab collection, S. Meyer	3042
pINDUCER20 FLAG -p97 E578Q	Buchberger lab collection, S. Meyer	3044
pINDUCER20 FLAG -p97 E305QE578Q	Buchberger lab collection, S. Meyer	3043

5.1.3 Antibodies

5.1.3.1 Primary Antibodies

Table 4: List of primary antibodies used in this study

Antigen	Species	Clonality	Identifier	Company	pAB	Dilution
alpha Tubulin	mouse	monoclonal	T 5168	Sigma-Aldrich	-	WB: 1:2000
CD63	mouse	monoclonal	sc-5275	Santa Cruz	305	WB: 1:500 IF: 1:50
CD71	mouse	monoclonal	sc-65882	Santa Cruz	286	WB: 1:500 IF: 1:50
EEA1	rabbit	polyclonal	2411	Cell Signaling	189	WB: 1:1000 IF: 1:100
FAF1	rabbit	polyclonal	-	-	65	WB: 1:10000
FLAG	rabbit	polyclonal	PA1-984B	Thermo Scientific	356	WB: 1:1000 IF: 1:200
HA	mouse	monoclonal	HA.11-MMS-101R	Biolegend	-	WB: 1:2000 IP: 6 µg
IgG	rabbit		011-000-003	Jackson Immunoresearch	-	IP: 6/10 µg
IgG2a	mouse		02-6200	Invitrogen	-	IP: 6/10 µg
LAMP1	rabbit	polyclonal	9091	Cell Signaling	275	WB: 1:1000 IF: 1:100
MYOF #1	rabbit	polyclonal	ab190264	Abcam	269	IP: 10 µg WB: 1:2500
MYOF #2	mouse	monoclonal	sc-376879	Santa Cruz	299	IF: 1:50
MYOF #3	rabbit	polyclonal	HPA014245	Sigma-Aldrich	268	WB: 1:500 IF: 1:75
PLAA #1	rabbit	polyclonal	HPA020996	Sigma-Aldrich	322	WB: 1:1000 IF: 1:75
PLAA #2	rabbit	polyclonal	HPA020994	Sigma-Aldrich	349	IF: 1:50
Rab5	rabbit	polyclonal	3547	Cell Signaling	274	IF: 1:100
UBXD1	rabbit	polyclonal	14706-1-AP	Proteintech Group	147	WB: 1:1000
VCP #1	rabbit	polyclonal	A300-589A	Bethyl Laboratories	247	IP: 6 µg WB: 1:2500
VCP #2	mouse	monoclonal	sc-57492	Santa Cruz	304	IP: 6 µg IF: 1:50
VCP #3	mouse	monoclonal	ab11433	Abcam	36	WB: 1:2000

5.1.3.2 Secondary Antibodies

Table 5: List of secondary antibodies used in this study

Antigen	Species	Catalog-Nr.	Company	Dilution
Mouse IgG HRP	goat	115-035-003	Dianova (Jackson ImmunoResearch)	1:7500
Rabbit IgG HRP	goat	111-035-045	Dianova (Jackson ImmunoResearch)	1:7500
Alexa Fluor 488 anti-Rabbit IgG	goat	A11070	Thermo Fisher	1:500
Alexa Fluor 488 anti-Mouse IgG	goat	A11017	Thermo Fisher	1:500
Alexa Fluor 594 anti-Rabbit IgG	goat	A11072	Thermo Fisher	1:500
Alexa Fluor 594 anti-Mouse IgG	goat	A11020	Thermo Fisher	1:500
Alexa Fluor 647 anti-Rabbit IgG	goat	A21246	Thermo Fisher	1:400
Alexa Fluor 647 anti-Mouse IgG	goat	A21236	Thermo Fisher	1:400

5.1.4 Strains and cell lines

5.1.4.1 *E.coli* strain

XL1 Blue: *supE44, hsd R17, rec A1, gyr A46, thi, rel A1, lac-, F' [proAB +, lac lq, lacZ M15, Tn10(tet r)]*

5.1.4.2 Cell lines

Table 6: List of mammalian cell lines used in this study

Cell line	Source
HeLa	ATCC # CCL-2
HEK293T	ATCC # CRL-3216
A549	ATCC # CCL-185; AG Diefenbacher
HeLa pINDUCER20 empty	This work
HeLa pINDUCER20 FLAG-p97WT	This work
HeLa pINDUCER20 FLAG-p97E305Q	This work
HeLa pINDUCER20 FLAG -p97E578Q	This work
HeLa pINDUCER20 FLAG-p97E305QE578Q	This work
HeLa UBXD1 -/- knockout (single clone)	Dr. Gabriella Marincola, Buchberger lab
HeLa wild-type control (single clone)	Dr. Gabriella Marincola, Buchberger lab
HeLa UBXD1 -/- knockout (cell pool)	Maria Körner, Buchberger lab
HeLa PLAA - /- knockout (cell pool)	Maria Körner, Buchberger lab
HeLa p97 -/- knockout (cell pool)	Maria Körner, Buchberger lab
HeLa non-human-target control (cell pool)	Maria Körner, Buchberger lab

5.1.5 Inhibitors

Table 7: List of inhibitors used in this study

Inhibitor	Manufacturer	Stock solution
CB-5083	Selleckchem	10 mM in DMSO
NMS-873	Selleckchem	10 mM in DMSO

5.1.6 Kits

Table 8: Kits used in this study

Kit	Manufacturer	Identifier
NucleoSpin Plasmid	Macherey-Nagel	740588.250
NucleoSnap Plasmid Midi	Macherey-Nagel	740494.50
Venor®GeM Classic: Mycoplasma detection kit	Minerva Biolabs	11
Pierce™ 660 nm Protein Assay Reagent	Thermo Fisher	22660

5.1.7 Cell culture

Table 9: Material used for mammalian cell culture

Material	Manufacturer	Identifier
DMEM	Gibco, Life Technologies	11966025
FBS	Gibco, Life Technologies	10500064
Trypsin-EDTA	Gibco, Life Technologies	25200056
PBS	Gibco, Life Technologies	10010023
Opti-MEM	Gibco, Life Technologies	31985602
Penicillin/Streptomycin	Gibco, Life Technologies	15140122
G418	InvivoGen	ant-gn-1
Puromycin	InvivoGen	ant-pr-1

5.1.8 Consumables

Table 10: Consumables used in this study

Chemical	Company	Identifier
ANTI-FLAG M2 Affinity Gel	Sigma-Aldrich	A2220
Oligofectamine™ Transfection Reagent	Thermo Fisher	12252011
Precision Plus Protein All Blue Standards	Biorad	1610373
Precision Plus Protein Dual Color Standards	Biorad	161-0374
ProLong™ Glass Antifade Mountant	Thermo Fisher	P36980
Protease-Inhibitor Tabletten *cOMPLETE edta free*	Roche	04693132001
Protein G Sepharose *4 fast flow* Beads	GE Healthcare	17-5132-01
Transferrin from human serum, Alexa Fluor™ 594 conjugate	Thermo Fisher	T13343
Vectrashield with DAPI	Vector Laboratories	H1200

5.1.9 Software

Table 11: Software used in this study

Software	Company	
ApE A plasmid Editior by M.Wayne Davis	-	http://jorgensen.biology.utah.edu/wayned/ape
Attune™ NxT Software.	Thermo Fisher	
Fiji	-	http://imagej.net/software/Fiji/
Leica confocal software	Leica Microsystems	
Mendeley Desktop	Mendeley	http://mendeley.com
Image Lab software	Bio-Rad Laboratories Inc.	
ZEN 2012 SP3 software	Zeiss	

5.2 Methods

5.2.1 Molecular biology methods

5.2.1.1 Sequencing

Sanger sequencing was performed by Eurofins Scientific SE (Luxemburg) and sequencing results were analyzed using the ApE software.

5.2.1.2 Transformation of *E. coli* cells

$CaCl_2$ competent *E. coli* cells were thawed on ice and plasmid DNA was added to 25 µl of competent cells. The mixture was incubated on ice for 30 min and heat shocked at 42 °C for 60 s. The cells were placed on ice for 5 min and LB medium was added. The cells incubated for 1 h on the shaker at 37 °C and dilutions of the mixture were prepared. *E. coli* cells were plated onto selection plates with the appropriate antibiotics and incubated over night at 37 °C.

5.2.1.3 Plasmid isolation from *E. coli*

Cultures of single *E. coli* colonies were grown in LB medium containing the appropriate antibiotics over night at 37 °C. Isolation of Plasmid DNA via Mini-Prep or Midi-Prep was performed according to the manufacturer's instructions (Machery-Nagel).

5.2.2 Mammalian cell culture

5.2.2.1 Cultivation of cells

All eukaryotic cells were cultured in Dulbecco's Modified Eagle medium (DMEM) (GIBCO), supplemented with 10% fetal bovine serum (FBS) and 1% Penicillin/Streptomycin at 37 °C and 5% CO_2. Additional antibiotics were added to the culture media for HeLa pINDUCER20 cell pools (G418: 400 µg/ml) and HeLa KO cell pools (puromycin: 2 µg/ml). Cells were seeded at a density of 20% and split when the cells reached around 90% confluence. For splitting, the medium was removed and the cells were washed with PBS and detached from the culture dish by 1 - 2 min trypsinization. Trypsin was inhibited by the addition of fresh DMEM medium and cells were split in a ratio of 1:8 with the fresh medium and added into a new culture dish.

5.2.2.2 Transfection with plasmid DNA

HeLa, HEK293T and A549 cells were transfected at 40-70% confluence with Polyethylenimine (PEI). The plasmids were diluted in serum-free media (DMEM or Opti-MEM) and PEI was added (Table 12). The mixture was incubated for 15 min at room temperature and then added drop-wise to the cells.

Table 12: Transfection mixture for different plate formats and cell lines

	DMEM (µl)	PEI (µl)	DNA (µg)
12 well plate	100	1.5	0.5
15 cm dish	2000	70	35

5.2.2.3 Transfection with small interfering RNAs (siRNAs)

Cells were grown on coverslips in 12 well plates and transfected with 50 nM siRNA and 1.5 µl Oligofectamine (Thermo Fisher) diluted in Opti-MEM. The mixture was incubated for 15 min at room temperature and then added drop-wise to the cells. The myoferlin siRNA pool (L-013584-01-0005 ON-TARGET plus Human MYOF siRNA –SMARTpool) or the non-targeting siRNA pool (D-001810-10-05 ON-TARGET plus Non-targeting Pool) from Dharmacon™ was used. After 20 h the medium was changed to fresh growth medium and knockdown was performed for a total of 72 h.

5.2.2.4 Production of lentiviruses

18 - 24 h before transfection, HEK293T cells were seeded in 6 well plates and grown until they reached 75 - 85% confluent. The plasmids encoding viral proteins, psPAX2 (2.5 µg) and pMD2G (0.8 µg) as well as the pINDUCER20 plasmid (3.8 µg), were diluted with 200 µl DMEM medium

without serum. 20 µl of PEI were added, and the mixture was incubated for 15 min at room temperature. The medium of HEK293T cells was changed to serum free DMEM medium and the DNA-PEI mixture was added drop-wise to the cells. The plate was placed in an S2 safety level incubator. After 24 h and 48 h, the supernatant was harvested and stored at 4 °C. Fresh culture medium was added to the cells. The collected supernatants were combined, filtered through a 0.45 µm filter and stored at 4°C.

5.2.2.5 Transduction and treatment of HeLa cells

About 20 h before transduction, HeLa cells were seeded in 6 well plates and transduced at 40 - 60% confluence. The medium was removed, and the lentivirus-containing supernatant mixed with 8 µg/ml polybrene was added to the cells. After 20 h fresh culture medium containing 1000 µg/ml G418 was added to the lentivirus-infected and control cells and selection was performed for 12 days. During this time the cells were splitted and the fresh growth medium containing 1000 µg/ml G418 was added. To express the p97 variants the cells were treated with 500 ng/ml doxycycline for 22 h.

5.2.3 Protein analysis

5.2.3.1 SDS-PAGE

Denatured protein samples were separated according to their molecular weight by sodium dodecylsulfate polyacrylamide gel electrophoresis (SDS-PAGE). The different compositions of the gels are listed in Table 13. SDS-PAGE was carried out by using Laemmli running buffer (25 mM Tris-HCl pH 8.3; 192 mM glycine; 0.1% SDS) in a Hoefer mini-gel system, applying a current of 20 mA per gel.

Table 13: Composition of SDS gels used in this study

Composition	stacking gel	8% separating gel	10% separating gel	12% separating gel
H_2O	1.4 ml	2.3 ml	1.9 ml	1.6 ml
Acrylamide/Bis solution, 37. 5:1 (30% w/v), 2.6% C	0.33 ml	1.3 ml	1.7 ml	2.0 ml
1.5 M Tris pH 8.8	-	1.3 ml	1.3 ml	1.3 ml
1 M Tris pH 6.8	0.25 ml	-	-	-
10% SDS	0.02 ml	0.05 ml	0.05 ml	0.05 ml
10% APS	0.02 ml	0.05 ml	0.05 ml	0.05 ml
TEMED	0.002 ml	0.006 ml	0.004	0.004 ml

5.2.3.2 Semi-dry western blot

The separated proteins (5.2.3.1) were electrotransferred to a PVDF membrane (Millipore immobilon) by semi-dry western blot (blotting buffer: 25 mM Tris; 192 mM glycine; 20% (v/v) methanol) applying a current of 150 mA per membrane for two hours. The membrane was blocked with 5% milk in Tris-buffered saline (50 mM Tris-HCl. 150 mM NaCl, pH 7.5) with 0.1% Tween® 20 (TBST) for 1 h.

To identify target proteins on the membrane, primary antibodies diluted in blocking solution were incubated overnight at 4 °C. The membrane was washed three times (5 min each) with TBST, incubated in TBST with the appropriate HRP-conjugated secondary antibody for 1 h at room temperature, and washed again three times (10 min each) with TBST. The membrane was incubated with Clarity Western ECL Substrate (Bio-Rad), and chemiluminescence signals were detected using the Molecular Imager® Gel Doc™ XR+ System (Biorad). The Image Lab software (Biorad) was used for quantification of the band intensity.

5.2.3.3 Cell lysates for western blot

Cells were grown in 12 well plates until 90% confluent and washed twice with cold PBS. Cells were lysed 1x sample buffer (0.0005% bromophenol blue, 10% glycerol, 2% SDS, 63 mM Tris-HCl, pH 6.8) supplemented with 100 mM DTT. The lysates were collected and boiled at 95°C for 5 min. Samples were centrifuged and analyzed by western blot as described in 5.2.3.2.

5.2.4 Cell biology

5.2.4.1 Crosslinking

HeLa, HEK293T or A549 cells were grown on 15 cm dishes until 80-90% confluent and washed two times with PBS. The cells were treated with the indicated concentration of DSP in PBS (50 mM DSP stock solution in DMSO) for 30 min at room temperature. The crosslinker was quenched with 25 mM Tris-HCl pH 7.6 for 10 min at room temperature and the supernatant was removed. PBS was added to the cells and the cells were collected and harvested at 1200 rpm, 4°C for 8 min. The cell pellet was flash frozen and stored at -80°C.

5.2.4.2 Immunoprecipitation experiments

Immunoprecipitation with crosslinking

For immunoprecipitation of endogenous p97 or MYOF, parental or genome-edited HeLa cells or A549 cells were grown on 15 cm dishes until 80-90% confluent and crosslinked as described in 5.2.4.1. Frozen cell pellets were resuspended in lysis buffer (50 mM Tris pH 7,6; 150 mM NaCl; 2 mM $MgCl_2$; 1% Nonidet P40; 10% Glycerol) containing protease inhibitors (1 mM PMSF, 1x Roche complete protease inhibitor mix) and incubated for 10 min on ice. Cell debris was removed by centrifugation (13000 rpm, 15 min, 4 °C) and the supernatant was collected. Protein concentration was determined with the Pierce™ 660 nm Protein-Assay-Kit and adjusted if needed. Lysates were pre-cleared using 20 µl of protein G sepharose beads (1 h, 4 °C, on a rotating wheel). After centrifugation (1200 rpm, 3 min, 4 °C), the pre-cleared supernatants were transferred to fresh 1.5 ml reaction tubes. 50 µl of the samples were collected as input sample, mixed with 2x sample buffer (125 mM Tris-HCl pH 6.8; 4% (w/v) SDS; 20% glycerol, 0.002% bromophenolblue) supplemented with DTT and heat denatured for 5 min at 95 °C. Pre-cleared lysates were either incubated with antibody against endogenous p97 (6 µg: p97 #1 and p97 #2) or MYOF (10 µg: MYOF #1 and MYOF #2) or the control IgG (IgG – rabbit or IgG2a – mouse) for 1 h, 4 °C on a rotating wheel. The lysates were incubated with 25 µl of protein G sepharose beads for 2 h at 4 °C on a rotating wheel. Beads were washed two times with lysis buffer with inhibitors and once without inhibitors, and a final washing step was performed with 1 x TBS buffer. The remaining supernatant was removed and 2x sample buffer with DTT was added to the beads. The samples were heat denatured for 5 min at 95°C and analyzed by western blot (5.2.3.2).

For the p97 interactome via mass spectrometry, HeLa cells were grown on 15 cm dishes until 80-90% confluent and crosslinked as described in 5.2.4.1. Non-crosslinked control cells were treated with PBS with equivalent amounts of DMSO for 30 min at room temperature. The immunoprecipitation was done as described above (Immunoprecipitation with crosslinking). The samples were analyzed and statistically evaluated by Prof. Andreas Schlosser (see 5.2.4.3). Three separate experiments were performed for the non-crosslinked samples and four for the crosslinked samples. Two of the four crosslinked samples oriented from the same lysate, but different p97 antibody lots (p97 #1) were used. Maria Körner generated one set of the non-crosslinked and crosslinked immunoprecipitations.

To determine the MYOF interactome via mass spectrometry, immunoprecipitations of crosslinked HeLa cells were performed with 10 µg antibodies (MYOF #1 and the control IgG) as described above (Immunoprecipitation with crosslinking). The samples were analyzed and statistically evaluated by

Prof. Andreas Schlosser (see 5.2.4.3). The data was generated from three separate experiments. Each of the experiments contained a pool of three immunoprecipitations from the same lysate.

Immunoprecipitation of p97 complexes from HEK293T cells with crosslinking

HEK293T cells were seeded on 15 cm dishes and transfected with a plasmid encoding MYOF-HA. Cells were grown until 90% confluent and crosslinked (see 5.2.4.1) 48 h post transfection. Lysates were generated as described above (Immunoprecipitation with crosslinking). The lysate was pre-cleared using 20 µl of protein G sepharose beads (1 h, 4 °C, on a rotating wheel). After centrifugation, the pre-cleared supernatant was transferred and 50 µl were taken as input sample. Pre-cleared lysate was separated into different 1.5 ml reaction tubes and 6 µg of antibody against p97 #1, HA or MYOF #1 or the corresponding control IgGs (IgG – rabbit or IgG2a – mouse) were added. The immunoprecipitation was done as described above (Immunoprecipitation with crosslinking).

FLAG-Immunoprecipitation of p97 complexes

HeLa pINDUCER20 cell lines were seeded on 15 cm dishes and grown until 60-70% confluent. The expression of the different p97 variants was induced by treatment of the cells with 500 ng/ml doxycycline for 20 h. Cells were washed two times with cold PBS, harvested and cell pellets were flash frozen and stored at -80°C. The pellets were resuspended in lysis buffer (50 mM Tris pH 7,6; 150 mM NaCl; 2 mM $MgCl_2$; 1 % Nonidet P40; 10 % Glycerin; 1mM DTT) containing protease inhibitors (1 mM PMSF, 1x Roche complete protease inhibitor mix) and incubated for 10 min on ice. The cell debris was removed by centrifugation (13000 rpm, 15 min, 4°C) and supernatant was collected. The protein concentration was determined with the Pierce™ 660 nm Protein-Assay-Kit and concentrations were adjusted. 50 µl of each lysate was taken as input sample, mixed with 2x sample buffer with DTT and heat denatured. The remaining sample was added to 30 µl FLAG-M2 agarose beads and incubated for 3 h 30 min at 4°C on a rotating wheel. Beads were washed twice with lysis buffer containing inhibitors for 10 min and 5 min respectively at 4°C on a rotating wheel. An additional washing step was performed for 5 min with lysis buffer without inhibitors, and the final washing step was performed using 1x TBS. The supernatant was removed and the beads were boiled in 30 µl 2x sample buffer with DTT at 95 °C for 5 min.

5.2.4.3 Mass spectrometry

The samples were analyzed and statistically evaluated by Prof. Andreas Schlosser as described before (Turakhiya et al., 2018). Further data analysis was performed using R scripts developed in-house (AG Schlosser). LFQ intensities were used and missing LFQ intensities in the control samples were

imputed with values close to the baseline. Data imputation was performed with values from a standard normal distribution with a mean of the 5% quantile of the combined log10-transformed LFQ intensities and a standard deviation of 0.1. For the identification of significantly co-immunoprecipitated proteins, median log2 transformed protein ratio were calculated from the three replicate experiments and boxplot outliers were identified in intensity bins of at least 300 proteins. Log2 transformed protein ratios of co-immunoprecipitation versus control with values outside a 1.5x (potential; significance 1) or 3x (extreme; significance 2) interquartile range (IQR), respectively, were considered as significantly co-immunoprecipitated (significance 0 labeled in blue, significance 1 labeled in green and significance 2 labeled in red).

5.2.4.4 Indirect immunofluoroscence

HeLa or A549 cells were seeded on coverslips 24 h prior to the indicated treatment (see 5.2.2.2 or 5.2.2.3 for transfection; p97 inhibitor treatment: DSMO, NMS-873 (10 µM) or CB-5083 (10 µM) was added for 3 h 30 min prior to fixation) to achieve about 60% confluence at the time point of fixation. Then, cells were washed twice with cold PBS, fixed by using 3.7% formaldehyde in PBS for 12 min at room temperature, and washed again twice with cold PBS. Cells were permeabilized with 0.2% Triton X-100 and 1% bovine serum albumin (BSA) in PBS for at least 10 min, washed with PBS and blocked by incubation in 1% BSA diluted in PBS. Incubation with primary antibody, diluted in 1% BSA in PBS, was performed overnight at 4 °C. Cells were washed for 5 min with cold PBS and incubated with the secondary antibody diluted in 1% BSA in PBS for 2 h at room temperature. Next, cells were washed again for 10 min with PBS, and a last washing step was performed with ddH_2O. Coverslips were mounted for microscopy with mounting medium containing DAPI (Vectashield®) or ProLong™ Glass Antifade Mountant, sealed with nail polish and stored at 4 °C.

5.2.4.5 Confocal microscopy and image processing

Immunofluorescence microscopy was performed at the Imaging Core Facility (Biocenter, University of Würzburg) using a Leica TCS SP2 confocal microscope equipped with an acousto-optical beam splitter. Images were acquired using the laser sources Ar laser (488 nm), HeNe laser (561 nm, 633 nm) and Diode UV laser (405 nm) for excitation with a 63x/1.4 oil immersion objective. Where higher resolution was required, 2x digital zooming was applied. Single planes or Z-stacks were acquired using the Leica confocal software. Representative images were processed using Fiji software.

5.2.4.6 Structured illumination microscopy (SIM)

SIM was performed at the Imaging Core Facility (Biocenter, University of Würzburg), using a Zeiss Elyra S.1 SIM equipped with a PCO Edge 5.5 sCMOS camera. The ZEN 2012 SP3 software (Zeiss) was used to acquire and process images. Images were acquired using a Plan-Apochromat 63x/1.4 oil objective, an HR Diode 488-100 nm laser with a BP495 - 550, LP750 emission filter and an HR DPSS 561-100 nm laser with a BP570 - 620, LP750 emission filter. With the help of N. Tolay, seven slices were captured at 400 nm Z-step size and Fourier transformation with all slices was performed to acquire the images. Representative images were further processed using Fiji software. Maximum intensity projections of the Z-stack SR-SIM images were generated and brightness/contrast was adapted.

5.2.4.7 Transferrin assay for immunofluoroscence microscopy

HeLa cells were grown on coverslips until 60% confluent. The cells were washed twice with PBS and starved for 30 min in serum-free medium containing 25 mM HEPES pH 7.4 and 0.5% BSA. The cells were washed with cold PBS and labeled with 20 µg/ml transferrin conjugated with Alexa Fluor™ 594 (Thermo Fisher) diluted in serum-free medium containing 25 mM HEPES pH 7.4 and 0.5% BSA for the indicated times at 37°C. The cells were washed with cold PBS and the cover slips were transferred to pre-warmed growth medium and placed in the incubator. The cells were chased for the indicated times, washed twice with cold PBS and fixed for 15 min with 3.7% formaldehyde in PBS.

5.2.4.8 Transferrin assay for FACS

HeLa cells were grown on 15 cm dishes until 80-90% confluent. The medium was removed and fresh medium containing DSMO, NMS-873 (10 µM) or CB-5083 (10 µM) was added for 3 h 30 min. The cells were washed twice with PBS and starved for 30 min in serum-free medium containing 25 mM HEPES pH 7.4 and 0.5 % BSA. DSMO, NMS-873 (10 µM) or CB-5083 (10 µM) was added to the respective plates. The cells were washed with PBS and incubated with 5 mM EDTA in PBS for 5 min at 37°C and the supernatant was removed. The cells were collected, harvested at 1300 x rpm, 3 min at 4°C and washed twice with cold PBS. One control sample without labeled transferrin was collected. Cell pellets were resuspended in 1 ml cold serum-free medium containing 25 mM HEPES pH 7.4, 0.5% BSA, 50 µg/ml transferrin conjugated with Alexa Fluor™ 594 and DSMO, NMS-873 (10 µM) or CB-5083 (10 µM). Cells were incubated at 37°C for 5 min and washed twice with cold PBS. Cell pellets were resuspended in pre-warmed growth medium containing, NMS-873 (10 µM) or CB-5083 (10 µM). The samples were aliquoted and incubated for the indicated times at 37°C. Then, the

samples were washed twice with cold PBS and resuspended in 1 ml cold PBS and placed on ice. The transferrin fluorescence signal was measured for 10 000 single cells with the Attune™ NxT Acoustic Focusing Cytometer (Laser: 561 nm, Detector/Channel: YL2; Filter: 620/15 nm) and the Attune™ NxT Software. The mean signal (YL2-A) from 10000 single cells was measured, background signal was subtracted and the data was normalized to time point 0 min. Mean values and standard deviation was calculated from three independent experiments and significance was determined by *t*-test (two tailed, unpaired, equal variance; *p≤0.05, **p≤0.01).

HeLa pINDUCER20 cell pools were grown on 15 cm dishes, induced with 500 ng/ml doxycycline for 22 h at a final confluence of 80-90%. The transferrin assay was performed as described above. All media used during the sample preparation contained 500 ng/ml doxycycline. The mean transferrin fluorescence signal was measured for 10000 single cells with the Attune™ NxT Acoustic Focusing Cytometer (Laser: 561 nm, Detector/Channel: YL2; Filter: 620/15 nm) and analyzed with the Attune™ NxT Software.

6 References

Akutsu, M., Dikic, I., & Bremm, A. (2016). Ubiquitin chain diversity at a glance. *Journal of Cell Science*, *129*(5), 875–880.

Arakel, E. C., & Schwappach, B. (2018). Formation of COPI-coated vesicles at a glance. *Journal of Cell Science*, *131*(7).

Arendt, C. S., & Hochstrasser, M. (1997). Identification of the yeast 20S proteasome catalytic centers and subunit interactions required for active-site formation. *Proc. Nati. Acad. Sci. USA*, *94*(14), 7156–7161.

Banerjee, S., Bartesaghi, A., Merk, A., Rao, P., Bulfer, S. L., Yan, Y., Green, N., Mroczkowski, B., Neitz, R. J., Wipf, P., Falconieri, V., Deshaies, R. J., Milne, J. L. S., Huryn, D., Arkin, M., & Subramaniam, S. (2016). 2.3 Å resolution cryo-EM structure of human p97 and mechanism of allosteric inhibition. *Science.*, *351*(6275), 871–875.

Barefield, D. Y., Sell, J. J., Tahtah, I., Kearns, S. D., McNally, E. M., & Demonbreun, A. R. (2021). Loss of dysferlin or myoferlin results in differential defects in excitation–contraction coupling in mouse skeletal muscle. *Scientific Reports*, *11*(1), 1–12.

Bernatchez, P. N., Sharma, A., Kodaman, P., & Sessa, W. C. (2009). Myoferlin is critical for endocytosis in endothelial cells. *American Journal of Physiology - Cell Physiology*, *297*(3), 484–492.

Beskow, A., Grimberg, K. B., Bott, L. C., Salomons, F. A., Dantuma, N. P., & Young, P. (2009). A Conserved Unfoldase Activity for the p97 AAA-ATPase in Proteasomal Degradation. *Journal of Molecular Biology*, *394*(4), 732–746.

Bodnar, N. O., & Rapoport, T. A. (2017a). Molecular Mechanism of Substrate Processing by the Cdc48 ATPase Complex. *Cell*, *169*(4), 722-735.e9.

Boom, J. Van Den, Kueck, A. F., Kravic, B., Müschenborn, H., Giesing, M., Pan, D., Kaschani, F., Kaiser, M., Musacchio, A., & Meyer, H. (2021). Targeted substrate loop insertion by VCP/p97 during PP1 complex disassembly. *Nature Structural & Molecular Biology*, *28*(December), 964–971.

Bottger, G., Nagelkerken, B., & Sluijs, P. Van Der. (1996). Rab4 and Rab7 Define Distinct Nonoverlapping Endosomal Compartments *. *Journal of Biological Chemistry*, *271*(46), 29191–29197.

Brandman, O., & Hegde, R. S. (2016). Ribosome-associated protein quality control. *Nat Struct Mol Biol.*, *23*(1), 7–15.

Buchan, J. R., Kolaitis, R., Taylor, J. P., & Parker, R. (2013). Eukaryotic stress granules are cleared by granulophagy and Cdc48 / VCP function. *Cell*, *153*(7), 1461–1474.

Buchberger, A., Schindelin, H., & Hänzelmann, P. (2015). Control of p97 function by cofactor binding. *FEBS Letters*, *589*(19), 2578–2589.

Bulankina, A. V., & Thoms, S. (2020). Functions of Vertebrate Ferlins. In *Cells* (Vol. 9, Issue 3).

Ciechanover, A., Elias, S., Heller, H., & Hershko, A. (1982). "Covalent affinity" purification of ubiquitin-activating enzyme. *The Journal of Biological Chemistry*, *257*(5), 2537–2542.

Ciechanover, A., Heller, H., Katz-Etzion, R., & Hershko, A. (1981). Activation of the heat-stable polypeptide of the ATP-dependent proteolytic system. *Proc. Nati. Acad. Sci. USA*, *78*(2), 761–765.

Clague, M. J., Liu, H., & Urbe, S. (2012). Review Governance of Endocytic Trafficking and Signaling by Reversible Ubiquitylation. *Developmental Cell*, *23*, 457–467.

Collins, G. A., & Goldberg, A. L. (2017). The Logic of the 26S Proteasome. *Cell*, *169*(5), 792–806.

Coux, O., Tanaka, K., & Goldberg, A. L. (1996). STRUCTURE AND FUNCTIONS OF THE 20S AND 26S. *Annual Review of Biochemistry*, *65*, 601–647.

Cullen, P. J., & Steinberg, F. (2018). To degrade or not to degrade: mechanisms and significance of endocytic recycling. *Nature Reviews Molecular Cell Biology*, *19*(november), 679–696.

Daro, E., Sluijst, P. V. A. N. D. E. R., & Galli, T. (1996). Rab4 and cellubrevin define different early endosome populations on the pathway of transferrin receptor recycling. *Proc. N. A. S.*, *93*, 9559–9564.

Davis, D. B., Delmonte, A. J., Ly, C. T., & Mcnally, E. M. (1999). Myoferlin, a candidate gene and potential modifier of muscular dystrophy. *Human Molecular Genetics*, *9*(2), 217–226.

Davis, D. B., Doherty, K. R., Delmonte, A. J., & McNally, E. M. (2002). Calcium-sensitive Phospholipid Binding Properties of Normal and Mutant Ferlin C2 Domains *. *Journal of Biological Chemistry*, *277*(25), 22883–22888.

DeLaBarre, B., & Brunger, A. T. (2003). Complete structure of p97/valosin-containing protein reveals communication between nucleotide domains. *Nature Structural Biology*, *10*(10), 856–863.

Demonbreun, A. R., Lapidos, K. A., Heretis, K., Levin, S., Dale, R., Pytel, P., Svensson, E. C., & McNally, E. M. (2010). Myoferlin regulation by NFAT in muscle injury, regeneration and repair. *Journal of Cell Science*, *123*(14), 2413–2422.

Demonbreun, A. R., Posey, A. D., Heretis, K., Swaggart, K. A., Earley, J. U., Pytel, P., & McNally, E. M. (2010). Myoferlin is required for insulin-like growth factor response and muscle growth. *The FASEB Journal*, *24*(4), 1284–1295.

Dobson, C. M., Andrej, S., & Karplus, M. (1998). Protein Folding : A Perspective from Theory and Experiment. *Angewandte Chemie*, *37*(7), 868–893.

Doherty, K. R., Cave, A., Davis, D. B., Delmonte, A. J., Earley, J. U., Hadhazy, M., & Mcnally, E. M. (2005). Normal myoblast fusion requires myoferlin. *Development*, *132*(24), 5565–5575.

Doherty, K. R., Demonbreun, A. R., Wallace, G. Q., Cave, A., Posey, A. D., Heretis, K., Pytel, P., & Mcnally, E. M. (2008). The Endocytic Recycling Protein EHD2 Interacts with Myoferlin to Regulate Myoblast Fusion *. *The Journal of Biological Chemistry*, *283*(29), 20252–20260.

Dowling, J. J., Gibbs, E. M., & Feldman, E. L. (2008). Membrane Traffic and Muscle: Lessons from Human Disease. *Traffic.*, *9*, 1035–1043.

Fang, S., & Weissman, a M. (2004). A field guide to ubiquitylation. *Cellular and Molecular Life Sciences : CMLS*, *61*(13), 1546–1561.

Fernández-Sáiz, V., & Buchberger, A. (2010). Imbalances in p97 co-factor interactions in human proteinopathy. *EMBO Reports*, *11*(6), 479–485.

Ferro, E., Bosia, C., & Campa, C. C. (2021). RAB11-Mediated Trafficking and Human Cancers: An Updated Review. *Biology*, *10*(26), 1–15.

Finley, D. (2009). Recognition and Processing of Ubiquitin-Protein Conjugates by the Proteasome. *Annu Rev Biochem.*, *78*, 477–513.

Fleming, A., Bourdenx, M., Fujimaki, M., Karabiyik, C., Krause, G. J., Lopez, A., Martín-Segura, A., Puri, C., Scrivo, A., Skidmore, J., Son, S. M., Stamatakou, E., Wrobel, L., Zhu, Y., Cuervo, A. M., & Rubinsztein, D. C. (2022). The different autophagy degradation pathways and neurodegeneration. *Neuron*, *110*, 935–966.

Franz, A., Ackermann, L., & Hoppe, T. (2016). Ring of Change : CDC48 / p97 Drives Protein Dynamics at Chromatin. *Frontiers in Genetics*, *7*(May), 1–14.

French, M. E., Koehler, C. F., & Hunter, T. (2021). Emerging functions of branched ubiquitin chains. *Cell Discovery*, *7*(1).

Gamayun, I., O'Keefe, S., Pick, T., Klein, M. C., Nguyen, D., McKibbin, C., Piacenti, M., Williams, H. M., Flitsch, S. L., Whitehead, R. C., Swanton, E., Helms, V., High, S., Zimmermann, R., & Cavalié, A. (2019). Eeyarestatin Compounds Selectively Enhance Sec61-Mediated Ca 2+ Leakage from the Endoplasmic Reticulum. *Cell Chemical Biology*, *26*(4), 571-583.e6.

Gershlick, D. C., & Lucas, M. (2017). Endosomal Trafficking: Retromer and Retriever Are Relatives in Recycling. *Current Biology*, *27*(22), R1233–R1236.

Glickman, M. H., & Ciechanover, A. (2002). The ubiquitin-proteasome proteolytic pathway: destruction for the sake of construction. *Physiological Reviews*, *82*(2), 373–428.

Goldstein, G., Scheid, M., Hammerling, U., Schlesinger, D. H., Niall, H. D., & Boyse, E. a. (1975). Isolation of a polypeptide that has lymphocyte-differentiating properties and is probably represented universally in living cells. *Proceedings of the National Academy of Sciences of the United States of America*, *72*(1), 11–15.

Groll, M., Ditzel, L., Löwe, J., Stock, D., Bochtler, M., Bartunik, H., & Huber, R. (1997). Structure of 20S proteasmome from yeast at 2.4 A resolution. *Nature*, *386*(3), 463–471.

Guerra, F., & Bucci, C. (2016). Multiple Roles of the Small GTPase Rab7. *Cells*, *5*(34), 1–28.

Gundry, C., Marco, S., Rainero, E., Miller, B., Dornier, E., Mitchell, L., Caswell, P. T., Campbell, A. D., Hogeweg, A., Sansom, O. J., Morton, J. P., & Norman, J. C. (2017). Phosphorylation of Rab-coupling protein by LMTK3 controls Rab14-dependent EphA2 trafficking to promote cell:cell repulsion. *Nature Communications*, *8*, 1–15.

Gupta, S., Yano, J., Mercier, V., Htwe, H., Shin, H., Rademaker, G., Cakir, Z., Ituarte, T., Wen, K., Kim, G., Zoncu, R., Roux, A., Dawson, D., & RM, P. (2021). Lysosomal retargeting of Myoferlin mitigates membrane stress to enable 2 pancreatic cancer growth. *Nat Cell Biol*, *23*(March), 232–242.

Haines, D. S., Lee, J. E., Beauparlant, S. L., Kyle, D. B., Den Besten, W., Sweredoski, M. J., Graham, R. L. J., Hess, S., & Deshaies, R. J. (2012). Protein interaction profiling of the p97 adaptor UBXD1 points to a role for the complex in modulating ERGIC-53 trafficking. *Molecular and Cellular Proteomics*, *11*(6), 1–11.

Hales, C. M., Griner, R., Hobdy-henderson, K. C., Dorn, M. C., Hardy, D., Kumar, R., Navarre, J., Chan, E. K. L., Lapierre, L. A., & Goldenring, J. R. (2001). Identification and Characterization of a Family of Rab11-interacting Proteins *. *Journal of Biological Chemistry*, *276*(42), 39067–39075.

Hall, E. A., Nahorski, M. S., Murray, L. M., Shaheen, R., Perkins, E., Dissanayake, K. N., Kristaryanto, Y., Jones, R. A., Vogt, J., Rivagorda, M., Handley, M. T., Mali, G. R., Quidwai, T., Soares, D. C., Keighren, M. A., McKie, L., Mort, R. L., Gammoh, N., Garcia-Munoz, A., … Mill, P. (2017). PLAA Mutations Cause a Lethal Infantile Epileptic Encephalopathy by Disrupting Ubiquitin-Mediated Endolysosomal Degradation of Synaptic Proteins. *American Journal of Human Genetics*, *100*(5), 706–724.

Hänzelmann, P., Galgenmüller, C., & Schindelin, H. (2019). Structure and Function of the AAA+ ATPase p97, a Key Player in Protein Homeostasis. In *Subcellular Biochemistry* (Vol. 93).

Hänzelmann, P., & Schindelin, H. (2017). The Interplay of Cofactor Interactions and Post-translational Modifications in the Regulation of the AAA + ATPase p97. *Frontiers in Molecular Biosciences |*, *4*(April), 1–22.

Hayer, A., Stoeber, M., Ritz, D., Engel, S., Meyer, H. H., & Helenius, A. (2010). Caveolin-1 is ubiquitinated and targeted to intralumenal vesicles in endolysosomes for degradation. *Journal of Cell Biology*, *191*(3), 615–629.

He, Y., Kan, W., Li, Y., Hao, Y., Huang, A., Gu, H., Wang, M., Wang, Q., Chen, J., Sun, Z., Liu, M., Chen, Y., & Yi, Z. (2021). A potent and selective small molecule inhibitor of myoferlin attenuates colorectal cancer progression. *Clinical and Translational Medicine*, *11*(2).

Henne, W. M., Buchkovich, N. J., & Emr, S. D. (2011). The ESCRT Pathway. *Developmental Cell*, *21*, 77–91.

Heo, J. M., Livnat-Levanon, N., Taylor, E. B., Jones, K. T., Dephoure, N., Ring, J., Xie, J., Brodsky, J. L., Madeo, F., Gygi, S. P., Ashrafi, K., Glickman, M. H., & Rutter, J. (2010). A Stress-Responsive System for Mitochondrial Protein Degradation. *Molecular Cell*, *40*(3), 465–480.

Her, N.-G., Toth, J. I., Ma, C.-T., Wei, Y., Motamedchaboki, K., Sergienko, E., & Petroski, M. D. (2016). p97 composition changes caused by allosteric inhibition are suppressed by an on-target mechanism that increases the enzyme's ATPase activity. *Cell Chem Biol.*, *23*(4), 517–528.

Hershko, A., & Ciechanover, A. (1998). The ubiquitin system. *Annual Review of Biochemistry*, *67*, 425–479.

Hershkos, A., Heller, H., Elias, S., & Ciechanover, A. (1983). Components of Ubiquitin-Protein Ligase System. *The Journal of Biological Chemistry*, *258*(13), 8206–8214.

Homma, Y., Hiragi, S., & Fukuda, M. (2021). Rab family of small GTPases : an updated view on their regulation and functions. *The FEBS Journal 288*, *288*, 36–55.

Hui, E., Johnson, C. P., Yoa, J., Dunning, F. M., & Chapman, E. R. (2012). Synaptotagmin-mediated bending of the target membrane is a critical step in Ca2+ -regulated fusion. *Bone*, *23*(1), 1–7.

Huotari, J., & Helenius, A. (2011). Endosome maturation. *EMBO Journal*, *30*(17), 3481–3500.

Jackson, M. P., & Hewitt, E. W. (2016). Cellular proteostasis: Degradation of misfolded proteins by lysosomes. *Essays in Biochemistry*, *60*(2), 173–180.

Jayaraj, G. G., Hipp, M. S., & Ulrich Hartl, F. (2019). Functional modules of the proteostasis network. *Cold Spring Harbor Perspectives in Biology*, *12*(1).

Ji, Z., Li, H., Peterle, D., Paulo, J. A., Ficarro, S. B., Wales, T. E., Marto, J. A., Gygi, S. P., Engen, J. R., & Rapoport, T. A. (2022). Translocation of polyubiquitinated protein substrates by the hexameric Cdc48 ATPase. *Angewandte Chemie International Edition*, *82*(3), 570–584.

Jovic, M., Sharma, M., Rahajeng, J., & Caplan, S. (2010). The early endosome: a busy sorting station for proteins at the crossroads. *Histol Histopathol.*, *25*(1), 99–112. ht

Ju, J.-S., Fuentealba, R. A., Miller, S. E., Jackson, E., Piwnica-Worms, D., Baloh, R. H., & Weihl, C. C. (2009). Valosin-containing protein (VCP) is required for autophagy and is disrupted in VCP disease. *Journal of Cell Biology*, *187*(6), 875–888.

Junutula, J. R., De Maziere, A. M., Peden, A. A., Ervin, K. E., Advani, R. J., van Dijk, S. M., Klumperman, J., & Scheller, R. H. (2004). Rab14 Is Involved in Membrane Trafficking between the Golgi Complex and Endosomes. *Molecular Biology of the Cell*, *15*(May), 2218–2229.

Kaur, J., & Debnath, J. (2015). Autophagy at the crossroads of catabolism and anabolism. *Nature Reviews Molecular Cell Biology*, *16*(8), 461–472.

Kawabata, H. (2019). Transferrin and transferrin receptors update. *Free Radical Biology and Medicine*, *133*, 46–54.

Kelly, E. E., Horgan, C. P., Goud, B., & Mccaffrey, M. W. (2012). The Rab family of proteins : 25 years on. *Biochem. Soc. Trans.*, *June*, 1337–1347.

Kelly, E., Horgan, C. P., Adams, C., Patzer, T. M., Ni Shuilleabhain, D MNorman, J. C., & Mccaffrey, M. W. (2010). Class I Rab11-family interacting proteins are binding targets for the Rab14 GTPase. *Biol. Cell (2010)*, *102*(1), 51–62.

Kim, Y. E., Hipp, M. S., Bracher, A., Hayer-Hartl, M., & Hartl, F. U. (2013). Molecular chaperone functions in protein folding and proteostasis. In *Annual review of biochemistry* (Vol. 82).

Kirchner, P., Bug, M., & Meyer, H. (2013). Ubiquitination of the n-terminal region of caveolin-1 regulates endosomal sorting by the VCP/p97 AAA-ATPase. *Journal of Biological Chemistry*, *288*(10), 7363–7372.

Kiselev, A., Vaz, R., Knyazeva, A., Sergushichev, A., Dmitrieva, R., Khudiakov, A., Jorholt, J., Smolina, N., Sukhareva, K., Fomicheva, Y., Mikhaylov, E., Mitrofanova, L., Predeus, A., Sjoberg, G., Rudenko, D., Sejersen, T., Lindstrand, A., & Kostareva, A. (2019). Truncating variant in myof gene is associated with limb-girdle type muscular dystrophy and cardiomyopathy. *Frontiers in Genetics*, *10*(JUN), 1–10.

Komander, D., & Rape, M. (2012). The ubiquitin code. *Annual Review of Biochemistry*, *81*, 203–229.

Kondo, H., Rabouille, C., Newman, R., Levine, T. P., Pappin, D., Freemont, P., & Warren, G. (1997). p47 is a cofactor for p97- mediated membrane fusion. *Letters to Nature*, *7184*, 75–78.

Korb, M. K., Kimonis, V. E., & Mozaffar, T. (2020). Multisystem proteinopathy: Where myopathy and motor neuron disease converge. *Muscle and Nerve*, *63*(4), 442–454.

Körner/Schultz, M. (2018). *Bachelor's Thesis: Proteomische Analyse endogener p97-Kofaktor-Interaktionen*.

Kumari, S., Mg, S., & Mayor, S. (2010). Endocytosis unplugged : multiple ways to enter the cell. *Cell Research*, *20*, 256–275.

Labbadia, J., & Morimoto, R. I. (2015). The biology of proteostasis in aging and disease. *Annual Review of Biochemistry*, *84*, 435–464.

Leventis, P. A., & Grinstein, S. (2010). The Distribution and Function of Phosphatidylserine in Cellular Membranes. *Annual Review of Biophysics*, *39*, 407–427.

Li, X., & DiFiglia, M. (2012). The recycling endosome and its role in neurological disorders. *Progress in Neurobiology, 97*(2), 127–141.

Linford, A., Yoshimura, S. I., Bastos, R. N., Langemeyer, L., Gerondopoulos, A., Rigden, D. J., & Barr, F. A. (2012). Rab14 and Its Exchange Factor FAM116 Link Endocytic Recycling and Adherens Junction Stability in Migrating Cells. *Developmental Cell*, *22*(5), 952–966.

Lopata, A., Kniss, A., Löhr, F., Rogov, V. V., & Dötsch, V. (2020). Ubiquitination in the erad process. *International Journal of Molecular Sciences*, *21*(15), 1–21.

Madeo, F., Schlauer, J., Zischka, H., Mecke, D., & Fro, K. (1998). Tyrosine Phosphorylation Regulates Cell Cycle- dependent Nuclear Localization of Cdc48p. *Molecular Biology of the Cell*, *9*(January), 131–141.

Magnaghi, P., D'Alessio, R., Valsasina, B., Avanzi, N., Rizzi, S., Asa, D., Gasparri, F., Cozzi, L., Cucchi, U., Orrenius, C., Polucci, P., Ballinari, D., Perrera, C., Leone, A., Cervi, G., Casale, E., Xiao, Y., Wong, C., Anderson, D. J., … Isacchi, A. (2013). Covalent and allosteric inhibitors of the ATPase VCP/p97 induce cancer cell death. *Nature Chemical Biology*, *9*(9), 548–559.

Marty, N. J., Holman, C. L., Abdullah, N., & Johnson, C. P. (2014). The C2 Domains of Otoferlin, Dysferlin, and Myoferlin Alter the Packing of Lipid Bilayers. *Biochemistry*, *52*(33).

Mauthe, M., Orhon, I., Rocchi, C., Zhou, X., Luhr, M., & Hijlkema, K. (2018). Chloroquine inhibits autophagic flux by decreasing autophagosome-lysosome fusion. *Autophagy*, *14*(8), 1435–1455.

Maxfield, F. R., & Mcgraw, T. E. (2004). ENDOCYTIC RECYCLING. *Nature Reviews Molecular Cell Biology*, *5*(February), 121–132.

Mayle, M. K., Le, M. A., & Kamei, D. (2012). The Intracellular Trafficking Pathway of Transferrin. *Biochim Biophys Acta*, *23*(1), 1–7.

Mayor, S., & Pagano, R. E. (2007). Pathways of clathrin-independent endocytosis. *Nature Reviews Molecular Cell Biology*, *8*(August), 603–612.

Mayor, S., Preslely, J. F., & Maxfield, F. R. (1993). Sorting of Membrane Components from Endosomes and Subsequent Recycling to the Cell Surface Occurs by a Bulk Flow Process. *The Journal of Cell Biology*, *121*(6), 1257–1269.

Meerbrey, K. L., Hu, G., Kessler, J. D., Roarty, K., Li, M. Z., Fang, J. E., Herschkowitz, J. I., Burrows, A. E., Ciccia, A., Sun, T., Schmitt, E. M., Bernardi, R. J., Fu, X., Bland, C. S., Cooper, T. A., Schiff, R., Rosen, J. M., Westbrook, T. F., & Elledge, S. J. (2011). The pINDUCER lentiviral toolkit for inducible RNA interference in vitro and in vivo. *Proceedings of the National Academy of Sciences of the United States of America*, *108*(9), 3665–3670.

Metzger, M. B., Hristova, V. A., & Weissman, A. M. (2012). HECT and RING finger families of E3 ubiquitin ligases at a glance. *Journal of Cell Science*, *125*(3), 531–537.

Meyer, H., Bug, M., & Bremer, S. (2012). Emerging functions of the VCP / p97 AAA-ATPase in the ubiquitin system. *Nature Cell Biology*, *14*(2), 117–123.

Meyer, H., & Weihl, C. C. (2014). The VCP/p97 system at a glance: Connecting cellular function to disease pathogenesis. *Journal of Cell Science*, *127*(18), 3877–3883.

Miyatake, Y., Yamano, T., & Hanayama, R. (2018). Myoferlin-Mediated Lysosomal Exocytosis Regulates Cytotoxicity by Phagocytes. *The Journal of Immunology*, *201*(10), 3051–3057.

Mullally, J. E., Chernova, T., & Wilkinson, K. D. (2006). Doa1 Is a Cdc48 Adapter That Possesses a Novel Ubiquitin Binding Domain. *Molecular and Cellular Biology*, *26*(3), 822–830.

Nalbandian, A., Donkervoort, S., Dec, E., Badadani, M., Katheria, V., Rana, P., Nguyen, C., Mukherjee, J., Caiozzo, V., Martin, B., Watts, G. D., Vesa, J., Smith, C., & Kimonis, V. E. (2011). The multiple faces of valosin-containing protein-associated diseases: Inclusion body myopathy with Paget's disease of bone, frontotemporal dementia, and amyotrophic lateral sclerosis. *Journal of Molecular Neuroscience*, *45*(3), 522–531.

Naslavsky, N., & Caplan, S. (2011). EHD proteins: Key conductors of endocytic transport. *Trends Cell Biol.*, *21*(2), 122–131. https://doi.org/10.1016/j.tcb.2010.10.003.EHD

Naslavsky, N., & Caplan, S. (2018). The enigmatic endosome – sorting the ins and outs of endocytic trafficking. *Journal of Cell Science*, *131*. https://doi.org/10.1242/jcs.216499

Ohashi, Y. (2021). Activation mechanisms of the vps34 complexes. *Cells*, *10*(11). https://doi.org/10.3390/cells10113124

Olszewski, M. M., Williams, C., Dong, K. C., & Martin, A. (2019). The Cdc48 unfoldase prepares well-folded protein substrates for degradation by the 26S proteasome. *Communications Biology*, *2*(1). https://doi.org/10.1038/s42003-019-0283-z

Papadopoulos, C., Kirchner, P., Bug, M., Grum, D., Koerver, L., Schulze, N., Poehler, R., Dressler, A., Fengler, S., Arhzaouy, K., Lux, V., Ehrmann, M., Weihl, C. C., & Meyer, H. (2017). VCP/p97 cooperates with YOD1, UBXD1 and PLAA to drive clearance of ruptured lysosomes by autophagy. *The EMBO Journal Vol*, *36*(2), 135–150. https://doi.org/10.15252/embj.201695148

Pavlos, N. J., Grønborg, M., Riedel, D., Chua, J. J. E., Boyken, J., Kloepper, T. H., Urlaub, H., Rizzoli, S. O., & Jahn, R. (2010). Quantitative analysis of synaptic vesicle Rabs uncovers distinct yet overlapping roles for Rab3a and Rab27b in Ca2+-triggered exocytosis. *Journal of Neuroscience*, *30*(40), 13441–13453. https://doi.org/10.1523/JNEUROSCI.0907-10.2010

Peden, A., Schonteich, E., Chun, J., Junutula, J. R., Scheller, R. H., & Prekeris, R. (2004). The RCP–Rab11 Complex Regulates Endocytic Protein Sorting. *Molecular Biology of the Cell*, *15*(August), 3530–3541.

Peters, J. M., Walsh, M. J., & Franke, W. W. (1990). An abundant and ubiquitous homo-oligomeric ring-shaped ATPase particle related to the putative vesicle fusion proteins Sec18p and NSF. *EMBO Journal*, *9*(6), 1757–1767.

Peulen, O., Rademaker, G., Anania, S., Turtoi, A., Bellahcène, A., & Castronovo, V. (2019). Ferlin Overview: From Membrane to Cancer Biology. *Cells*, *8*(9), 1–21.

Pickart, C. M. (2001). Mechanisms underlying ubiquitination. *Annual Review of Biochemistry*, *70*, 503–533.

Piper, R. C., Dikic, I., & Lukacs, G. L. (2014). Ubiquitin-Dependent Sorting in Endocytosis. *Cold Spring Harb Perspect Biol*, *6*, 1–21.

Pohl, C., & Dikic, I. (2019). Cellular quality control by the ubiquitin-proteasome system and autophagy. *Science*, *366*(6467), 818–822. https://doi.org/10.1126/science.aax3769

Posey, A. D., Pytel, P., Gardikiotes, K., Demonbreun, A. R., Rainey, M., George, M., Band, H., & Mcnally, E. M. (2011). Endocytic Recycling Proteins EHD1 and EHD2 Interact with Fer-1-like-5 (Fer1L5) and Mediate Myoblast Fusion * □. *The Journal of Biological Chemistry*, *286*(9), 7379

Poteryaev, D., Datta, S., Ackema, K., Zerial, M., & Spang, A. (2010). Identification of the Switch in Early-to-Late Endosome Transition. *Cell*, *141*(3), 497–508.

Princiotto, J. V., & Zapolski, E. J. (1976). Functional heterogeneity and pH-dependent dissociation properties of human transferrin. *BBA - General Subjects*, *428*(3), 766–771.

Proikas-Cezanne, T., Gaugel, A., Frickey, T., & Nordheim, A. (2006). Rab14 is part of the early endosomal clathrin-coated TGN microdomain. *FEBS Letters*, *580*(22), 5241–5246.

Rabouille, C., Levine, T. P., Peters, J., & Warren, G. (1995). An NSF-like ATPase , p97 , and NSF Mediate Cisternal Regrowth from Mitotic Golgi Fragments. *Cell*, *82*(September), 905–914.

Raman, M., Sergeev, M., Gernaas, M., Lydeard, J. R., Huttlin, E. L., Goessling, W., Shah, J. V, & Harper, J. W. (2015). Systematic VCP-UBXD Adaptor Network Proteomics Identifies a Role for UBXN10 in Regulating Ciliogenesis. *Nat Cell Biol. 2015*, *17*(10), 1356–1369.

Ramanathan, H. N., & Ye, Y. (2012). The p97 ATPase associates with EEA1 to regulate the size of early endosomes. *Cell Research*, *22*(2), 346–359. 0

Redpath, G. M. I., Sophocleous, R. A., Turnbull, L., Whitchurch, C. B., & Cooper, S. T. (2016). Ferlins Show Tissue-Specific Expression and Segregate as Plasma Membrane/Late Endosomal or Trans-Golgi/Recycling Ferlins. *Traffic*, *17*(3), 245–266.

Reed, S. E., Hodgson, L. R., Song, S., May, M. T., Kelly, E. E., McCaffrey, M. W., Mastick, C. C., Verkade, P., & Tavare, J. M. (2013). A role for Rab14 in the endocytic trafficking of GLUT4 in 3T3-L1 adipocytes. *Journal of Cell Science*, *126*(9), 1931–1941.

Rink, J., Ghigo, E., Kalaidzidis, Y., & Zerial, M. (2005). Rab conversion as a mechanism of progression from early to late endosomes. *Cell*, *122*(5), 735–749.

Ritz, D., Vuk, M., Kirchner, P., Bug, M., Schütz, S., Bremer, S., Lusk, C., Baloh, R. H., Lee, H., Glatter, T., Gstaiger, M., Aebersold, R., Weihl, C. C., & Meyer, H. (2011b). Endolysosomal sorting of ubiquitinated caveolin-1 is regulated by VCP/p97 and UBXD1 and impaired by VCP disease mutations. *Nat Cell Biology*, *13*(9), 1116–1123.

Rosenfeld, J. L., Moore, R. H., Zimmer, K. P., Alpizar-Foster, E., Dai, W., Nader Zarka, M., & Knoll, B. J. (2001). Lysosome proteins are redistributed during expression of a GTP-hydrolysis-defective rab5a. *Journal of Cell Science*, *114*(24), 4499–4508.

Rosey, A. jr, Demonbreun, A., & McNally, E. (2011). Ferlin proteins in myoblast fusion and muscle growth. *Curr Top Dev Biol*, *96*(12), 203–230.

Rouiller, I., DeLaBarre, B., May, A. P., Weis, W. I., Brunger, A. T., Milligan, R. A., & Wilson-kubalek, E. M. (2002). Conformational changes of the multifunction p97 AAA ATPase during its ATPase cycle. *950 Nature Structural Biology •*, *9*(January), 950–957.

Saftig, P., & Klumperman, J. (2009). Lysosome biogenesis and lysosomal membrane proteins : trafficking meets function. *Nature Reviews Molecular Cell Biology*, *10*(September), 623–635.

Schnell, J. D., & Hicke, L. (2003). Non-traditional functions of ubiquitin and ubiquitin-binding proteins. *The Journal of Biological Chemistry*, *278*(38), 35857–35860.

Schuetz, A. K., & Kay, L. E. (2016). A dynamic molecular basis for malfunction in disease mutants of p97/VCP. *ELife*, *5*(NOVEMBER2016), 1–25.

Sönnichsen, B., De Renzis, S., Nielsen, E., Rietdorf, J., & Zerial, M. (2000). Distinct membrane domains

on endosomes in the recycling pathway visualized by multicolor imaging of Rab4, Rab5, and Rab11. *Journal of Cell Biology*, *149*(4), 901–913.

Sula, A., Cole, A. R., Yeats, C., Orengo, C., & Keep, N. H. (2014). Crystal structures of the human Dysferlin inner DysF domain. *BMC Structural Biology*, *14*, 1–9.

Sullivan, M. J. O., & Lindsay, A. J. (2020). The Endosomal Recycling Pathway — At the Crossroads of the Cell. *International Journal of Molecular Sciences*, *21*.

Tang, W. K., & Xia, D. (2016). Mutations in the Human AAA + Chaperone p97 and Related Diseases. *Frontiers in Molecular Biosciences |*, *3*(December), 1–12.

Taylor, E., & Rutter, J. (2011). Mitochondrial quality control by the ubiquitin-proteasome system. *Biochem Soc Trans.*, *39*(5), 21936843.

Thrower, J. S., Hoffman, L., Rechsteiner, M., & Pickart, C. M. (2000). Recognition of the polyubiquitin proteolytic signal. *The EMBO Journal*, *19*(1), 94–102.

Tresse, E., Salomons, F. A., Vesa, J., Bott, L. C., Kimonis, V., Yao, P., Dantuma, N. P., & Taylor, J. P. (2010). VCP/p97 is essential for maturation of ubiquitin-containing autophagosomes and this function is impaired by mutations that cause IBMPFD. *Autophagy*, *6*(2), 217–227.

Tu, Y., Zhao, L., Billadeau, D. D., & Jia, D. (2020). Endosome-to-TGN Trafficking : Organelle-Vesicle and Organelle-Organelle Interactions. *Frontiers in Cell and Developmental Biology*, *8*(March).

Turakhiya, A., Meyer, S. R., Marincola, G., Schlosser, A., & Hofmann, K. (2018). ZFAND1 Recruits p97 and the 26S Proteasome to Promote the Clearance of Arsenite-Induced Stress Granules. *Molecular Cell*, *70*, 906–919.

Turtoi, A., Blomme, A., Baellahcene, A., Gilles, C., Hennequi, V., Peixoto, P., Bianchi, E., Noel, A., Pauw, E. De, Lifrange, E., & Delvenne, P. (2013). Myoferlin Is a Key Regulator of EGFR Activity in Breast Cancer. *Cancer Res*, *2*(17), 5438–5449.

Ullrich, O., Reinsch, S., Urbe, S., Zerial, M., & Parton, R. G. (1996). Rab11 Regulates Recycling through the Pericentriolar Recycling Endosome. *The Journal of Cell Biology*, *135*(4), 913–924.

van den Boom, J., & Meyer, H. (2018). VCP/p97-Mediated Unfolding as a Principle in Protein Homeostasis and Signaling. *Molecular Cell*, *69*(2), 182–194.

Vesa, J., Su, H., Watts, G. D., Krause, S., Walter, M. C., Wallace, D. C., & Kimonis, V. E. (2009). Valosin containing protein associated inclusion body myopathy: abnormal vacuolization, autophagy and cell fusion in myoblasts. *Neuromuscul Disord*, *19*(NOvember), 1–7.

Vietri, M., Radulovic, M., & Stenmark, H. (2020). The many functions of ESCRTs. *Nature Reviews Molecular Cell Biology*, *21*(January), 25–42.

Walden, H., & Rittinger, K. (2018). RBR ligase-mediated ubiquitin transfer: A tale with many twists and turns. *Nature Structural and Molecular Biology*, *25*(6), 440–445.

Wandinger-Ness, A., & Zerial, M. (2014). Rab proteins and the compartmentalization of the endosomal system. *Cold Spring Harbor Perspectives in Biology*, *6*(11).

Wang, Y., Ballar, P., Zhong, Y., Zhang, X., Liu, C., Zhang, Y., & Mervyn, J. (2011). SVIP Induces Localization of p97 / VCP to the Plasma and Lysosomal Membranes and Regulates Autophagy. *PLoS ONE*, *6*(8).

Weihl, C. C., Dalal, S., Pestronk, A., & Hanson, P. I. (2006). Inclusion body myopathy-associated

mutations in p97 / VCP impair endoplasmic reticulum-associated degradation. *Human Molecular Genetics*, *15*(2), 189–199.

Weith, M., Seiler, J., van den Boom, J., Kracht, M., Hülsmann, J., Primorac, I., del Pino Garcia, J., Kaschani, F., Kaiser, M., Musacchio, A., Bollen, M., & Meyer, H. (2018). Ubiquitin-Independent Disassembly by a p97 AAA-ATPase Complex Drives PP1 Holoenzyme Formation. *Molecular Cell*, *72*(4), 766-777.e6.

Wolf, D. H., & Hilt, W. (2004). The proteasome: a proteolytic nanomachine of cell regulation and waste disposal. *Biochimica et Biophysica Acta*, *1695*(1–3), 19–31.

Xu, L., Pallikkuth, S., Hou, Z., Mignery, G. A., Robia, S. L., & Han, R. (2011). Dysferlin Forms a Dimer Mediated by the C2 Domains and the Transmembrane Domain In Vitro and in Living Cells. *PLoS ONE*, *6*(11).

Xue, L., Blythe, E. E., Freiberger, E. C., Mamrosh, J. L., Hebert, A. S., Reitsma, J. M., Hess, S., Coon, J. J., & Deshaies, R. J. (2016). Valosin-containing protein (VCP)-adaptor interactions are exceptionally dynamic and subject to differential modulation by a VCP inhibitor. *Molecular and Cellular Proteomics*, *15*(9), 2970–2986.

Yamamoto, H., Koga, H., Katoh, Y., Takahashi, S., Nakayama, K., & Shin, H. W. (2010). Functional cross-talk between Rab14 and Rab4 through a dual effector, RUFY1/Rabip4. *Molecular Biology of the Cell*, *21*(15), 2746–2755.

Yarwood, R., Hellicar, J., Woodman, P. G., & Lowe, M. (2020). Membrane trafficking in health and disease. *DMM Disease Models and Mechanisms*, *13*(4). https://doi.org/10.1242/dmm.043448

Ye, Y., Meyer, H. H., & Rapoport, T. A. (2001). The AAA ATPase Cdc48 / p97 and its partners transport proteins from the ER into the cytosol. *Letters to Nature*, *414*(December), 6–10.

Ye, Y., Meyer, H. H., & Rapoport, T. A. (2003). Function of the p97-Ufd1-Npl4 complex in retrotranslocation from the ER to the cytosol: Dual recognition of nonubiquitinated polypeptide segments and polyubiquitin chains. *Journal of Cell Biology*, *162*(1), 71–84.

Yip, M. C. J., Keszei, A. F. A., Feng, Q., Chu, V., McKenna, M. J., & Shao, S. (2019). Mechanism for recycling tRNAs on stalled ribosomes. *Nature Structural and Molecular Biology*, *26*(5), 343–349.

Zhang, T., Li, J., He, Y., Yang, F., Hao, Y., Jin, W., Wu, J., Sun, Z., Li, Y., Chen, Y., Yi, Z., & Liu, M. (2018). A small molecule targeting myoferlin exerts promising anti-tumor effects on breast cancer. *Nature Communications*, *9*(1), 1–13.

Zhen, Y., & Stenmark, H. (2015). Cellular functions of Rab GTPases at a glance. *Journal of Cell Science*, *128*, 3171–3176.

Zhou, H. J., Wang, J., Yao, B., Wong, S., Djakovic, S., Kumar, B., Rice, J., Valle, E., Soriano, F., Menon, M. K., Madriaga, A., Kiss Von Soly, S., Kumar, A., Parlati, F., Yakes, F. M., Shawver, L., Le Moigne, R., Anderson, D. J., Rolfe, M., & Wustrow, D. (2015). Discovery of a First-in-Class, Potent, Selective, and Orally Bioavailable Inhibitor of the p97 AAA ATPase (CB-5083). *Journal of Medicinal Chemistry*, *58*(24), 9480–9497. https://doi.org/10.1021/acs.jmedchem.5b01346

Zhu, W., Zhou, B., Zhao, C., Ba, Z., Xu, H., Yan, X., Liu, W., Zhu, B., Wang, L., & Ren, C. (2019). Myoferlin, a multifunctional protein in normal cells, has novel and key roles in various cancers. *Journal of Cellular and Molecular Medicine*, *23*(11), 7180–7189.

7 Appendix

7.1 Mass spectrometry analysis: p97 interactome without crosslinking

Table 14: Mass spectrometry analysis for p97 binding proteins without crosslinking. Gene names of positive enriched interactors are shown (n=3), with significance levels of 0, 1, or 2.

Gene name	significance	Gene name	significance	Gene name	significance	Gene name	significance
ACTN4	0	FASN	0	PDE12	0	TUBB6	0
AHCY	0	FSCN1	0	PDIA3	0	TUFM	0
AHNAK	0	FUBP1	0	PGAM1;		UBAP2	0
ALDOA	0	FUS	0	PGAM2	0	UBAP2L	0
ANXA1	0	G6PD	0	PGK1	0	VCL	0
ANXA7	0	GAPDH	0	PHB	0	VIM	0
ATP5A1	0	GBE1	0	PHGDH	0	XRCC6	0
ATP5B	0	GNAI2	0	PKM	0	YTHDF3	0
ATXN2L	0	GNB2L1	0	PNMA2	0	CALR	1
BAG4	0	GOT2	0	PPP1R7	0	CKAP4	1
BASP1	0	GRPEL1	0	PPP2R1A	0	COPA	1
CALD1	0	HADHA	0	PRKCSH	0	IMPDH2	1
CASP14	0	HADHB	0	PRPF39	0	LDHA	1
CCT2	0	HLA-A	0	PSMB6	0	LDHB	1
CCT3	0	HNRNPA3	0	RBM14	0	LUZP1	1
CCT4	0	HNRNPD	0	RNMT	0	PHLDB2	1
CCT6A	0	HNRNPD	0	RPL22	0	RPA1	1
CCT8	0	HNRNPF	0	RPN1	0	RPS15A	1
CDKN2AIP	0	HNRNPK	0	RPS14	0	YWHAZ	1
COPB2	0	HNRNPM	0	RPS21	0	ASPSCR1	2
CPSF7	0	HSP90AA1	0	RPS3	0	CAMSAP2	2
CRBN	0	HSP90AB1;		RPSA	0	CAV1	2
CSTF1	0	HSP90AB3P	0	RTCB	0	FAF2	2
CTTN	0	HSP90B1	0	RUVBL1	0	GOLGA3	2
DARS	0	HSPA5	0	RUVBL2	0	NPLOC4	2
DAZAP1	0	HSPB1	0	SDHA	0	NSFL1C	2
DCD	0	HSPD1	0	SEC16A	0	OSBPL3	2
DDOST	0	HSPE1	0	SEC23A	0	PFN1	2
DDX17	0	IGF2BP3	0	SEC31A	0	PRDX1	2
DDX3X;		KHDRBS1	0	SFPQ	0	PRKCDBP	2
DDX3Y	0	KIF7	0	SLC25A5	0	PTRF	2
DDX5	0	KPNA2	0	SLC3A2	0	RPS20	2
DHX9	0	LANCL1	0	SMARCB1	0	RPS27A;	
DNAJA1	0	LGALS3BP	0	SMARCE1	0	UBB;	
DSP	0	LMNA	0	STOM	0	UBC;	
DYNC1H1	0	MAP4	0	SYVN1	0	UBA52	2
EEF1A1P5;		MATR3	0	TAF15	0	SCYL2	2
EEF1A1;		MRPS2	0	TCP1	0	SNRPD2	2
EEF1A2	0	MRPS22	0	TFRC	0	UBXN6	2
EEF1G	0	MRPS23	0	TIA1	0	UFD1L	2
EIF4A1	0	MRPS9	0	TKT	0	VCP	2
ENDOD1	0	MSN	0	TLN1	0	YWHAG	2
ENO1	0	NCL	0	TPI1	0		
ERAL1	0	NONO	0	TPM3;			
ERLIN1	0	NUDC	0	DKFZp686J1372	0		
EZR	0	PAICS	0	TRNAU1AP	0		
FAM120A	0	PCBP1	0	TUBA1B	0		
		PDCD6IP	0	TUBB4B	0		

7.2 Mass spectrometry analysis: p97 interactome with crosslinking

Table 15: Mass spectrometry analysis for p97 binding proteins with crosslinking. Gene names of positive enriched interactors are shown (n=4), with significance levels of 0, 1, or 2.

Gene name	significance
ABCD3	0
ACAD9	0
ACADM	0
ACADVL	0
ACAT2	0
ACOT9	0
ACTL6A	0
ACTR2	0
AHCY	0
AK2	0
AKAP8L	0
ALDH7A1	0
ANKFY1	0
ANXA11	0
ANXA3	0
ANXA7	0
APOL2	0
ARID1A	0
ARID1B	0
ARPC4-TTLL3;	
ARPC4	0
ATAD3A	0
ATL2	0
ATL3	0
ATP1A1;	
ATP1A3;	
ATP1A2	0
ATP2B1;	
ATP2B2;	
ATP2B4	0
ATP5A1	0
ATP5B	0
ATP5H	0
ATP5J2-PTCD1;	
PTCD1	0
ATP5O	0
ATP6V1A	0
ATXN2L	0
BAG2	0
BAG4	0
BCKDK	0
BCS1L	0
BSG	0
CALR	0
CALU	0
CAPRIN1	0
CARM1	0
CASP14	0

Gene name	significance
CCDC47	0
CCT3	0
CCT7	0
CD44	0
CFL1	0
CHD4;	
CHD5;	
CHD3	0
CKAP4	0
CLPB	0
CPNE8	0
CPS1	0
CPSF1	0
CPSF6	0
CPT1A	0
CS	0
CSRP1	0
CSTF1	0
CSTF3	0
CTPS1	0
CUL1	0
DAP3	0
DCTN1;	
DKFZp686E0752	0
DCTN2	0
DDX21	0
DDX28	0
DDX3X;	
DDX3Y	0
DHCR7	0
DHX30	0
DHX8	0
DHX9	0
DLST	0
DNAJB14	0
DNAJC13	0
DPM1	0
DSG1	0
DSP	0
DYNC1I2	0
ECH1	0
ECHS1	0
ECI1;	
DCI	0
EGFR	0
EIF2S1	0
EIF2S3;	
EIF2S3L	0

Gene name	significance
EIF3A	0
EIF3F	0
EIF3H	0
EIF3I	0
EIF3L	0
EIF4A3	0
EIF4B	0
EPPK1	0
ESYT2	0
ETFB	0
FADS1	0
FAP	0
FASTKD2	0
FBLN5	0
FH	0
FKBP10	0
FLNA	0
FLNB	0
FUS	0
GALNT1	0
GALNT7	0
GAPDH	0
GCDH	0
GFM1	0
GLG1	0
GLS	0
GNB2	0
GNB2L1	0
GOLIM4	0
GOT2	0
GPD2	0
GPS1	0
GRSF1	0
HADHA	0
HDAC2	0
HK1;HK2	0
HNRNPA0	0
HNRNPA3	0
HNRNPAB	0
HNRNPF	0
HNRNPH2	0
HNRNPM	0
HNRNPR	0
HNRNPU	0
HNRNPUL1	0
HNRNPUL2;	
HNRNPUL2-BSCL2	0
HSP90B1	0

Gene name	significance
HSPA1B; HSPA1A	0
HSPA4	0
HSPA5	0
HSPA8	0
HSPH1	0
IGF2BP3	0
IMPDH2	0
IPO7	0
ITGB1	0
KARS	0
KPNA6	0
KPNB1	0
KRT1	0
LANCL1	0
LARS2	0
LDHA	0
LEPREL4; P3H4	0
LMNA	0
LMNB1	0
LOXL2	0
LRPPRC	0
MAP1B	0
MAT2B	0
MATR3	0
MCAM	0
MCM2	0
MCM3	0
MCM5	0
MCM7	0
MDH2	0
ME2	0
MRPL1	0
MRPL11	0
MRPL15	0
MRPL16	0
MRPL38	0
MRPL43	0
MRPL44	0
MRPL45	0
MRPL48	0
MRPS16	0
MRPS18A	0
MRPS2	0
MRPS23	0
MRPS27	0
MRPS28	0
MRPS7	0
MRPS9	0
MTA2	0
NASP	0
NCSTN	0
NDUFS1	0
NNT	0
NONO	0
NPM1	0
NT5DC2	0

Gene name	significance
NUMA1	0
OGT	0
OXCT1	0
P4HB	0
PC	0
PDCD6IP	0
PDE12	0
PDHB	0
PDIA3	0
PDIA4	0
PDIA6	0
PDPR	0
PFKP	0
PGAM1; PGAM2	0
PGAM5	0
PLEC	0
PLOD1	0
PNPT1	0
PODXL	0
POLR2A	0
POLR2B	0
POLR2C	0
POR	0
PPP1R7	0
PPP2R1A	0
PRDX1	0
PRKAR1A	0
PRKDC	0
PRPF19	0
PRPF39	0
PSAP	0
PSPC1	0
PTCD3	0
PTRF	0
PUF60	0
PYCR1	0
RAB11A; RAB11B	0
RAB18	0
RAB1B	0
RAB2A; RAB2B	0
RAB3GAP1	0
RAB5C	0
RAC1; RAC3; RAC2	0
RAN	0
RAP1B; RAP1A	0
RBM12	0
RBM14	0
RBM39	0
RFC3	0
RFC4	0
RFC5	0
RNF213	0

Gene name	significance
RPS10; RPS10P5; RPS10-NUDT3	0
RPS11	0
RPS13	0
RPS14	0
RPS19	0
RPS5	0
RTCB	0
RUVBL2	0
SEC23A	0
SEC23B	0
SEC24B	0
SEC24C	0
SEPT7; DKFZp586I031	0
SERBP1	0
SERPINB12	0
SF3A1	0
SF3A2	0
SF3A3	0
SF3B1	0
SF3B3	0
SFXN3	0
SH3BP4	0
SKIV2L2	0
SLC1A5	0
SLC25A5	0
SLC7A5	0
SMARCA4	0
SMARCC1	0
SMARCC2	0
SMC1A	0
SND1	0
SNRNP200	0
SNRPA	0
SNRPA1	0
SNRPN; SNRPB	0
SNX9	0
SPTAN1	0
SRRT	0
SRSF3	0
SRSF6	0
SRSF7	0
SSBP1	0
STIP1	0
SUCLG1	0
SUCLG2	0
SUMF2	0
SUPT6H	0
TAF15	0
TAGLN2	0
TARDBP	0
TARS	0
TCERG1	0
TFB1M	0

Gene name	significance
TMED7-TICAM2; TMED7	0
TMEM259	0
TNPO1	0
TPI1	0
TPM1	0
TPM3; DKFZp686J1372	0
TPR	0
TRAFD1	0
TRAP1	0
TRIM28	0
TUBA1B	0
TXNDC5	0
U2SURP	0
UBAP2	0
UBE2J1	0
UBR4	0
UGDH	0
UPF1	0
UQCRC2	0
USO1	0
VPS35	0
YTHDF3	0
YWHAB	0
YWHAG	0
ZFR	0
SEPT2	1
ABCD1	1
ACAA2	1
ACAD8	1
ACAT1	1
ACLY	1
ACTN1	1
ADAR	1
AGL	1
AHNAK	1
AHNAK2	1
AKAP8	1
ALDH3A2	1
ALDOA	1
ANXA1	1
ARPC3	1
ATP5F1	1
BASP1	1
CAD	1
CAMSAP2	1
CAND1	1
CAP1	1
CCT2	1
CCT4	1
CCT8	1
CDC2;CDK1	1
CLU	1
COL5A1	1
COPS3	1
CTNND1	1
CTTN	1

Gene name	significance
CUL4A	1
CYC1	1
CYFIP1; CYFIP2	1
DAZAP1	1
DDX1	1
DDX39A; DDX39B	1
DPYSL3	1
DSC1	1
EEF1A1P5; EEF1A1; EEF1A2	1
EFTUD2	1
EIF3B	1
EIF3C; EIF3CL	1
EIF3E	1
EIF4A1	1
EIF4G1	1
EMC1	1
EMC2	1
EMD	1
EPRS	1
ERP29	1
EWSR1	1
EZR	1
FAM120A	1
G3BP1	1
GALNT2	1
GANAB	1
GOLGA2	1
GOLGA3	1
GOSR2	1
GPX8	1
GSTP1	1
GTPBP10	1
H3F3B; H3F3A; HIST2H3A; HIST3H3; HIST1H3A; HIST2H3PS2; H3F3C	1
HDLBP	1
HLA-A	1
HLA-C	1
HNRNPDL	1
IARS	1
IDH3A	1
IGF2R	1
IKBIP	1
IMMT	1
IPO5	1
IQGAP1	1
ITGA11	1
ITPR1	1
KIF4A	1
KIF5B	1

Gene name	significance
KRT18	1
L1CAM	1
LEPREL2	1
LMAN2	1
LRP1	1
MRPL13	1
MRPL21	1
MRPL3	1
MRPL4	1
MRPL49	1
MRPS25	1
MRPS30	1
MRPS35	1
MSN	1
MTDH	1
MTERF3	1
MTHFD1	1
MYL6	1
NOA1	1
NQO1	1
NSUN2	1
NUP210	1
P4HA1	1
P4HA2	1
PARP1	1
PCNA	1
PHGDH	1
PKM	1
PLS3	1
POLDIP2	1
POLR2H	1
PON2	1
PPP1CB	1
PRDX2	1
PRKCSH	1
PSME3	1
RAB10	1
RAB7A	1
RABL3	1
RAD50	1
RALY	1
RBMX	1
RCN1	1
RNF5	1
RPA1	1
RPSA	1
RPUSD3	1
RRBP1	1
RTN4	1
SCFD1	1
SEC23IP	1
SEC31A	1
SELK	1
SEPT9	1
SERPINH1	1
SFXN1	1
SLC25A13	1
SLC3A2	1

Gene name	significance
SMARCA5	1
SMARCD1	1
SMARCD2	1
SMC4	1
SNRPD3	1
SRPR	1
SRSF1	1
SSR4	1
TALDO1	1
TIMM44	1
TIMM50	1
TMED10	1
TMPO	1
TMUB1	1
TMX1	1
TPM4	1
TRNAU1AP	1
TUBA4A	1
U2AF1; U2AF1L4	1
UBA1	1
USP5	1
USP9X	1
VAT1	1
VDAC1	1
VWA8	1
XRCC5	1
YME1L1	1
ACACA	2
ACSL3	2
ACTC1; ACTG2; ACTA1; ACTA2	2
ACTN4	2
ACTR3	2
AGPS	2
AHCYL1; AHCYL2	2
AMFR	2
ANXA2; ANXA2P2	2
ANXA5	2
APMAP	2
ARCN1	2
ARF4	2
ARF5	2
ARFGAP2	2
ARFGAP3	2
ARG1	2
ASPH	2
ASPSCR1	2
ATP2A2	2
ATP5C1	2
AUP1	2
BAT3; BAG6	2
BCAP31	2

Gene name	significance
BUB3	2
C14orf166	2
CANX	2
CAT	2
CAV1	2
CCT5	2
CCT6A	2
CHCHD3	2
CLTC	2
COL12A1	2
COLGALT1	2
COPA	2
COPB1	2
COPB2	2
COPE	2
COPG1	2
COPG2	2
COPS4	2
COPZ1	2
CRTAP	2
CTSD	2
CUL2	2
DARS	2
DDB1	2
DDOST	2
DERL1	2
DLAT	2
DNAJA1	2
DNAJA3	2
DNAJB11	2
DNAJB12	2
DNM1L	2
DYNC1H1	2
EEA1	2
EEF1D	2
EEF1G	2
ENO1	2
ERGIC1	2
ERGIC3	2
ERLEC1	2
ERLIN1	2
ERLIN2	2
ERP44	2
ESYT1	2
ETFA	2
FAF1	2
FAF2	2
FAM8A1	2
FASN	2
FSCN1	2
GADD45GIP1	2
GOLPH3	2
HACD3	2
HERPUD1	2
HSP90AA1	2
HSP90AB1; HSP90AB3P	2
HSPB1	2

Gene name	significance
HUWE1	2
HYOU1	2
IARS2	2
IDH3B	2
ILF2	2
IP6K1	2
ITGB4	2
KPNA2	2
KTN1	2
LARP1	2
LARS	2
LDHB	2
LGALS7	2
LMAN1	2
LOX	2
LPCAT1	2
LRRC59	2
MAP4	2
MARCKS	2
MCAT	2
MRPL37	2
MRPL39	2
MRPL47	2
MYH9	2
MYOF	2
NAPA	2
NCLN	2
NGLY1	2
NME1-NME2; NME2; NME1; NME2P1	2
NOMO3; NOMO2	2
NPLOC4	2
NSFL1C	2
NUP155	2
OS9	2
PABPC1; PABPC3	2
PABPC4	2
PAICS	2
PDCD6	2
PDP1	2
PFN1	2
PGK1	2
PGRMC2	2
PHB	2
PHB2	2
PLAA	2
POLR2E	2
POLRMT	2
PPIA	2
PPIB	2
PRMT1	2
PRPF8	2
PSMA1	2
PSMA2	2

Gene name	significance
PSMA3	2
PSMA4	2
PSMA5	2
PSMA6	2
PSMA7	2
PSMB1	2
PSMB3	2
PSMB4	2
PSMB5	2
PSMB6	2
PSMB7	2
PSMC1	2
PSMC2	2
PSMC3	2
PSMC4	2
PSMC5	2
PSMC6	2
PSMD1	2
PSMD11	2
PSMD12	2
PSMD13	2
PSMD14	2
PSMD2	2
PSMD3	2
PSMD4	2
PSMD5	2
PSMD6	2
PSMD7	2
PSMD8	2
PXDN	2
QKI	2
RAB14	2
RAB3GAP2	2
RAD23B	2
RARS	2
RBBP4	2
RPN1	2
RPN2	2
RPS16	2
RPS17	2
RPS18	2
RPS20	2
RPS27A; UBB; UBC; UBA52	2
RPS3A	2
RUVBL1	2
SACM1L	2
SCYL1	2
SCYL2	2
SDCBP	2
SEC22B	2
SEC24A	2
SEC61A1; SEC61A2	2
SEL1L	2
SF3B2	2

Gene name	significance
SLC25A3	2
SMARCA2	2
SMARCB1	2
SMC2	2
SMC3	2
SPTBN1	2
SQSTM1	2
SRPRB	2
SRRM2	2
STOML2	2
STT3B	2
SUPT5H	2
SYNCRIP	2
SYVN1	2
TCP1	2
TECR	2
TFRC	2
TGM3	2
TKT	2
TLN1	2
TMED9	2
UBAC2	2
UBAP2L	2
UBE4A	2
UBE4B	2
UBL7	2
UBQLN1	2
UBXN1	2
UBXN4	2
UBXN6	2
UBXN7	2
UBXN8	2
UCHL5	2
UFD1L	2
VAPB	2
VARS	2
VCL	2
VCP	2
VCPIP1	2
VDAC2	2
VIMP	2
VPRBP	2
XRCC6	2
YBX1	2
YWHAE	2
ZC3HAV1	2

7.3 Mass spectrometry analysis: MYOF interactome

Table 16: Mass spectrometry analysis for MYOF binding proteins. Gene names of positive enriched interactors are shown (n=3), with significance levels of 0, 1, or 2.

Gene name	significance
A2M	0
ABCB7	0
ABCD1	0
ACAA1	0
ACAA2	0
ACAT2	0
ACLY	0
ACOT8	0
ACSF3	0
ACSL3	0
ACTB	0
ACTC1; ACTG2; ACTA1; ACTA2	0
ACTL6A	0
ACTR2	0
AGMAT	0
AGPS	0
AGRN	0
AHNAK2	0
AIMP1	0
AK2	0
AKR1C1	0
AKR1C3	0
ALDH1B1	0
ALDH3A2	0
ALDOA	0
ANKFY1	0
ANXA1	0
ANXA11	0
ANXA2; ANXA2P2	0
ANXA5	0
AP2A1	0
AP3M1	0
AP3S1	0
APOL2	0
ARF4	0
ARFGAP2	0
ARG1	0
ARL2	0
ARMCX3	0
ARPC2	0
ARPC3	0
ASPH	0
ATAD1	0
ATAD3A	0
ATP5A1	0
ATP5B	0
ATP5C1	0
ATP5EP2; ATP5E	0
ATP5I	0
ATP5O	0

Gene name	significance
ATP6V1A	0
B2M	0
BASP1	0
BCAP31	0
BCS1L	0
BLMH	0
BSG	0
BZW1	0
CALR	0
CAND1	0
CANX	0
CAP1	0
CAPZA1	0
CAPZB	0
CARM1	0
CAT	0
CAV1	0
CBR1	0
CCAR2	0
CCDC47	0
CCDC80	0
CCT2	0
CCT3	0
CCT4	0
CCT5	0
CCT6A	0
CCT7	0
CCT8	0
CD59	0
CDIPT	0
CFH	0
CFL1	0
CHCHD2; CHCHD2P9	0
CHCHD3	0
CKAP4	0
CKAP5	0
CLIC1	0
CLTA	0
CLTB	0
CLTC	0
CLU	0
CNBP	0
CNOT1	0
COA3	0
COL12A1	0
COL4A2	0
COL5A1	0
COLGALT1	0
COPS6	0
COPZ1	0
COX20	0
COX5A	0
COX5B	0
COX6C	0

Gene name	significance
CPNE1	0
CPNE8	0
CRIP2	0
CSRP1	0
CSTF1	0
CTNNA1	0
CTNNBL1	0
CTNND1	0
CTSC	0
CTSZ	0
CTTN	0
CYB5R3	0
DAP3	0
DARS	0
DAZAP1	0
DCTPP1	0
DDB1	0
DDOST	0
DDRGK1	0
DDX39B; DDX39A	0
DECR2	0
DNAJB1	0
DNAJC10	0
DNAJC7	0
DNMT1	0
DPF2	0
DPM1	0
DSTN	0
DTYMK	0
DYNC1H1	0
DYNC1LI1	0
ECI2	0
EEA1	0
EEF1A1P5; EEF1A1; EEF1A2	0
EEF1B2	0
EEF1D	0
EEF1E1; EEF1E1-BLOC1S5	0
EEF1G	0
EEF2	0
EFTUD2	0
EGFR	0
EIF2S1	0
EIF3B	0
EIF3E	0
EIF3F	0
EIF3G	0
EIF3I	0
EIF3K	0
EIF3L	0
EIF4A1	0
EIF4A3	0

Gene name	significance
EIF4B	0
ELAVL1	0
EMC1	0
EMC2	0
EMD	0
ENO1	0
EPHX1	0
EPRS	0
ERGIC1	0
ERGIC2	0
ERLIN1	0
ERO1L	0
ERP44	0
ESYT1	0
ESYT2	0
ETFB	0
EXOSC2	0
EXOSC6	0
FAF2	0
FAM129B	0
FASTKD2	0
FECH	0
FERMT2	0
FH	0
FIS1	0
FKBP10	0
FKBP9	0
FLOT1	0
FN3KRP	0
FUS	0
G3BP1	0
GADD45GIP1	0
GANAB	0
GAPDH	0
GAPVD1	0
GCDH	0
GCN1L1	0
GEMIN5	0
GGCX	0
GIPC1	0
GLA	0
GLS	0
GLUL	0
GNAI2	0
GNAI3	0
GNAS	0
GNB2	0
GNB2L1	0
GNG12	0
GOLGA2	0
GRPEL1	0
GSR	0
GSTK1	0
GSTP1	0
GTPBP10	0

Gene name	significance
H3F3B; H3F3A; HIST2H3A; HIST3H3; HIST1H3A; H3F3C	0
HACL1	0
HADH	0
HAT1	0
HDLBP	0
HEXA	0
HEXB	0
HIBCH	0
HINT2	0
HLA-A	0
HLA-B	0
HLA-C	0
HMGB1; HMGB1P1	0
HMGCL	0
HNRNPA1; HNRNPA1L2	0
HNRNPA2B1	0
HNRNPAB	0
HNRNPC	0
HNRNPD	0
HNRNPF	0
HNRNPH2	0
HNRNPL	0
HNRNPR	0
HNRNPUL2; HNRNPUL2-BSCL2	0
HSD17B4	0
HSD17B8	0
HSDL2	0
HSP90AA1	0
HSP90AB1; HSP90AB3P	0
HSPA1B; HSPA1A	0
HSPA4	0
HSPA4L	0
HSPA5	0
HSPA8	0
HSPB1	0
HSPG2	0
HSPH1	0
IDH1	0
IGF2R	0
ILF2	0
ILF3	0
INPP5K	0
IPO5	0
IPO7	0
IQGAP1	0

Gene name	significance
ITGB1	0
KIAA0368; ECM29	0
KIF2A	0
KIF4A	0
KIF5B	0
KLHL13; KLHL9	0
KPNA6	0
KRT18	0
L1CAM	0
LANCL1	0
LARP4	0
LASP1	0
LDHA	0
LDHB	0
LEPRE1	0
LEPREL2	0
LGALS1	0
LGALS3BP	0
LMAN2	0
LOX	0
LRP1	0
LRRC59	0
LUC7L2; C7orf55	0
LUC7L3	0
MAGED2	0
MARCKS	0
MCAM	0
MLEC	0
MRPL14	0
MRPL15	0
MRPL17	0
MRPL20	0
MRPL22	0
MRPL23	0
MRPL24	0
MRPL38	0
MRPL4	0
MRPL43	0
MRPL44	0
MRPL45	0
MRPL47	0
MRPL49	0
MRPL50	0
MRPL9	0
MRPS10	0
MRPS11	0
MRPS12	0
MRPS14	0
MRPS15	0
MRPS21	0
MRPS27	0
MRPS33	0

Gene name	significance
MRPS34	0
MRPS35	0
MRPS7	0
MRPS9	0
MRRF	0
MSN	0
MTCH2	0
MT-CO2	0
MTERF3	0
MTHFD1	0
MTOR	0
MTPAP	0
MYH9	0
MYL12A; MYL12B	0
MYL6	0
MYO1C	0
MYO1E	0
NASP	0
NDUFA12	0
NDUFA2	0
NDUFA4	0
NDUFA6	0
NDUFAF7	0
NDUFB1	0
NDUFB10	0
NDUFB4	0
NDUFB5	0
NDUFB8	0
NDUFB9	0
NDUFS1	0
NDUFS2	0
NELFB	0
NME1-NME2; NME2; NME1; NME2P1	0
NME3	0
NOA1	0
NOMO1	0
NONO	0
NQO1	0
NSUN4	0
NT5DC2	0
NTPCR	0
NUMA1	0
NUP155	0
OAT	0
P4HA1	0
P4HA2	0
PABPC4	0
PAFAH1B1	0
PAICS	0
PAIP1	0
PAPSS1	0

Gene name	significance
PARK7	0
PCBP1	0
PCBP2	0
PCK2	0
PDS5A	0
PDXK	0
PEBP1	0
PFKP	0
PFN1	0
PGK1	0
PIGS	0
PKM	0
PLD3	0
PLOD1	0
PLOD2	0
PLS3	0
PLXDC2	0
PLXNB2	0
PMPCA	0
PMPCB	0
PNP	0
POLA1	0
POLR1C	0
POLR2E	0
POLRMT	0
PON2	0
PPIA	0
PPIL1	0
PPME1	0
PPP1CA	0
PPP1CB	0
PPP2R1A	0
PRADC1	0
PRDX1	0
PRDX2	0
PRDX4	0
PRDX5	0
PRDX6	0
PRKCDBP	0
PRKCSH	0
PRKDC	0
PRMT5	0
PRMT6	0
PRPS1	0
PRRC2C	0
PSAP	0
PSMA1	0
PSMA4	0
PSMA5	0
PSMA6	0
PSMA7	0
PSMB1	0
PSMB2	0
PSMB5	0
PSMB6	0

Gene name	significance
PSMC1	0
PSMC4	0
PSMC5	0
PSMC6	0
PSMD1	0
PSMD11	0
PSMD13	0
PSMD2	0
PSMD3	0
PSMD6	0
PTCD2	0
PTCD3	0
PTGES2	0
PTPMT1	0
PTRF	0
PXDN	0
PYCR1	0
PYGL	0
QARS	0
QKI	0
RAB10	0
RAB18	0
RAB1A	0
RAB2A; RAB2B	0
RAB32	0
RAB3GAP1	0
RAB5C	0
RAB8A	0
RALY	0
RAN	0
RAP1B; RAP1A	0
RARS	0
RBBP4	0
RBM12	0
RBM3	0
RBM39	0
RBM4	0
RBMX	0
RBX1	0
RDH11	0
RDX	0
RFC2	0
RFC3	0
RFC4	0
RFC5	0
RHOA	0
RNF5	0
ROCK2	0
RPA2	0
RPL11	0
RPL22	0
RPL26; RPL26L1	0

Gene name	significance
RPL27	0
RPL30	0
RPL38	0
RPL7	0
RPLP0; RPLP0P6	0
RPN1	0
RPN2	0
RPS11	0
RPS12	0
RPS13	0
RPS14	0
RPS15A	0
RPS16	0
RPS17	0
RPS18	0
RPS19	0
RPS20	0
RPS23	0
RPS25	0
RPS27	0
RPS27A	0
RPS3	0
RPS3A	0
RPS4X	0
RPUSD4	0
RRM1	0
RTCB	0
S100A11	0
SACM1L	0
SCAMP3	0
SCFD1	0
SDCBP	0
SDF4	0
SDHA	0
SEC22B	0
SEC23A	0
SEC23B	0
SEC23IP	0
SEC24A	0
SEC24B	0
SEC24C	0
SEC31A	0
SEC61A1; SEC61A2	0
SEPT2	0
SEPT7	0
SEPT9	0
SERBP1	0
SET; SETSIP	0
SFN	0
SFXN1	0
SFXN3	0
SLC16A1	0

Gene name	significance
SLC1A5	0
SLC25A1	0
SLC25A13	0
SLC25A20	0
SLC25A22	0
SLC25A29	0
SLC25A3	0
SLC25A5	0
SLC25A6	0
SLC35A4	0
SLC3A2	0
SLC7A5	0
SMARCB1	0
SMARCD1	0
SMARCE1	0
SMC2	0
SND1	0
SNX1	0
SRP68	0
SRPR	0
SRSF11	0
SRSF7	0
SS18L1	0
SSR1	0
SSR4	0
STAM	0
STAM2	0
STAT1	0
STAT3	0
STIP1	0
STMN1	0
STOM	0
STRAP	0
STT3B	0
SUB1	0
SUCLG2	0
SYNCRIP	0
TAGLN	0
TAGLN2	0
TAPBP	0
TBRG4	0
TCEB1	0
TCP1	0
TFB2M	0
TFG	0
THOC1	0
THOC3	0
TIA1	0
TIMM50	0
TMED10	0
TMEM106B	0
TMEM165	0
TNPO1	0
TOMM20	0
TOMM22	0

Gene name	significance
TPI1	0
TPM3; DKFZp686J1372	0
TPM4	0
TRA2B	0
TRIM28	0
TTLL12	0
TUBA1B	0
TUBB	0
TUBB4B	0
TUFM	0
TXN	0
TXNDC12	0
TXNDC5	0
UBA1	0
UBAP2L	0
UBR4	0
UBXN1	0
UFD1L	0
UGGT1	0
UPF1	0
UQCRC1	0
UQCRC2	0
UQCRQ	0
USO1	0
VARS	0
VAT1	0
VCL	0
VDAC2	0
VDAC3	0
VPS18	0
VPS29	0
VPS35	0
VPS45	0
WASF2	0
WBSCR16	0
WDR1	0
WDR5	0
WDR82	0
WNK1	0
XPO1	0
YARS2	0
YBX1	0
YIPF5	0
YWHAG	0
YWHAQ	0
YWHAZ	0
ZADH2	0
ZC3HAV1	0
ABCD3	1
ACTR1A	1
ACTR3	1
ANAPC7	1
ANXA3	1
ANXA6	1

Gene name	significance
ANXA7	1
AP1B1	1
ARFIP1	1
ASCC3	1
ATP6V1G1	1
BABAM1	1
BRE	1
CALU	1
CCDC127	1
CDC42	1
CDKN2A	1
CNP	1
CNTNAP1	1
COPS8	1
CPD	1
CPOX	1
CRTAP	1
CSNK2A2	1
DNAJA1	1
DNAJA2	1
DNAJC13	1
EHD4	1
ERLIN2	1
EXOC4	1
FAM98A	1
FKBP4	1
FTH1	1
GBA	1
GLB1	1
GNE	1
GPX8	1
HIST1H2BN; HIST1H2BM; HIST1H2BH; HIST2H2BF; HIST1H2BC; HIST1H2BD; HIST1H2BK; H2BFS; HIST1H2BL	1
HSP90AB2P	1
IKBIP	1
IKBIP	1
IKBKAP	1
IPO9	1
ITGA11	1
KDELC1	1
KNSTRN	1
LAMA5	1
LAMTOR1	1
LARS	1
LEPREL4; P3H4	1
LRRC8A	1
MAGT1	1
MANF	1

Gene name	significance
MIF	1
MRPL32	1
NAPA	1
NHP2L1	1
P4HB	1
PABPC1; PABPC3	1
PDIA3	1
PEX13	1
PGAM1; PGAM2	1
PGRMC2	1
POFUT1	1
PPIB	1
PPP2CA	1
PRPF19	1
PRPSAP1	1
PSMB4	1
PSMC2	1
PSMD14	1
RAC1; RAC3; RAC2	1
RAE1	1
RBBP7	1
RCN1	1
RPL23	1
RUFY1	1
SCP2	1
SEC11A; SEC11B	1
SEC16A	1
SEH1L	1
SEL1L	1
SNAPIN	1
SORD	1
SPAG5	1
SRP14	1
SRPRB	1
ST13; ST13P4; ST13P5	1
STK4	1
TBL2	1
TFRC	1
TMEM33	1
TMX1	1
TPP1	1
TTC37	1
UBAP2	1
UBE2V1; TMEM189-UBE2V1	1
USP14	1
VAMP8	1
VIMP	1

Gene name	significance
VPS26A	1
WDR77	1
YWHAB	1
ZMPSTE24	1
ABI1	2
ACAD9	2
ACOX1	2
ACOX3	2
AHNAK	2
AIFM1	2
ALYREF	2
ANAPC1	2
AP1M1	2
ARPC4-TTLL3; ARPC4	2
ATP6AP1	2
ATP6AP2	2
ATP6V0D1	2
ATXN2L	2
BCL9	2
BRK1	2
C1orf109	2
C2orf47	2
C4B;C4A	2
CALD1	2
CALM2; CALM1	2
CAMK2D	2
CAMK2G	2
CARS2	2
CDC2; CDK1	2
CLN6	2
CLPTM1L	2
CNN3	2
CNPY2	2
CNPY3	2
COASY	2
COL2A1	2
COPS7A	2
COX7A2	2
CSNK2A1; CSNK2A3	2
CYFIP1	2
DNAJB11	2
DNAJC3	2
EDEM3	2
EFCAB14	2
EHD1	2
EIF2S3; EIF2S3L	2
ETV6	2
EZR	2
FAM64A	2
FN1	2

Gene name	significance
FSCN1	2
G6PD	2
GFER	2
GIGYF2	2
GPI	2
hCG_1984214; MRPS17	2
HK1	2
HSD17B12	2
HSP90B1	2
HYOU1	2
IFITM2; I FITM3; IFITM1	2
IGKV4-1	2
IGSF10	2
KPNA2	2
LMF2	2
LMO7	2
LPL	2
LRBA	2
LRPAP1	2
MAPRE1	2
MDN1	2
MESDC2	2
MOCOS	2
MTAP	2
MYDGF	2
MYOF	2
NARS	2
NCAPD2	2
NCKAP1	2
NCOA5	2
NDUFC2; KCTD14; NDUFC2-KCTD14	2
NRAS; HRAS	2
NUDC	2
NUP50	2
OCIAD1	2
OCIAD2	2
OLFML2A	2
PDIA4	2
PDIA6	2
PDP1	2
PEX1	2
PEX14	2
PEX5	2
PFDN2	2
PHKA2	2
PHKB	2
PHKG2	2
PLAA	2
POLDIP3	2

Gene name	significance
PROCR	2
PRUNE2	2
PSMD4	2
PSMD7	2
PSMD8	2
PTRH2	2
RAB11B; RAB11A	2
RAB11FIP1	2
RAB14	2
RAB31	2
RAB34	2
RAB6A	2
RAB7A	2
RCN2	2
RFX1	2
RNF213	2
RPL17; RPL17-C18orf32	2
RPL24	2
RTN4	2
RUVBL1	2
RUVBL2	2
SARNP	2
SDF2L1	2
SERPINH1	2
SLC9A3R1	2
SMAD2	2
SNAP29	2
SNX3	2
SPATA5	2
SPATA5L1	2
STX7	2
SUMF2	2
TECR	2
TGFBI	2
THOC2	2
THOC5	2
THOC6	2
TMX3	2
TOR1AIP1	2
TRIP10	2
TXNRD1	2
UGGT2	2
USP5	2
VAPB	2
VCP	2
WDR61	2

7.4 Shared interactors of p97 and MYOF

Table 17: Shared interactors of p97 and MYOF. Protein name and gene name of shared MYOF and p97 interactors with a significance of 1 and 2.

Protein name	Gene name
Actin-related protein 3	ACTR3
Neuroblast differentiation-associated protein AHNAK	AHNAK
Cyclin-dependent kinase 1	CDC2;CDK1
Cartilage-associated protein	CRTAP
Cytoplasmic FMR1-interacting protein 1;Cytoplasmic FMR1-interacting protein 2	CYFIP1;CYFIP2
DnaJ homolog subfamily A member 1	DNAJA1
DnaJ homolog subfamily B member 11	DNAJB11
Erlin-2	ERLIN2
Ezrin	EZR
Fascin	FSCN1
Glutathione peroxidase;Probable glutathione peroxidase 8	GPX8
Hypoxia up-regulated protein 1	HYOU1
Inhibitor of nuclear factor kappa-B kinase-interacting protein	IKBIP
Integrin alpha-11	ITGA11
Importin subunit alpha-1	KPNA2
Leucine--tRNA ligase, cytoplasmic	LARS
Myoferlin	MYOF
Alpha-soluble NSF attachment protein	NAPA
Polyadenylate-binding protein 1;Polyadenylate-binding protein;Polyadenylate-binding protein 3	PABPC1;PABPC3
Membrane-associated progesterone receptor component 2	PGRMC2
Phospholipase A-2-activating protein	PLAA
Peptidyl-prolyl cis-trans isomerase B	PPIB
Proteasome subunit beta type-4	PSMB4
26S protease regulatory subunit 7	PSMC2
26S proteasome non-ATPase regulatory subunit 14	PSMD14
26S proteasome non-ATPase regulatory subunit 4	PSMD4
26S proteasome non-ATPase regulatory subunit 7	PSMD7
26S proteasome non-ATPase regulatory subunit 8	PSMD8
Ras-related protein Rab-14	RAB14
Ras-related protein Rab-7a	RAB7A
Reticulocalbin-1	RCN1
Reticulon-4;Reticulon	RTN4
RuvB-like 1	RUVBL1
Protein sel-1 homolog 1	SEL1L
Serpin H1	SERPINH1
Signal recognition particle receptor subunit beta	SRPRB
Very-long-chain enoyl-CoA reductase	TECR
Transferrin receptor protein 1;Transferrin receptor protein 1, serum form	TFRC
Thioredoxin-related transmembrane protein 1	TMX1
Ubiquitin carboxyl-terminal hydrolase 5	USP5
Vesicle-associated membrane protein-associated protein B/C	VAPB
Transitional endoplasmic reticulum ATPase	VCP
Selenoprotein S	VIMP

Acknowledgements

I would like to express my gratitude to all those who helped me during my doctoral studies and without whose support this work would not have been possible.

First and foremost, I am deeply grateful to Prof. Dr. Alexander Buchberger for supervising this thesis and for providing me with the opportunity to work on this project. I very much enjoyed the time I spent on this project and I want to thank you for your encouragement, great support, helpful suggestions, and scientific discussions during the past years!

I am also thankful to the members of my thesis committee, Prof. Dr. Hermann Schindelin and Dr. Mathias Rosenfeldt, for their valuable suggestions, support, and guidance at every stage of this project.

I want to thank Dr. Andreas Schlosser for the mass spectrometry analysis. Additionally, I would like to thank Prof. Dr. Thomas Rudel and Dr. Kathrin Stelzner for the initial help with the FACS, Dr. Ursula Eilers and Dr. Christina Schülein-Völk for their support with the Operetta system, and the core imaging facility at the Biocenter.

I would also like to express my gratitude to all past and current members of Buchberger group, Dr. Ankit Turakhiya, Dr. Beyenech Binotti, Maria Körner, Nazife Tolay, Susanne Meyer, and Sven Spielhaupter, for the great atmosphere, support, and advice. Thank you for the time we spent together, it was much fun and I will miss you. Special thanks to Ankit for all the initial help when I first joined our group, to Beyenech for sharing your experience with Rab proteins and for all your practical advice, to Maria for all your motivation and hard work you gave during your time as my student. I very much enjoyed it. Thank you, Maria and Sven, for sharing your experience with working with the lentivirus system, Nazife for your help with microscopy and the SIM, and Susanne for all technical support, your jokes and the jogging sessions. Thanks to my students Rebecca Hobrecht and Joshua Grubb.

Additionally, I would like to thank all GRK2243 members, I enjoyed the discussions and friendly atmosphere of the GRK2243. Thanks to all current and former members of the department, especially Prof. Dr. Utz Fischer and the members of the Fischer group for the discussions during the department seminars.

Finally, I wish to thank my husband Frank and my parents, for all their support and love.

Publication list

Manuscript in preparation:

Authors: **Mona Kawan**, Maria Körner, Andreas Schlosser and Alexander Buchberger

Working title: p97 promotes the recycling of endocytic cargo

Previous publications:

Nguyen AT, Prado MA, Schmidt PJ, Sendamarai AK, Wilson-Grady JT, Min M, Campagna DR, Tian G, Shi Y, Dederer V, **Kawan M**, Kuehnle N, Paulo JA, Yao Y, Weiss MJ, Justice MJ, Gygi SP, Fleming MD, Finley D. UBE2O remodels the proteome during terminal erythroid differentiation. Science. 2017 Aug 4;357(6350).

Amm I, **Kawan M**, Wolf DH. Characterization of protein quality control components via dual reporter-containing misfolded cytosolic model substrates. Anal Biochem. 2016 Dec 15;515:14-21.

Curriculum Vitae